

Development of Closed-Loop Control System for Microwave Freeze-
Drying of Carrot Slices



NARATHIP SUJINDA

DOCTOR OF ENGINEERING IN FOOD ENGINEERING

MAEJO UNIVERSITY

2021

Development of Closed-Loop Control System for Microwave Freeze-
Drying of Carrot Slices



A DISSERTATION SUBMITTED IN PARTIAL FULFILLMENT
OF THE REQUIREMENTS FOR THE DEGREE OF DOCTOR OF ENGINEERING
IN FOOD ENGINEERING
ACADEMIC ADMINISTRATION AND DEVELOPMENT MAEJO UNIVERSITY
2021

Copyright of Maejo University

Development of Closed-Loop Control System for Microwave
Freeze-Drying of Carrot Slices

NARATHIP SUJINDA

THIS DISSERTATION HAS BEEN APPROVED IN PARTIAL FULFLLMENT
OF THE REQUIREMENTS FOR THE DEGREE OF DOCTOR OF ENGINEERING
IN FOOD ENGINEERING

APPROVED BY

Advisory Committee

Chair

(Associate Professor Dr. Jaturapatr Varith)

...../...../.....

Committee

(Professor Dr. Rosnah Shamsudin)

...../...../.....

Committee

(Associate Professor Dr. Somkiat

Jaturonglumlert)

...../...../.....

Program Chair, Doctor of Engineering

in Food Engineering (Associate Professor Dr. Somkiat

Jaturonglumlert)

...../...../.....

CERTIFIED BY ACADEMIC

.....

ADMINISTRATION AND DEVELOPMENT

(Associate Professor Dr. Yanin Opatpatanakit)

Vice President for the Acting President of Maejo

University

...../...../.....

ชื่อเรื่อง	การพัฒนาระบบควบคุมวงปิดสำหรับการอบแห้งชิ้นแครอทด้วยการอบแห้งแบบแช่เยือกแข็งร่วมกับคลื่นไมโครเวฟ
ชื่อผู้เขียน	นายนราธิป สุจินดา
ชื่อปริญญา	วิศวกรรมศาสตรดุษฎีบัณฑิต สาขาวิชาวิศวกรรมอาหาร
อาจารย์ที่ปรึกษาหลัก	รองศาสตราจารย์ ดร.จตุรภัทร วาฤทธิ

บทคัดย่อ

การอบแห้งแบบแช่เยือกแข็งร่วมกับไมโครเวฟ (Microwave freeze-drying) เป็นกระบวนการที่ใช้พลังงานไมโครเวฟเป็นแหล่งพลังงานความร้อนในการอบแห้งแบบแช่เยือกแข็ง (freeze drying) เพื่อการลดระยะเวลาการอบแห้งของกระบวนการทำแห้งแบบแช่เยือกแข็ง กระบวนการอบแห้งแบบแช่เยือกแข็งร่วมกับไมโครเวฟเป็นกระบวนการที่มีความซับซ้อนระหว่างระดับพลังงานไมโครเวฟ ปริมาณความชื้น อุณหภูมิวัสดุ และระดับแรงดันสุญญากาศ ซึ่งมีผลต่ออัตราการอบแห้ง คุณภาพของผลิตภัณฑ์ และการใช้พลังงานในกระบวนการอบแห้ง การควบคุมสถานะของการอบแห้งแบบแช่เยือกแข็งร่วมกับไมโครเวฟให้เหมาะสม เพื่อให้ได้ประสิทธิภาพการอบแห้งและคุณภาพของผลิตภัณฑ์ที่ดีที่สุด จึงเป็นสิ่งที่ผู้วิจัยต้องการค้นคว้าในงานวิจัยนี้ ดังนั้นงานวิจัยนี้จึงมีวัตถุประสงค์เพื่อออกแบบกลยุทธ์การควบคุมกระบวนการอบแห้งแบบแช่เยือกแข็งร่วมกับคลื่นไมโครเวฟ โดยใช้ชื่อว่า ตรรกะการควบคุมไมโครเวฟแบบพลวัต (Dynamic microwave logic control) โดยประยุกต์เข้ากับระบบควบคุมแบบวงปิด (Closed-loop control system) เพื่อเพิ่มประสิทธิภาพของการอบแห้งแบบแช่เยือกแข็งร่วมกับไมโครเวฟ

ในส่วนแรกของงานวิจัยนี้ ได้ทำการประเมินความไม่แน่นอนของระบบตรวจวัดและการคำนวณความชื้นวัสดุตามคู่มือการประเมินความไม่แน่นอนในการตรวจวัด (GUM) เพื่อตรวจสอบความความแม่นยำของระบบตรวจวัดและการคำนวณความชื้นของวัสดุ ผลการประเมินพบว่า ความไม่แน่นอนของการวัดอุณหภูมิ คือ ± 1.5 องศาเซลเซียส หรือ 3.9% ในช่วงการวัด 30 ถึง 50 องศาเซลเซียส ความไม่แน่นอนของการวัดน้ำหนัก คือ ± 0.347 กรัม ในช่วงการวัด 0 ถึง 150 กรัม และความไม่แน่นอนในการคำนวณปริมาณความชื้น คือ ± 1 เปอร์เซ็นต์ (มาตรฐานเป็ยก) ผลการประเมินนี้ ระบบการวัดและการคำนวณความชื้นสามารถยอมรับในการใช้งานร่วมกับระบบควบคุมแบบวงปิดได้ โดยไม่ส่งผลกระทบต่อกระบวนการควบคุมกระบวนการและคุณภาพของผลิตภัณฑ์ ซึ่งยืนยันได้จากผลลัพธ์ที่มีความใกล้เคียงกันในการทำซ้ำของงานวิจัยนี้

ในส่วนที่สอง ได้ศึกษาการแปรผันของอุณหภูมิระหว่างการอบแห้งชิ้นแครอท ด้วยการอบแห้งแบบแช่เยือกแข็งร่วมกับไมโครเวฟ โดยใช้ระบบควบคุมอุณหภูมิแบบวงปิด (Closed-loop temperature control system) เพื่อควบคุมอุณหภูมิของชิ้นแครอทในขั้นตอนสุดท้ายของกระบวนการ ผลการศึกษาพบว่าระบบควบคุมอุณหภูมิแบบวงปิดสามารถเพิ่มประสิทธิภาพในการควบคุมอุณหภูมิของชิ้นแครอทได้ถึง 60 เปอร์เซ็นต์ เมื่อเทียบกับการอบแห้งแบบแช่เยือกแข็งร่วมกับไมโครเวฟที่ไม่มีระบบควบคุมอุณหภูมิแบบวงปิด โดยคุณภาพของผลิตภัณฑ์เทียบเท่ากับการอบแห้งแบบแช่เยือกแข็ง ด้วยเหตุนี้จึงนำระบบควบคุมอุณหภูมิแบบวงปิดมาใช้เพื่อพัฒนาระบบควบคุมวงปิดสำหรับการอบแห้งแบบแช่เยือกแข็งร่วมกับไมโครเวฟในส่วนที่สุดท้ายของงานวิจัยนี้

ในส่วนสุดท้าย ระบบควบคุมวงปิดได้รับการพัฒนาเพื่อปรับปรุงกระบวนการอบแห้งแบบแช่เยือกแข็งร่วมกับไมโครเวฟ และเพื่อศึกษาผลกระทบของตรรกะการควบคุมไมโครเวฟแบบพลวัตต่อคุณลักษณะเฉพาะของกระบวนการอบแห้งแบบแช่เยือกแข็งร่วมกับไมโครเวฟ การพัฒนาดังกล่าวประกอบด้วยสองส่วนย่อย ในส่วนย่อยแรกของการพัฒนาระบบ ได้ศึกษากระบวนการอบแห้งแบบแช่เยือกแข็งร่วมกับไมโครเวฟเพื่อให้ได้มาซึ่งกลยุทธ์ในการอบแห้งชิ้นแครอท โดยใช้กำลังไมโครเวฟ 100, 200 และ 300 วัตต์ อุณหภูมิวัสดุในช่วง -15 องศาเซลเซียส ถึง 40 องศาเซลเซียส และความชื้นสุดท้าย 6 เปอร์เซ็นต์ (มาตรฐานเปียก) ในส่วนย่อยที่สอง ตรรกะการควบคุมไมโครเวฟแบบพลวัต ได้ถูกพัฒนาเชิงกลยุทธ์ตามการกำหนดค่าเฟสการอบแห้งและการควบคุมแบบพลวัตระหว่างพลังงานไมโครเวฟและความชื้น ณ เวลาปัจจุบัน เพื่อป้องกันไปยังระบบควบคุม หลังจากนั้นตรรกะการควบคุมไมโครเวฟแบบพลวัตจะถูกรวมเข้ากับระบบควบคุมแบบวงปิด

ผลการวิจัยพบว่า การพัฒนาระบบควบคุมแบบวงปิดโดยประยุกต์ใช้ตรรกะการควบคุมไมโครเวฟแบบพลวัต สามารถทำงานร่วมกับกระบวนการอบแห้งแบบแช่เยือกแข็งร่วมกับไมโครเวฟได้ดี โดยสามารถลดระยะเวลาการอบแห้งได้ 62.4 เปอร์เซ็นต์ และ 23.4 เปอร์เซ็นต์ เมื่อเปรียบเทียบกับกระบวนการอบแห้งแบบแช่เยือกแข็งและการอบแห้งแบบแช่เยือกแข็งร่วมกับไมโครเวฟที่ไม่มีการใช้ตรรกะการควบคุมไมโครเวฟแบบพลวัต โดยที่คุณภาพของผลิตภัณฑ์เทียบเท่ากับการอบแห้งแบบแช่เยือกแข็ง แต่มีอัตราการระเหยน้ำจำเพาะ (Specific moisture extraction rate) ดีกว่าถึง 44.3% การค้นพบนี้แสดงให้เห็นว่า การพัฒนาระบบควบคุมแบบวงปิดโดยประยุกต์ใช้ตรรกะการควบคุมไมโครเวฟแบบพลวัต สามารถเพิ่มประสิทธิภาพของการอบแห้งแบบแช่เยือกแข็งร่วมกับไมโครเวฟได้ในขณะที่ยังสามารถรักษาคุณภาพผลิตภัณฑ์ได้ดีเทียบเท่ากับการอบแห้งแบบแช่เยือกแข็งอย่างมีนัยสำคัญ

คำสำคัญ : การอบแห้งแบบแช่เยือกแข็งร่วมกับไมโครเวฟ, ระบบควบคุมแบบวงปิด, ตรรกะการควบคุมไมโครเวฟแบบพลวัต, คุณลักษณะการอบแห้ง, แครอท



Title	Development of Closed-Loop Control System for Microwave Freeze-Drying of Carrot Slices
Author	Mr. Narathip Sujinda
Degree	Doctor of Engineering in Food Engineering
Advisory Committee Chairperson	Associate Professor Dr. Jaturapatr Varith

ABSTRACT

Microwave freeze-drying (MFD) is the process that applies the microwave as the heating source to freeze-dry the food product. It is a complex process due to the combination of microwave power, vacuum pressure, drying time, material temperature, and moisture content that affects the drying rate, product quality, and energy consumption. The proper control of MFD process conditions to achieve the optimum drying performance and quality of products is a challenge for researcher. Therefore, the objective of this research was to design the MFD process strategy called dynamic microwave logic control (DMLC) and integrated it into the closed-loop control (CLC) system for improving the MFD performance.

In the first part of this research, the uncertainty of the measurement system and moisture content calculation were evaluated following the Guide to the expression of uncertainty in measurement or GUM (ISO, 2008) to verify the accuracy of the measurement systems and the calculation of the moisture content. The results show that the uncertainty of temperature measurement is $\pm 1.5^{\circ}\text{C}$ or 3.9% from a full-scale range of 30 – 50 $^{\circ}\text{C}$, the uncertainty of weight measurement is ± 0.347 grams or 0.8% from a full-scale range of 0 – 150 grams, and the uncertainty of real-time moisture content calculation is $\pm 1\%$ (wet basis). As the results, the measurement systems were acceptable for use in the CLC system with no affected in terms of process control and product quality which confirm by the same later results in repetition of each treatment in this research.

In the second part, the temperature variations during MFD of carrot slices

were studied by applying the closed-loop temperature (CLT) control system to control the carrot slice's temperature in the final stage of the MFD process. The MFD with CLT can improve the temperature control efficiency up to 60% compared to the MFD without CLT while providing the product quality similar to freeze-drying (FD). Therefore, the CLT was applied with the MFD process for developing the CLC system in the final part of this research.

In the final part, the CLC system was developed to improve the MFD process and to examine the effects of a DMLC on the drying characteristics of MFD. The development consists of two sections. In the first section, the MFD process was examined to obtain the strategy for drying the carrot slices using microwave powers of 100 W, 200 W, and 300 W, with a temperature profile of the sample from -15°C to 40°C , and the final moisture content of 6% (wet basis). The DMLC was strategically developed in the second section based on a drying-phase configuration and dynamic control between the microwave power and real-time moisture content sensing to provide feedback to the CLC system. After developed the DMLC, it was integrated into the CLC system.

The results showed that by applying the DMLC into the control logic, the CLC could work properly in the MFD process by shortening the drying time by 62.4% and 23.4% compared with those of FD and MFD with no DMLC, respectively. The MFD-DMLC provided the final product with a quality equivalent to that of the FD process but achieved 44.3% better SMER. The findings from this research suggested that the DMLC based on the moisture content and temperature of the samples could be combined with the MFD process to enhance its efficiency while maintaining the superior quality of the FD process.

Keywords : Microwave freeze-drying closed-loop control system dynamic
microwave logic control drying characteristics carrot slices

ACKNOWLEDGEMENTS

Pursuing this Ph.D. degree has been a truly life-changing experience for me, and it would not have been possible without the support and guidance I received from my advisors, lab mates, friends, and family.

Firstly, I would like to express my sincere gratitude to Associate Professor Dr. Jaturapatr Varith for his continued support throughout the course of my Ph.D. study. His patience, motivation, immense knowledge, and advice helped me tremendously as I conducted researches and wrote this dissertation. I could not have imagined having a better advisor and mentor during my Ph.D. study. His endless guidance will not be forgotten throughout my life.

Apart from Dr. Varith, I would also like to express gratitude to Professor Dr. Rosnah Shamsudin and Associate Professor Dr. Somkiat Jaturonlumlert for providing encouragement and sharing insightful suggestions.

I would like to thank my fellow lab mates for their suggestions, assistance, and friendship. I would also like to thank my friends from Universiti Putra Malaysia for their help when I stayed in Malaysia.

Last but not least, I am grateful to my parents, siblings, friends, and other acquaintances who gave me the moral support, encouragement, and motivation needed to accomplish my personal goals.

Narathip Sujinda

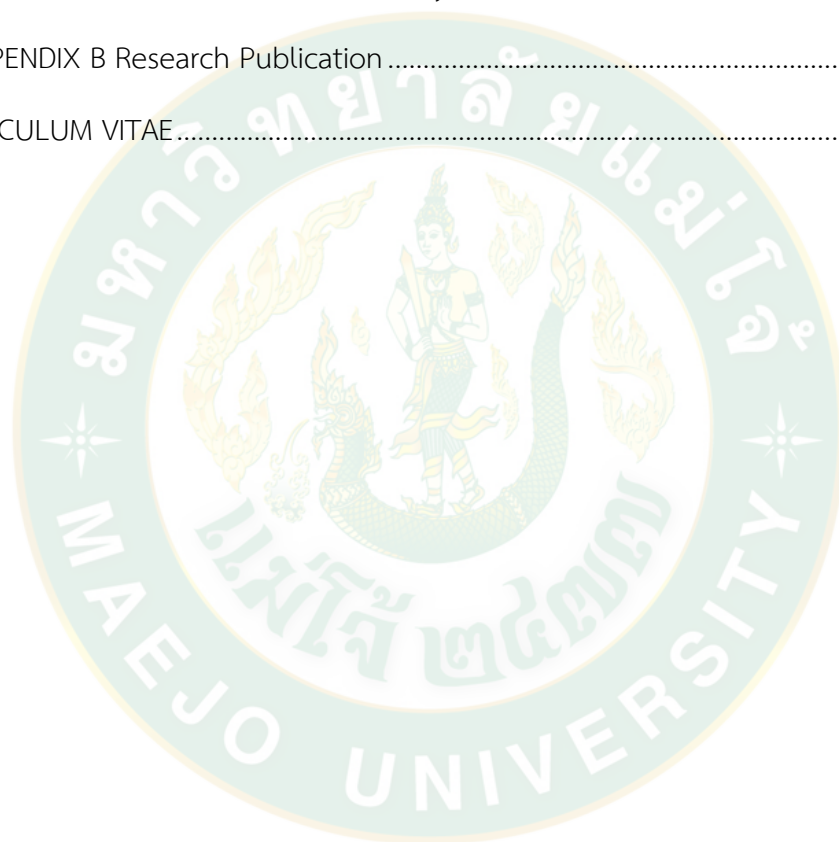
TABLE OF CONTENTS

	Page
ABSTRACT (THAI).....	C
ABSTRACT (ENGLISH).....	D
ACKNOWLEDGEMENTS.....	F
TABLE OF CONTENTS.....	G
CONTENT OF FIGURES.....	M
CONTENT OF TABLES.....	P
LIST OF SYMBOLS.....	Q
CHAPTER 1 INTRODUCTION.....	1
1.1 Significance of research.....	1
1.2 Objective of research.....	4
1.3 Scope of research.....	4
CHAPTER 2 THEORY AND LITERATURE REVIEW.....	5
2.1 Principles and Theory.....	5
2.1.1 Freeze drying.....	5
2.1.2 Microwave energy.....	9
2.1.3 Microwave freeze-drying.....	17
2.1.4 Drying kinetics.....	20
2.1.5 Closed-loop control system.....	28
2.1.6 Uncertainty of measurement.....	33
2.2 Literature review.....	44
2.2.1 Microwave freeze-drying characteristics and effect on product quality ...	44

2.2.2 Microwave freeze-drying with microwave dynamic loading scheme.....	51
2.2.3 Microwave freeze-drying kinetics.....	55
2.3 Summary of literature review.....	58
CHAPTER 3 RESEARCH METHODOLOGY.....	60
3.1 Sample preparation.....	61
3.2 Design of microwave freeze dryer.....	62
3.3 Hardware design for closed-loop control system.....	64
3.4 Part 0: Uncertainty of the measurement system.....	66
3.4.1 Uncertainty of temperature measurement.....	66
3.4.2 Uncertainty of weight measurement.....	70
3.4.3 Uncertainty of moisture content calculation.....	74
3.5 Part I: Variation of temperature during microwave-freeze drying process experiment.....	75
3.5.1 Experimental procedure.....	75
3.6 Part II: Development of closed-loop control system for microwave freeze- drying.....	76
3.6.1 Logic design of a closed-loop control system.....	76
3.6.2 Microwave freeze-drying experiment.....	79
3.6.3 Microwave freeze-drying characterization.....	80
3.6.4 Estimation of moisture diffusivity.....	81
3.7 Qualitative and statistical analysis.....	82
3.7.1 Color analysis.....	82
3.7.2 Texture analysis.....	82
3.7.3 Rehydration ratio.....	83

3.7.4 Shrinkage ratio	83
3.7.5 Energy consumption	83
3.7.6 Specific moisture extraction rate.....	84
3.7.7 Statistical analysis	84
CHAPTER 4 RESULTS AND DISCUSSION.....	85
4.1 Equipment setup for Microwave freeze dryer	85
4.2 Part 0: Uncertainty of the measurement system and moisture content calculation.....	92
4.2.1 Uncertainty of temperature measurement.....	92
4.2.2 Uncertainty of weight measurement.....	93
4.2.3 Uncertainty of moisture content calculation.....	94
4.3 Part I: Variation of temperature during microwave freeze-drying process.....	95
4.3.1 Effect of temperature variation during microwave freeze-drying process	95
4.3.2 Control of temperature variation in microwave freeze-drying with closed- loop temperature control system process	98
4.3.3 Improvement of closed-loop temperature control system	100
4.3.4 Quality of products and energy consumption.....	101
4.4 Part II: Development of closed-loop control system for microwave freeze- drying.....	104
4.4.1 MFD drying characteristics and kinetics.....	104
4.4.2 Moisture diffusivity (D)	108
4.4.2 Strategic development of dynamic microwave logic control (DMLC)	111
4.4.3 Product quality and energy consumption.....	118
4.5 Discussion.....	122
4.6 Novelty of this research.....	125

CHAPTER 5 CONCLUSIONS.....	126
5.1 Conclusions	126
5.2 Recommendations	127
REFERENCES	128
APPENDIX.....	141
APPENDIX A Results of statistical analysis	142
APPENDIX B Research Publication	154
CURRICULUM VITAE.....	157



CONTENT OF FIGURES

Figure 1 Cycle of FD process.....	6
Figure 2 Schematic diagram of a typical FD system.....	8
Figure 3 A typical magnetrons	11
Figure 4 A cut section of magnetron	12
Figure 5 MW applicator.....	15
Figure 6 The oscillating electric field causes the water molecules to oscillate up and down	16
Figure 7 Schematic diagram of a MFD system.....	19
Figure 8 A typical drying curve showing initial drying rate, constant rate and falling rate periods.....	21
Figure 9 Process to be controlled.....	28
Figure 10 Open-loop control system (without feedback).....	28
Figure 11 CLC system (with feedback)	29
Figure 12 Closed-loop temperature control system of the hot-air oven.....	30
Figure 13 The control system design process	31
Figure 14 Flowchart of summary for evaluating uncertainty of measurement.....	34
Figure 15 Rectangular distribution.....	38
Figure 16 Triangular distribution.	39
Figure 17 Gaussian distribution.	39
Figure 18 Conceptual overview of CLC system for MFD.	59
Figure 19 Research diagram and framework.....	60
Figure 20 Fresh carrots slices.....	61
Figure 21 3D model of laboratory-scale microwave freeze dryer.....	62

Figure 22 Schematic diagram of laboratory-scale microwave freeze dryer.	63
Figure 23 The schematic diagram of the CLC system hardware.	65
Figure 24 Temperature measurement equipment setup.....	68
Figure 25 Weight measurement equipment setup.....	71
Figure 26 A closed-loop control system diagram.....	78
Figure 27 Laboratory-scale microwave freeze dryer setup.....	85
Figure 28 Microwave freeze-drying chamber.	86
Figure 29 Microwave generation system.....	87
Figure 30 Installation of the load-cell, tray, and the rotating motor.....	88
Figure 31 A control system hardware.....	89
Figure 32 User interface of CLC system software.	90
Figure 33 A software processing diagram.....	91
Figure 34 Moisture content and temperature of carrot slices from MFD process.....	96
Figure 35 Moisture content and temperature of carrot slices from MFD process with CLT.....	97
Figure 36 Moisture content and temperature of carrot slices from FD process.	97
Figure 37 Temperature profile of carrot slices in MFD with CLT compared to MFD without CLT at 100W microwave power.	99
Figure 38 Carrot slices temperature controlled by CLT with and without on/off cycle.	101
Figure 39 Dried carrot slices from different drying methods.....	103
Figure 40 Moisture content (MC) and temperature profiles (Temp.) of carrot slices in MFD under various microwave power settings.....	105
Figure 41 The apparent moisture diffusivity (D_{APP}) of carrot during MFD process at different microwave power levels.	109

Figure 42 Flow process diagram of dynamic microwave logic control for microwave freeze drying of carrot slices. 113

Figure 43 Temperature and moisture content profiles of carrot slices during the MFD-DMLC. 115

Figure 44 Drying rate profiles of carrot slices during the MFD process. 117

Figure 45 Carrot slices dried a various microwave power levels compared with FD: 120



CONTENT OF TABLES

Table 1 Major regions of electromagnetic spectra.....	10
Table 2 The Moisture diffusivity of fruits and vegetables.....	23
Table 3 Thin-layer models for the drying of fruits and vegetables.	27
Table 4 The t-distribution table.	43
Table 5 Mathematical models used for fitting the experimental data.....	80
Table 6 Uncertainty budget table for the uncertainty of temperature measurement calculation.....	92
Table 7 Uncertainty budget table for uncertainty of weight measurement calculation.	93
Table 8 Product quality and energy consumption obtained from different drying methods.	102
Table 9 Statistical analysis of the drying kinetic models at different microwave power.	106
Table 10 The drying rate constant and coefficients for drying curves fitting of the carrot slices from Midilli et al. model.	108
Table 11 Regression coefficient and r^2 of apparent moisture diffusivity during the MFD.....	110
Table 12 The average moisture diffusivity for different microwave power levels. ...	111
Table 13 The average moisture diffusivity and drying rate constant of MFD-DMLC.	117
Table 14 The quality of carrot slices under different MFD and FD drying conditions.	119
Table 15 Energy consumption, specific moisture extraction rate, and total drying time of FD and MFD processes.....	122

LIST OF SYMBOLS

A_1	the coefficient of regression equation
a	the equation constants
B_1	the coefficient of regression equation
b	the equation constants
C_1	the coefficient of regression equation
c	the equation constants
D	the moisture diffusivity (m^2/s)
D_1	the coefficient of regression equation
D_{APP}	the apparent moisture diffusivity (m^2/s)
D_{AVG}	the average moisture diffusivity (m^2/s)
d	the equation constants
d_i	the diameter of the fresh carrot slices (m)
d_f	the diameter of the dried carrot slices (m)
F_0	the Fourier number
f	the functional relationship
h^*	the half thickness of slab (m)
k	the drying rate constant (min^{-1})
k_c	the coverage factor
L	the thickness of the carrot slices (m)
M	the moisture content (% wet basis)
M_e	the equilibrium moisture content (% wet basis)
M_f	the final moisture content (% wet basis)
M_i	the initial moisture content (% wet basis)
M_t	the initial moisture content at time t (% wet basis)
M_r	the real-time moisture content (% wet basis)
MR	the moisture ratio
$MR_{exp,i}$	the initial experimental moisture ratio
$MR_{pre,i}$	the initial prediction moisture ratio

N	the number of input quantity
n	the equation constants
n_t	the number of terms (a positive integer)
q	the expected value of a quantity
\bar{q}	the arithmetic mean
R	the equivalent radius
r	the cylinder radius
r^2	the corresponding values of coefficients of determination
$s(q_s)$	The experimental standard deviation
T_{air}	the air temperature (°C)
T_f	the final state temperature (°C)
T_h	the holding value of temperature (°C)
T_m	the pre-set values for the material temperature (°C)
T_r	the real-time material temperature (°C)
T_{rd}	the temperature reading of the OFT (°C)
T_x	the temperature measurement of the OFT
t	time (s)
t_p	the t-factor from the t-distribution table
U_{MC}	The uncertainty of real-time moisture content calculation (% wet basis)
U_T	the uncertainty of the temperature measurement (°C)
$U_{W,in}$	the uncertainty of the initial weight measurement (grams)
$U_{W,r}$	the uncertainty of the real-time weight measurement (grams)
U_y	the uncertainty of the measurement result
$u_{T,x}$	the combined standard uncertainty of the temperature measurement (°C)
$u_{T,rd}$	the standard uncertainty of the temperature reading (°C)
$u_{cb,t}$	the uncertainty of OFT base on its calibration data (°C)
$u_{cb,w}$	the uncertainty of load-cell base on its calibration data (grams)
$u_{rot,es}$	the estimated uncertainty of the load-cell due to the effect of the rotation tray (grams)

$u_{vc,es}$	the estimated uncertainty of OFT due to the effect of the vacuum pressure (°C)
$u_{W,rd}$	the standard uncertainty of the weight reading (grams)
$u_{W,x}$	the combined standard uncertainty of the weight measurement (grams)
$u_{x,i}$	the Type A standard uncertainty
u_y	the combined standard uncertainty
$u_{\Delta T,cert}$	the standard uncertainty of the OFT base on its calibration data correction (°C)
$u_{\Delta T,res}$	the standard uncertainty of the OFT resolution correction (°C)
$u_{\Delta T,vc}$	the standard uncertainty of OFT due to the effect of the vacuum pressure (°C)
$u_{\Delta W,cb}$	the standard uncertainty of the load-cell base on its calibration data (grams)
$u_{\Delta W,res}$	the standard uncertainty of the load-cell resolution (grams)
$u_{\Delta W,rot}$	the standard uncertainty of load-cell due to the effect of the rotation tray (grams)
$u_{\Delta W,vc}$	the standard uncertainty of load-cell due to the effect of the vacuum pressure (grams)
ν_{eff}	the effective degrees of freedom
ν_i	the degrees of freedom
$\nu_{T,eff}$	the effective degrees of freedom of the combined standard uncertainty of the temperature measurement
$\nu_{T,cb}$	the degrees of freedom of the standard uncertainty of the OFT base on its calibration data
$\nu_{T,rd}$	the degrees of freedom of the standard uncertainty of the temperature reading
$\nu_{T,res}$	the degrees of freedom of the standard uncertainty of the OFT resolution correction
$\nu_{T,vc}$	the degrees of freedom of the standard uncertainty of OFT due to the effect of the vacuum pressure

$\nu_{w,eff}$	the effective degrees of freedom of the combined standard uncertainty of the weight measurement
$\nu_{W,cb}$	the degrees of freedom of the standard uncertainty of the load-cell base on its calibration data
$\nu_{W,rd}$	the degrees of freedom of the standard uncertainty of the weight reading
$\nu_{W,res}$	the degrees of freedom of the standard uncertainty of the load-cell resolution
$\nu_{W,rot}$	the degrees of freedom of the standard uncertainty of load-cell due to the effect of the rotation tray
$\nu_{W,vc}$	the degrees of freedom of the standard uncertainty of load-cell due to the effect of the vacuum pressure
W_{in}	the initial materials weight (grams)
W_r	the real-time materials weight (grams)
W_{rd}	the weight reading of the load-cell (grams)
W_x	the weight measurement
X^2	the chi-square
X_N	the input quantity
x_N	the estimated input quantity
Y	the output of measured quantity
y	the measurement result
ΔT_{cb}	the temperature correction of the OFT reading based on its calibration data (°C)
ΔT_{res}	the temperature correction due to the resolution of the OFT (°C)
ΔT_{vc}	the temperature correction of the OFT due to the vacuum pressure (°C)
ΔW_{cb}	the weight correction of the load-cell based on its calibration data (grams)
ΔW_{res}	the weight correction due to the resolution of the load-cell (grams)
ΔW_{rot}	the weight correction of the load-cell due to the effect of rotation tray (grams)

ΔW_{vc} the weight correction of the load-cell due to the effect of the vacuum pressure (grams)

Acronyms

ANOVA	the analysis of variance
CLC	closed loop control system
CLT	closed loop temperature control system
DMLC	dynamic microwave logic control
EC	energy consumption
FD	freeze drying
MFD	microwave freeze-drying
OFT	optic fiber temperature sensor
OPC	open loop control system
RMSE	root mean square error
SMER	specific moisture extraction rate
SSE	sum of squared error
TDT	total drying time
USB	universal serial bus



CHAPTER 1

INTRODUCTION

1.1 Significance of research

Freeze-drying (FD) has been suggested as a way for the storage of fruits and vegetables in the food industries. This method is considered the most appropriate for retaining the organoleptic and nutritional properties compared to other typical drying methods. Nonetheless, the disadvantage of FD is the time-consuming drying period that utilizes much energy. It has a high operation cost and high energy consumption, resulting from the inadequate heat supply operated through a heated plate from the exterior to the interior of the material being dried (Cao et al., 2018b; Wu et al., 2020). Hence, decreases in the drying period and energy usage, and retaining the product's quality are significant concerns that need to be resolved.

Microwave freeze-drying (MFD) is a drying process that applies microwave energy as a heating source to the FD process (Duan et al., 2010a). Thus, microwave energy offers an alternative heat source to reduce the drying period and energy usage (Cao et al., 2018a; Huang et al., 2009) while considerably increases the drying rate (Ozcelik et al., 2019) due to rapid heating in materials through the use of microwave energy. The heat generation by microwave energy in the materials involves two mechanisms: ionic polarization and dipole rotation. These mechanisms occur simultaneously, as the electrical oscillation induces the ions to align the ions within the electromagnetic field. The electromagnetic energy in this process is converted to kinetic energy and absorbed in all parts of the material (Song et al., 2018; Varith et al., 2007), which is influenced by the dielectric properties of the food materials. For this reason, the MFD process can reduce the drying time by half (Duan et al., 2010b; Wang et al., 2010a) and up to 30% of the energy consumption while obtaining a product quality similar to FD (Jiang et al., 2013). Thus, MFD is an effective drying method that could solve the weakness of traditional FD. Moreover, microwave heating can eliminate microorganisms as well (Duan et al., 2007a)

In the MFD process, the complex parameters among the microwave power levels, moisture content, material temperature, and vacuum pressure affect the drying rate, product quality, and energy consumption. The higher microwave power could reduce the drying time and increase the drying rate by more than the lower power, but the higher microwave power could also result in low product quality (Ambros et al., 2018; Duan et al., 2007a; Wang et al., 2009). Additionally, the relationship between the microwave power levels, moisture content, and vacuum pressure level would need to be considered for the designing of the MFD process. This was because the possibility of corona discharging during the process could consume excessive microwave energy, burn the drying material, and damage the magnetrons (Duan et al., 2010b). Thus, it would be necessary to set the vacuum pressure to a range of 50 - 100 Pa to ensure that plasma discharge would not occur during the MFD process (Duan et al., 2008b; Li et al., 2019; Ren et al., 2015; Wang et al., 2009). The relationship among the material temperature, microwave power level, and moisture content of the material is also essential. This would affect the efficiency of the MFD process and the product quality of the result (Duan et al., 2010b). Ren et al. (2015) reported using a step-down microwave power loading scheme with mushrooms to be microwave freeze-dried to enhance their quality. Besides, Liu et al., 2017 found that the MFD process with a dynamic microwave loading scheme increased the mushrooms' porosity and shortened the drying time. According to dielectric properties, a multistage microwave loading scheme was also reported by Duan et al., 2012 and Li et al., 2019. These were able to reduce the drying time and obtain a better quality of dried products.

Even though the multistage microwave loading schemes proposed by Liu et al. (2017) and Duan et al. (2012) were not reported as real-time process control, they have shown a potential to the MFD process achieve better product quality and drying efficiency. Furthermore, Sujinda et al. (2020) examined MFD using a closed-loop temperature control system that incorporated a multistage microwave loading scheme. The results showed some improvement in the MFD process, which was denoted in this work as a dynamic microwave logic control (DMLC). There were two main types of loop control in the MFD process: the open-loop and closed-loop

controls. The open-loop control system is a single communication format with no feedback to control the MFD process and relies upon the output of the process; for example, the on-off control of a magnetron with a fixed timing cycle in a household microwave oven. On the other hand, the closed-loop control (CLC) system is a process control with the feedback of the output, e.g., moisture content or temperature of the product, to modify the input; such as the power level of the microwave, so to achieve better efficiency in the drying process (Drof and Bishop, 2017; Mayr and Bryant, 1971)

To develop the condition of the MFD process and improve the efficiency of the CLC system, a study of the drying kinetics would be useful for understanding the MFD profiles and their characteristics and to optimize the MFD to maximize the quality of the products. The studies on MFD of cabbage by Duan et al. (2007) and MFD of onion slices by Abbasi and Azari, 2009 have proven that the findings from drying kinetics could be used as the basis for the optimization of the MFD process; such as increasing the microwave power in the first stage of MFD was able to increase the drying rate, and decreasing the microwave power in last stages of MFD was able to maintain the product quality. Moreover, moisture diffusivity was another index to indicate the efficiency of the MFD process. Past studies have also shown effective diffusivity in the MFD process due to the altered appearance of the drying material, e.g., porosity and shrinkage of the sample. Because of the excessive heat levels, while conducting MFD, the samples experienced a high internal vapor gradient that increased the pore formation and moisture diffusivity (Feng et al., 2001; Narjes et al., 2018; Sharma and Prasad, 2001; Wang et al., 2007a). Thus, using drying kinetics and moisture diffusion were proposed to develop the CLC system, which was able to explain the phenomena of the MFD process in each stage. If the focus on the drying kinetics and moisture diffusion were intended to select appropriate drying conditions and control MFD processes, a better understanding of the drying rate would help develop a CLC system to enhance the MFD process.

Therefore, this research aimed to develop the logical design of the DMLC for the CLC-MFD. The study involved developing a MFD drying strategy that led to the design of the CLC system with the DMLC in the later part. As a food model, Carrot

slices were used in this work to evaluate the energy consumption and product quality to match that of the CLC-MFD. The researcher's goal was to enhance the efficiency of MFD and to improve the product quality when compared to that of the FD process.

1.2 Objective of research

1. To investigate the temperature variation during MFD of carrot slices using a closed-loop temperature control system (CLT) to improve temperature variations and study their effects on the product quality.
2. To develop a closed-loop control (CLC) system to improve the microwave freeze-drying (MFD) process and
3. To examine the effects of a dynamic microwave logic control (DMLC) on the drying characteristics of MFD.

1.3 Scope of research

This research involves designing a DMLC and developing a suitable CLC of microwave power levels in the range of 100 – 300 W at the frequency 2.45 GHz for the MFD process. The MFD process was examined to obtain the drying strategy on the carrot slices using microwave power of 100, 200, and 300 W with a temperature profile of the sample range from -15°C to 40°C. The material thickness was 10 mm, the diameter of about 35 mm, the material weight of 100 g, the constant vacuum pressure of 100 Pa, and a cold trap temperature of -40°C. The final moisture content of carrot slices for all MFD drying conditions and FD was 6% (wet basis). The DMLC was strategically developed based on the drying kinetics and drying characteristics of the MFD process. The drying time, color, texture, rehydration ratio, shrinkage, and energy consumption were compared with the FD to assess the performance of CLC-MFD.

CHAPTER 2

THEORY AND LITERATURE REVIEW

2.1 Principles and Theory

2.1.1 Freeze drying

Freeze-drying (FD) or lyophilization is how water is directly changed from a solid-state to a gaseous state to vapor through direct water transfer without passing through a liquid phase, then separates the layer of dry water (Franks and Auffret, 2008; Haseley and Oetjen, 2018; Mellor, 1978). In the food industry, it is established that it is a process to maintain the material's organoleptic and nutritional qualities. This is because the freezing of water in the substance eliminates the procedures related to chemistry, biochemistry, and microbiology before the FD process. However, there are no differences in the taste, smell, and content of various nutrients. Loads of water in raw food products are found, starting from 80% to 95%. The absorption of water by sublimation results in the development of the freeze-dried products' extremely porous structure; lyophilisate rehydration ensues instantly (Jia et al., 2019; Meda and Ratti, 2005). In some cases, water in the material possibly derives from free water or water bound to the matrix by different forces. Under the lyophilization mechanism, the emission of ice water and partially bound water emerges. Free water freezes, but there is no freezing of bound water. Lyophilization is an extraordinarily complex and multi-step procedure consisting of three phases of the FD process: freezing, primary drying, and secondary drying (Haseley and Oetjen, 2018; Lopez-Quiroga et al., 2012; Ratti, 2001). A FD process can be illustrated by the FD cycle, as shown in Figure 1.

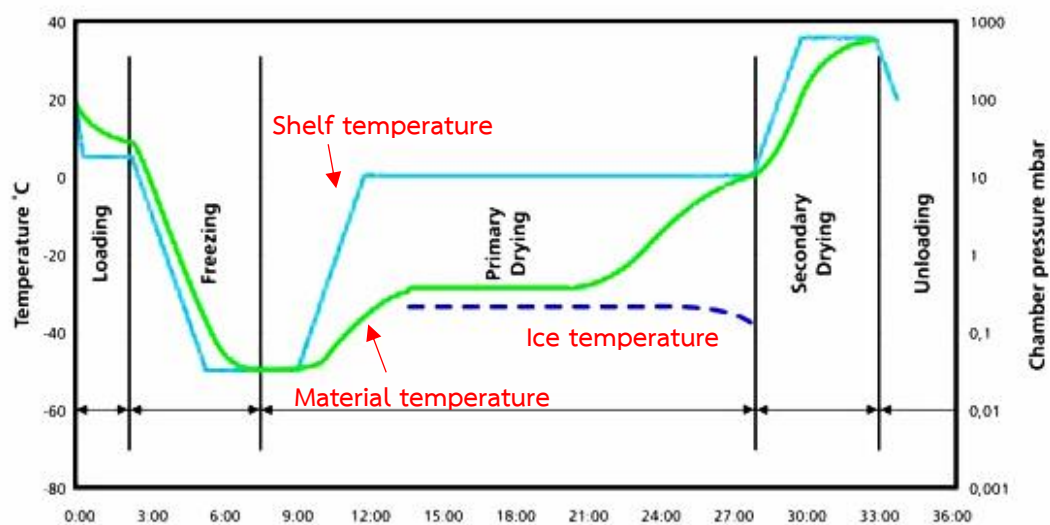


Figure 1 Cycle of FD process (adapted from Lopez-Quiroga et al., 2012).

From Figure 1, the water content of the material is converted into ice during the first stage of freezing. Freezing involves a rapid decrease of the sample's temperature, which controls the ice crystal size and growth, affecting the structure of the freeze-dried product. In the entire FD operation, the freezing step is the most important since, if incorrectly performed, the product may be ruined. It is quicker to freeze-dry large crystals. The substance can be gradually frozen to create larger crystals, but large ice crystals can weaken the pore structure when considering food products. Thus, to avoid the pore structure, the quick-freezing process should be adopted to offer the small size of the ice crystals. The final temperature of the freezing product must be below the eutectic point or collapse temperature to maintain the structural soundness.

The second stage, called the primary drying or sublimation stage, is the most extended FD cycle period. In this initial drying phase, about 95% of the water in the materials is sublimated under low vacuum pressure conditions. The power available as the heat must stay lower than the eutectic temperature of the product (the highest acceptable product temperature during the sublimation condition). Under the said procedure, the control of pressure is carried out with the partial use of vacuum. The sublimation is stimulated by vacuum pressure. In addition, the cold

condenser chamber or condenser plate will pay off steam along with the surface to re-solidify. This condenser does not play any part in preserving the frozen material. Instead, it prohibits the vacuum pump from touching water vapor, which could impair the efficiency of the pump. Usually, condenser temperatures are under -50°C . Nearly all the ice, free-water in solid form, is sublimated during this phase, which is a significant step for influencing the final product consistency. This adds to an integrated porous matrix that can subsequently be rehydrated very easily while maintaining the product's organoleptic and nutritional characteristics.

The final stage of FD is called the secondary drying or desorption phase. After the ice is melted in the principal drying process, secondary drying helps eliminate unfrozen water molecules. Under FD procedure, this part is controlled by adsorption isotherms of the substance. At this point, the temperature rises higher than in the prime drying process. It can also be higher than 0°C to sever any physicochemical associations between the water molecules and frozen product (bound water). At the completion of the process, the final residual water content in the dried product is around 1% to 4%, which is extremely low. At the completion of the FD process, the dried products were stored and sealed in the moisture-free package with offer oxygen absorber materials.

In addition to the FD process, which was previously mentioned, another important part of FD is the FD equipment. Including a cooling system, a vacuum system, a control system, a drying chamber, and a cold trap or condenser, a freeze-dryer consists of several simple components (Berk, 2018; Nail et al., 2002). The refrigeration system cools the condenser, typically positioned outside the drying chamber, as seen in Figure 2. Alternatively, it can comprise an internal scheme made of the chamber containing plates along the walls. The control system was used for temperature and pressure control and sensing. The vacuum mechanism operates as a separate vacuum pump linked to and fixed to the drying chamber by an airtight condenser. The rotary, oil-sealed configuration of the vacuum pumps for evacuating the system is normally able to maintain a system pressure lower than 10 Pa. A series of shelves/trays on which the stock is dried is used to mount the drying chambers. The food materials are distributed on the trays, and heat is delivered to the food

materials by radiation or conduction. The condenser draws the sublimated vapors from the product and converts them back into a solid form (ice).

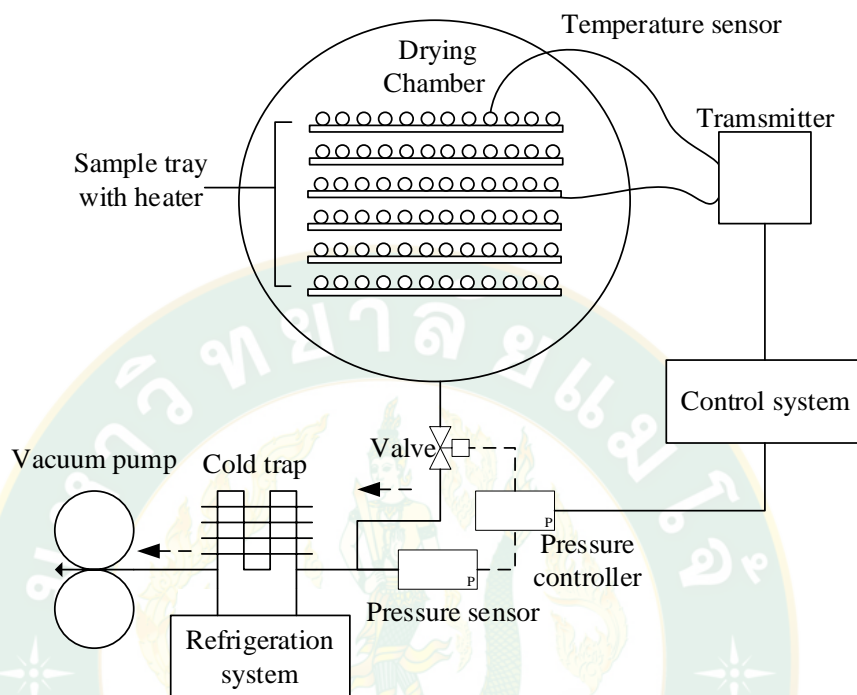


Figure 2 Schematic diagram of a typical FD system. (adapted from Nail et al., 2002)

The frozen products are arranged on a shelf, as indicated in Figure 2. After that, the dryer turns on the vacuum pump to push the air out of the drying chamber and reduced the pressure to 10 Pa or less in the drying chamber. Heating units add a small amount of heat to the racks, which allows the ice to shift. The ice transforms immediately into water vapor when the pressure is too low. The water vapor travels out of the drying chamber and through the cold trap. The water vapor concentrates in solid form on the coil inside the cold trap (ice). This lasts for a few hours as the content is eventually drying out. The method takes a long drying period because overheating the material will dramatically alter the composition and structure of the material. In addition, speeding the sublimation operation could create more water vapor than the pumping device would extract from the vacuum chamber. This could moisten and degrade the consistency of the material. If the substance has been

properly dried, it will maintain its shape, volume, original composition, and all its physical, chemical, and biological properties. Provided the commodity has been packaged in a moisture-free box and the package is safe, it can be kept for a nearly unlimited amount of time without deteriorating.

Compared to food items dehydrated by other processes, freeze-dried items exhibit superior consistency. As well as the low temperature of the procedure, the high consistency is because of the lack of a liquid phase. FD retains the taste, color, and appearance while mitigating heat-sensitive nutrient thermal impact. Furthermore, thanks to the solid-state phase, the texture is well maintained. Usually, freeze-dried goods are crisper and have four to six times the rehydration levels over traditional air-dried goods. Other main advantages of FD involve high volatile recovery, shape and surface area retention, high yield, long shelf life, and decreased weight for packaging, distribution, and supervision. Nevertheless, the FD procedure needs a longer drying time, often contributing to enhanced energy usage and high operating costs due to the low heat supply from the outside to the inside of the dried material via a heated layer (Cui et al., 2008; Wang et al., 2009). Consequently, reducing drying time and energy usage while retaining product consistency are serious challenges that should be tackled.

2.1.2 Microwave energy

Electromagnetic waves with wavelengths ranging from 1 GHz to 1000 GHz are microwaves. The higher frequency limit of microwaves surrounds the electromagnetic spectrum domains of infra-red and visible light, explaining why microwaves work more like light rays than typical radio waves do. Microwave wavelengths are analyzed quantitatively from radio waves due to this special property. As stated above, microwaves are electromagnetic waves; hence, to understand the properties of the microwave, we need to understand the electromagnetic spectra. Electromagnetic spectra can be defined as an arrangement of electromagnetic radiations in the order of their energy (which in turn is governed by their frequency or wavelength). The energy associated with each segment of the spectra is capable of producing a

characteristic effect on the molecules exposed to them. Table 1 depicts the major regions of electromagnetic spectra and their effects.

Table 1 Major regions of electromagnetic spectra.

Region	Wavelength (Angstroms)	Frequency (Hz)	Effects
Radio	1m–100km	$<3 \times 10^9$	Collective oscillation of charge carriers in bulk material (plasma oscillation)
Microwave	1mm–1m	3×10^9 – 3×10^{12}	Plasma oscillation, molecular rotation
Infrared	750nm–1mm	3×10^9 – 4.3×10^{14}	Molecular vibration, plasma oscillation
Visible	390nm–750nm	4.3×10^{14} – 7.5×10^{14}	Molecular electron excitation (including pigment molecules found in the human retina), plasma oscillations (in metals only)
Ultraviolet	10nm–400nm	7.5×10^{14} – 3×10^{17}	Excitation of molecular and atomic valence electrons, including ejection of the electrons.
X-rays	0.01nm–10nm	3×10^{17} – 3×10^{19}	Excitation and ejection of core atomic electrons, Compton scattering (for low atomic numbers)
Gamma rays	< 0.02 nm	$> 3 \times 10^{19}$	Creation of particle–antiparticle pairs. At very high energies a single photon can create a shower of high-energy particles and antiparticles upon interaction with matter.

At frequencies from approximately 300 MHz to 300 GHz, the microwave is electromagnetic radiation ranging from 1 mm to 1 m in duration. 915 MHz and 2.45 GHz are the primary microwave wavelengths used for commercial and household heating (Regier et al., 2016). Continuous-wave magnetrons effectively generate microwaves for household ovens and many commercial uses (Figure 3). The magnetron is a vacuum diode enclosed by a coaxial anode of the cathode (Love, 1995). From Figure 4a, anode consists of a certain number of vanes encompassing the cathode. The accessible regions between each of the vanes are modulated voids

that specify the magnetron's frequency. In polarity, alternating sections are opposite and are linked with conducting straps. The cathode passes through a high voltage direct current, heating the filament and releasing electrons. Electrons are repelled in a circular direction between the anode and cathode by a magnetic field created by permanent magnets outside the vacuum tube. Electrons form a cloud of spinning "spokes" as they pass across the cathode, hitting every other vane (Figure 4b). At microwave wavelengths, this generates an alternating current in the resonance gap. The radiofrequency energy is transmitted into a waveguide through an antenna placed in a deep void that emits the microwave into the oven chamber.

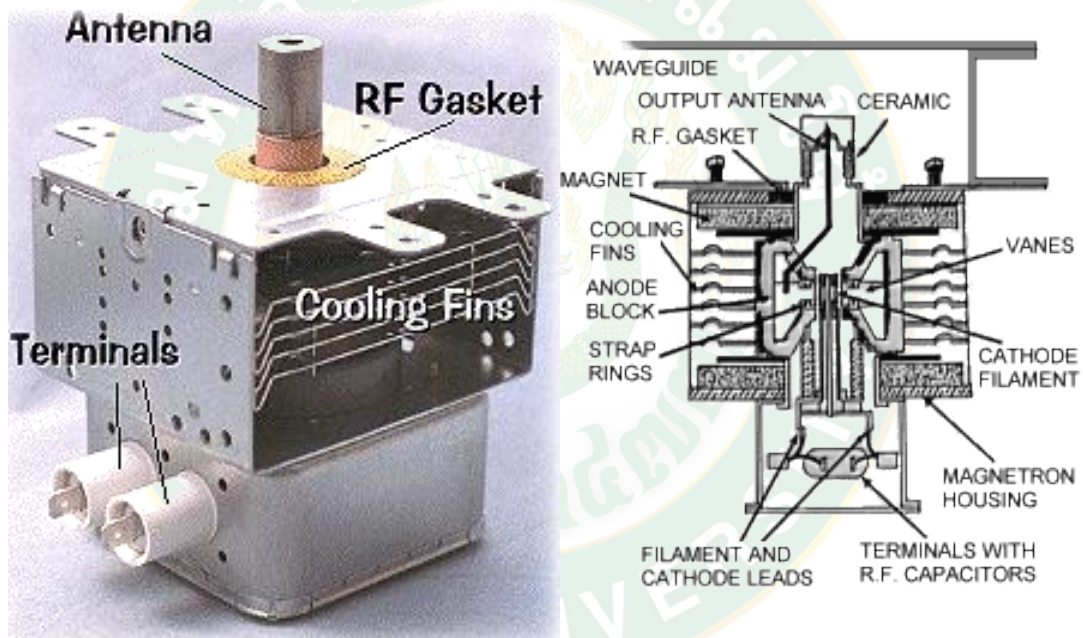


Figure 3 A typical magnetrons (Gallawa, 2000)

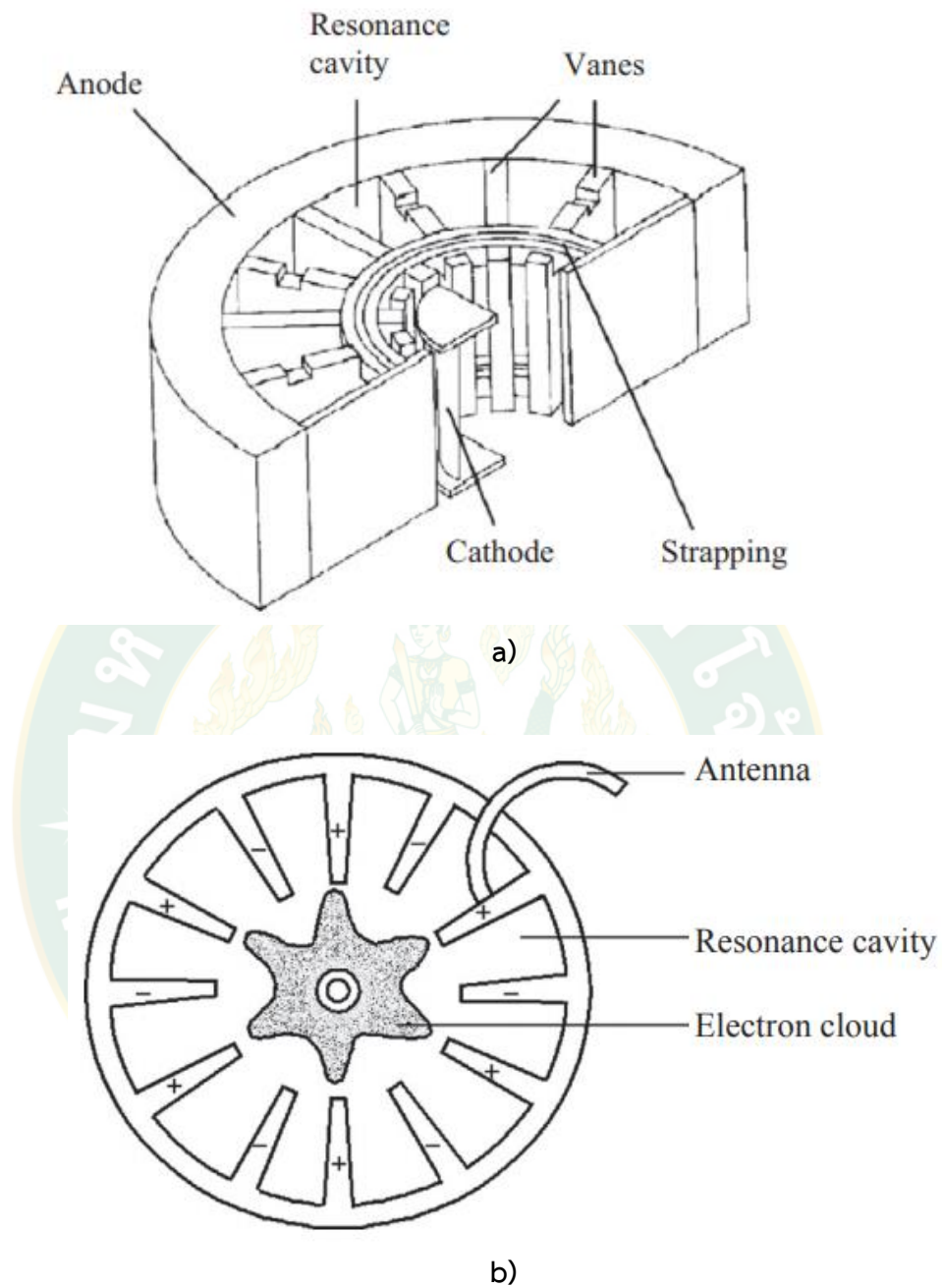


Figure 4 A cut section of magnetron (Scaman and Durance, 2005)

- a) Simplified diagram of a continuous wave magnetron.
- b) Cross-section of a magnetron.

The magnetron turns electricity into microwave energy. The microwave energy produced in the magnetron is directed to reach the microwave chamber via a

waveguide. To maximize microwave heating efficiency, the microwave chamber contains the sample to be heated and built with reflecting walls. In a traditional household microwave oven, a rectangular chamber representing a resonator enables the microwave applicator. The applicators widely used in microwave frameworks include single-mode applicators, multimode applicators, and moving wave devices. The validity of the practical operation, efficient power distribution, and low-cost systems are the basic requirements of a reliable microwave system.

1) Single-Mode Applicator

Only one mode of propagation is permitted within the single-mode chamber in a definite space with a particular volume. This function enables microwave energy to be effectively transmitted by the single-mode resonant chamber applicator. At fixed positions where the electrical field is strong, the material is positioned in a rectangular or cylindrical single-mode chamber. One waveguide, a tuning plunger, and a small microwave resonator have single-mode applicators (Figure 5a) with measurements in the spectrum of the microwave spectrum (Orsat et al., 2017). In TM_{10} mode, the simplest and most predominant single-mode chamber works and is practically the smallest. In the case of single-chamber applicators, the operational mode is that the target sample is stored in a position where the pitch strength is high. The restricted scale of the applicator is the main disadvantage because the material's diameter must be lower than half the wavelength of the incoming microwave. By rotating the tuning plunger in a rotational manner so that the time-average field is distributed over the material, this must be calibrated. Otherwise, a periodic heating sequence through the material will represent the periodicity of the unit.

2) Multimode Applicator

The multimode applicator is the most frequently utilized applicator (Figure 5b). Multimode applicators are used by about 50 percent of manufacturing systems. The concept is much like a domestic method but is meant for a greater amount to be handled. It is identical to a rectangular conductive metal box in which the substance

is located. Microwave energy is conveyed from the applicator to the chamber, passes through the waveguide, and sent through multiple reflections from the chamber walls. Inside the chamber and materials, there is an interaction between reflecting waves and the material within the chamber, resulting in the generation of an electric field distribution. As a result, a multimode applicator is produced, which induces stable electric field propagation processes at various points.

Field delivery in a multimode applicator is determined by the dielectric characteristics of the food materials, portion size, and position of the food materials inside the applicator. In food samples with a high dielectric loss factor, multimode applicators are ideal and take up greater areas of the applicator (> 50%) (Requena-Perez et al., 2005). The electric field is not equally dispersed for food substances with a lower loss factor and utilizing a small region of the applicator (<20%), contributing to uneven heat distribution. Inside the food sample, this will gradually produce hot-spots/cold-spots (Sumnu and Sahin, 2005). A constantly spinning turntable or mode stirrer (rotating reflector) must be built into the applicator to ensure consistent thermal performance (Fryer and Robbins, 2005). This helps to achieve an optimal and reliable application of the electric field within food products.

It is difficult to speculate the spatial distribution of the electric field within food materials because it is influenced by the dielectric properties of the food materials and their position and volume within the chamber. Therefore, in scaling up to the industrial level, the experimental results from a single research sample may not be relevant. Water is used as an experimental sample to map the field distribution inside the chamber. However, since the field distribution varies as a function of the fluid form inside the MW chamber due to the intrinsic dielectric characteristics of the material, the conversion to other liquids or materials generates distinct thermal performance.

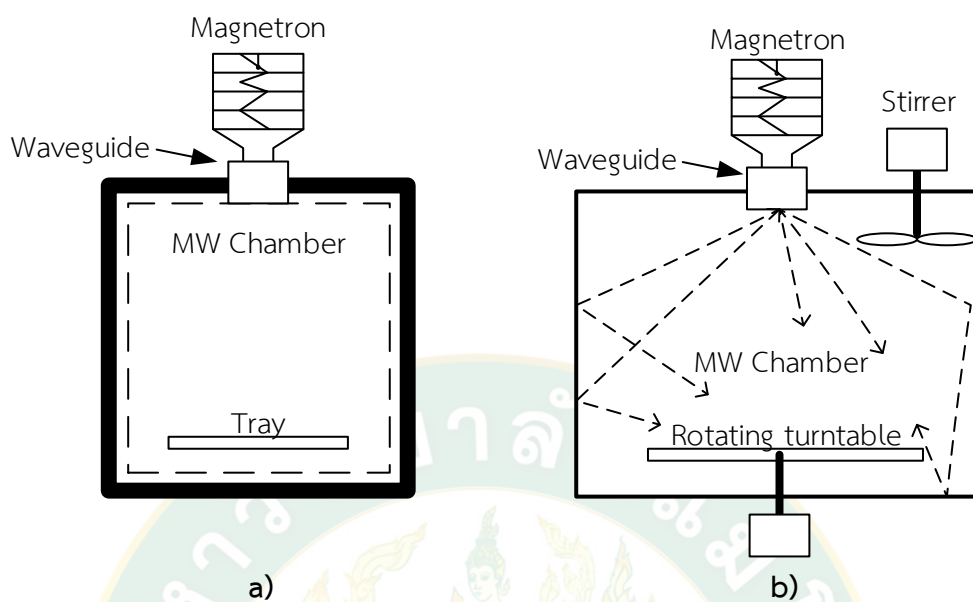


Figure 5 MW applicator (adapted from Mishra et al., 2015)

a) Single-mode

b) Multi-mode

Fundamentally, the microwave lacks heat. Instead, heating originates from the interface with two modes of motion with molecules, including dipolar rotation and ionic conduction (Figure 6). In dipolar rotation, a molecule continuously tilts back and forth, struggling to balance its dipole with an ever-oscillating electric field; heat generation derives from the friction between each spinning molecule. A free ion or ionic species travels conversationally through space in ionic conduction, seeking to coordinate with the shifting electric field. The resistance between these moving species leads to heat generation, as in dipolar rotation. The higher temperature in the reaction mixture results in more productive energy transfer. The more polar and/or ionic a species, the more powerful the rate of heat generation will be in both cases.

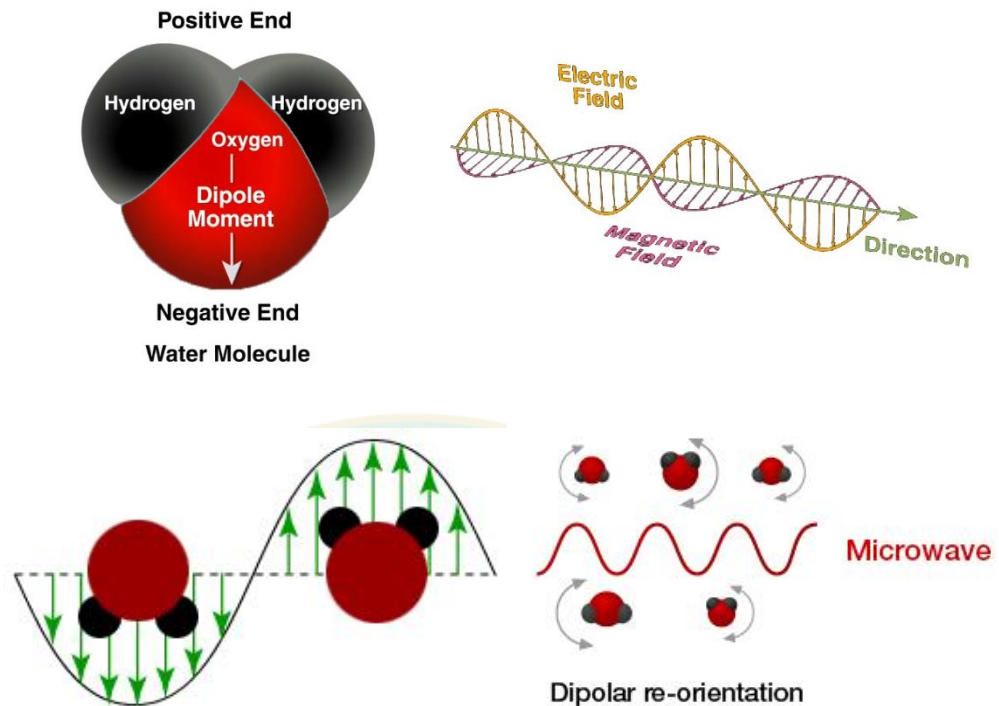


Figure 6 The oscillating electric field causes the water molecules to oscillate up and down (adapted from Hammack et al., 2012)

By way of conduction, the heat is transferred into the components. Water is also the critical element of a food material influenced by the microwave area due to its perpetual dipole and excess. Water's physical state has a significant impact on its reaction to microwave. In free water, water molecules form a hydrogen-bonded network with each other and can stabilize at microwave wavelengths. The relief time is the time necessary for a molecule to enter a dysfunctional state after eliminating the microwave field from which it was associated (Mudgett, 1985). Conversely, the dipole rotation of water bound to proteins or carbohydrates or water present as ice is impeded, limiting the level at which it eases to below the microwave range (Adams, 1981; Hasted, 1972; Kaatz, 1997). Water would also make a marginal contribution to MW heating in those conditions.

2.1.3 Microwave freeze-drying

As a delicate dehydration process for heat-sensitive food products, freeze-drying (FD) is used. It is established that, relative to other food drying processes, FD is the most effective method for removing water from heat-sensitive materials and producing high-quality dried goods. Even so, FD is an expensive and time-consuming dehydration process due to low drying rates, which result in relatively low throughputs and high capital and energy costs produced by vacuum and refrigeration equipment. Thus, reducing drying time and energy consumption while retaining the consistency of the commodity are serious challenges to address.

The usage of microwave energy as an energy supply for FD to minimize energy use and drying time is microwave freeze-drying (MFD) (Ambros et al., 2017; Cao et al., 2018a; Huang et al., 2009). Microwave energy is employed as the source of heat to provide the sublimation heat required in FD. Under vacuum conditions, it heats the substance volumetrically. For sublimation inside the food material, microwave energy is directly absorbed by water molecules without impacting the dry region. Therefore, the drying time and energy consumption in the sublimation and desorption process of the FD can be minimized.

The implementation of MFD can substantially shorten the FD process due to the following potential benefits: (1) automatic modification of the amount of microwave energy absorption by various moisture contents; (2) potential selective heating of the interior segments (microwave concentrating effect); (3) rapid dissipation of energy within the material; (4) more effective drying during the dropping rate cycle and overall energy savings (Duan et al., 2007b; Feng and Tang, 1998; Nijhuis et al., 1998; Torringa et al., 2001). Multiple studies have revealed that MFD is one of the most suitable approaches for speeding up the drying process and enhancing overall efficiency (Sochanski et al., 1990). For items of intermediate value, such as fruits and vegetables, this is incredibly beneficial. Several MFD-based laboratory experiments have shown that MFD offers a 50-60% improvement in drying time relative to FD approaches (Duan et al., 2008a; Duan et al., 2007a; Sochanski et al., 1990). In addition, tests and computational projections demonstrate that the cost of drying can be minimized when using MFD, while the efficiency of MFD products

does not vary from that of other FD methods for end products (Duan et al., 2010b; Jiang et al., 2010; Wu et al., 2004). However, concerning the initial asset value, MFD devices are obviously higher than those of the FD devices. However, they are balanced by more effective usage of the devices with an improved drying rate later.

As seen in Figure 7, a microwave freeze dryer is a traditional freeze dryer with the additional capacity to apply microwave to the drying chamber in basic terms (Duan et al., 2007a). The refrigeration system cools the condenser, which is usually located externally to the drying chamber. The control system was used for sensing the temperature and control the microwave power levels. The vacuum mechanism comprises a separate vacuum pump linked to and fixed to the drying chamber by an airtight condenser. A rotary, oil-sealed design for vacuum pumps is typically used to vacate the system. The whole MFD process proceeds under a vacuum environment in the range of 0.5 to 2.5 mbar (50 to 250 Pa) by sublimation. A vacuum pump maintained the vacuum pressure. The cold trap temperature is typically below -40°C to condense the vapor during the MFD process. This stops water vapor from accessing the vacuum pump, which could impair the pump operations. The frozen materials are spread on the rotating trays. The magnetron converts electric energy to microwave energy. Microwave energy generated in the magnetron is guided through a waveguide to arrive at the drying chamber. The materials absorbed microwave energy and converted to heat for the sublimation. In order to detect the temperature of the materials being dried, the surface temperature of materials can detect by the infrared temperature detection system and the core temperature of materials can monitor by using the optical fiber temperature sensor system (core temperature detection) which can be used in the electrical field.

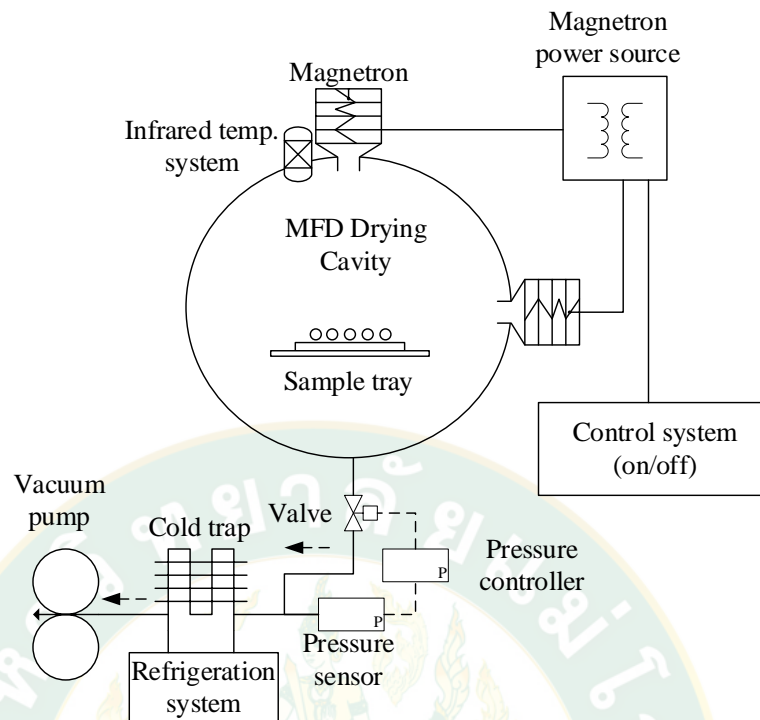


Figure 7 Schematic diagram of a MFD system. (adapted from Duan et al., 2007a)

Even though the MFD has many advantages and the equipment is simple, MFD is often challenging to use in commercial processes because of plasma discharge concerns. This occurs when there is a threshold value above the electric field amplitude in the vacuum chamber. The ionization of the remaining gases contained in the vacuum chamber results in a purple light emerging, allowing the surface of the substance to a flame. The presence of this condition causes significant losses of energy and unnecessary heating in the material's dry region, seriously harming the end product. The threshold of the electric field is usually a chamber pressure feature. In the pressure spectrum usually used in FD processes, it tends to have the lowest value. Therefore, it is important to monitor the process parameters (vacuum pressure and microwave power intensity) to prevent the occurrence of this phenomenon. The specification of a chamber with minimal localized electromagnetic field density is also essential.

The electric field strength is equal to the voltage that the microwave generator applies in a vacuum chamber. The power of the microwave reactor should be

regulated below the predefined threshold in order to prevent plasma leakage. As the electric field has a transition time after the generator is switched on before it hits a stable, steady-state, variable power levels should be used during this period to prevent the risk of arcing. The microwave function with the cyclic pressure technique was equal to a power-directly operated unit, as per (Lombraña et al., 2001). As an appropriate power management process, a microwave on/off cycled solution with simultaneous up/down pressure adjustment was identified. Chamber pressure is a useful control parameter in this situation to prevent plasma discharge and eventual melting of the product.

In general, MFD has a complex function among microwave power levels, moisture content, materials temperature, and vacuum pressure levels that affect the drying rate, product quality, and energy consumption. The relationship between microwave power levels, moisture content, and vacuum pressure levels needs to be considered because the possibility of corona discharging during the process, which consumes excessive microwave energy, and the plasma can also lead to material being burnt and can damage the magnetrons as well (Duan et al., 2010b). Therefore, if the MFD conditions are controlled properly, it can simultaneously improve the MFD performance and quality of products.

2.1.4 Drying kinetics

Drying kinetics indicates variations in the total moisture content of the substrate and temperature over time. They are used to calculate the quantity of moisture evaporated, the drying period, energy use, and the consistency of the substance. The shift in the content and temperature of material moisture is generally regulated by heat and mass transfer between the solid surface, the atmosphere, and the interior of the drying material. The drying process is represented through graphical form based on the material moisture content and drying duration (drying curve), the drying rate and drying time (drying rate curve), and the material temperature and drying time (temperature curve) As seen in Figure 8, the system can also be expressed by exchanging the drying time with the moisture ratio for related curves.

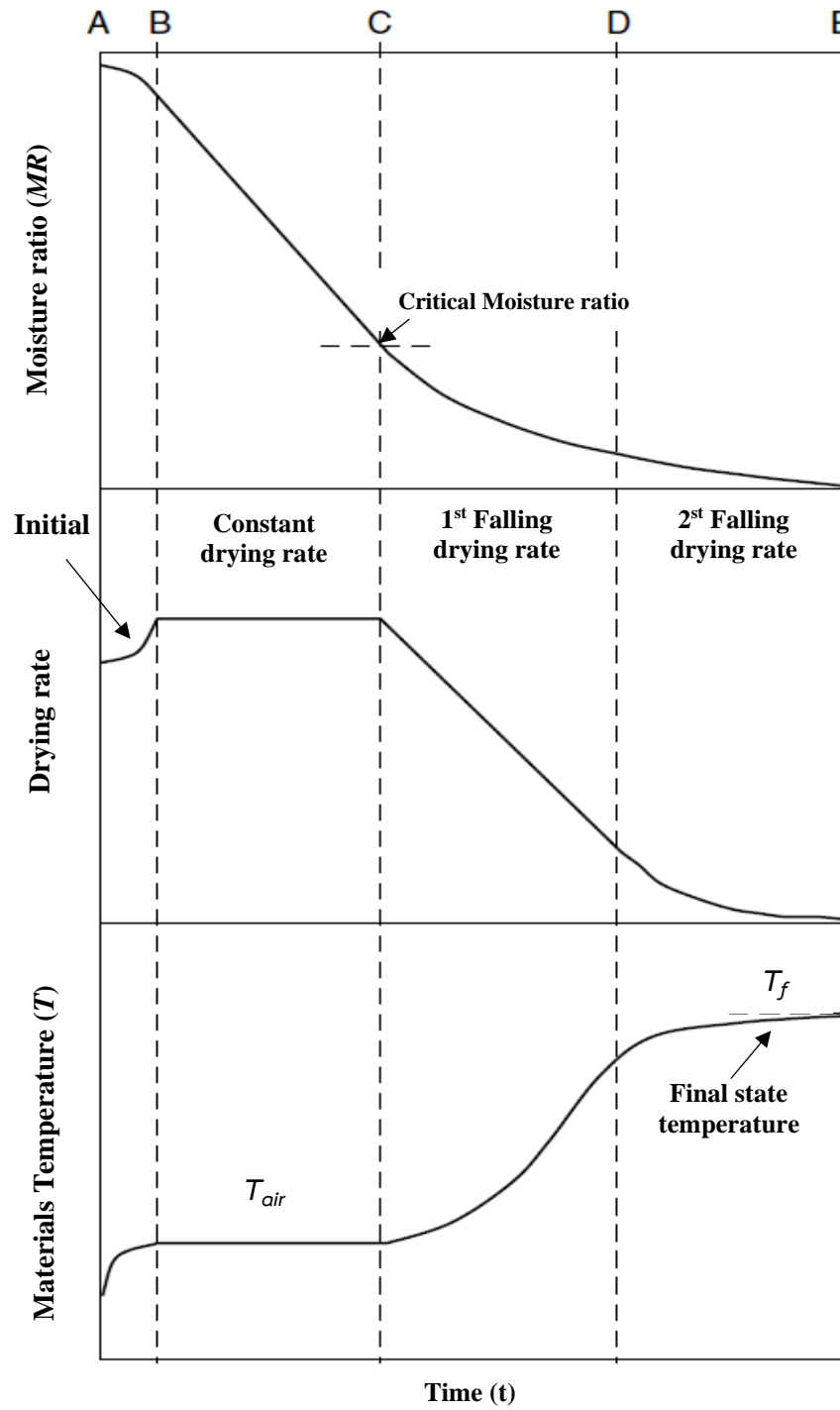


Figure 8 A typical drying curve showing initial drying rate, constant rate and falling rate periods. (adapted from Carrin and Crapiste 2008).

The drying rate and temperature as a function of time are defined in Figure 8. This rating curve may be used to define the prevailing process of the commodity while drying. Drying may be separated into three phases: the initial drying time, the constant rate phase, and the declining rate stage. An initial drying cycle (points A to B) occurs, while heat and mass transfer mechanisms between the substance and the ambient atmosphere reach an immediate stable level. Air temperature (T_{air}) is typically higher than the product's temperature in the initial drying period (Carrin and Crapiste, 2008). Thus, the drying rate between the preliminary drying cycle surges with an increase in the temperature of the commodity until the surface temperature is balanced (Corresponding to line B to C). The initial drying period duration is typically very brief and can be ignored in implementation.

The first cycle of the dropping drying rate (points C to D) starts when the moisture ratio has achieved the significance level. The pivotal factor of moisture relies strongly on the characteristics of the material and the environmental conditions. High drying rates will increase the critical point, and low drying rates will reduce the critical point (Okos et al., 1992). At this stage, the relative humidity on the drying surface tends to decline steadily. As a consequence, the vapor pressure above the material surface decreases, slowing the drying process. Based on the drying conditions and material parameters, internal and external resistance may be important. The water moves to the surface through capillary motion at the beginning of the lowering period (point C in Figure 8). As the drying process progresses, nonetheless, the water surface layer begins to recede. Assume that the water is continuously removed and replaced by air. In that case, a point is reached where there is not enough water remaining to hold consistent films through the pores, and the rate of drying unexpectedly declines, beginning with the second cycle of the dropping rate (point D to E). As a result, water vapor diffusion in the pores can become the controlling mode of mass transfer.

In fine porous solids, the drying rate curve in the next falling rate cycle will comply with the Diffusion Act, and the curve is contoured upwards. For rather porous solids with large pores, the drying rate curve is often straight at this time, and no diffusion algorithms are used. The flow of water during the decreasing period in

the drying of many food products was defined by the diffusion theory. Moisture diffusivity is usually lower than during the first falling process. However, the temperature rises to the final temperature (T_f) since the diffusion of the vapor is the dominant factor at this point.

1) Moisture diffusivity model

The diffusivity of the moisture, which is a utility of the temperature and moisture content of the matter, is an efficient delivery factor in the simulation of the fruit and vegetable drying process. The Fick Second Diffusion Law equation details the mass and heat transfer equation for the processing of fruits and vegetables as seen in the equation given:

$$\frac{dM}{dt} = D\nabla^2 M \quad \text{Eq. (1)}$$

Table 2 shows the most extensively used geometries for drying fruits and vegetables, including slab, infinite slab, sphere, and cylinder.

Table 2 The Moisture diffusivity of fruits and vegetables.

Product	Geometry	D (m ² /s)	Reference
Banana slices	Infinite slab	4.89×10 ⁻¹⁰ to 1.69×10 ⁻⁹	(Omolola et al., 2014)
Basil leaves	Slap	2.65×10 ⁻¹⁰ to 5.69×10 ⁻¹⁰	(Kadam et al., 2011)
Carrot (pomace)	Slap	2.74×10 ⁻⁹ to 4.64×10 ⁻⁹	(Kumar et al., 2012)
Green peas	Sphere	3.95×10 ⁻¹⁰ to 6.23×10 ⁻¹⁰	(Pardeshi et al., 2009)
Green bean	Slap	2.64×10 ⁻⁹ to 5.71×10 ⁻⁹	(Doymaz, 2005)
Kiwifruit	Infinite slab	3.0×10 ⁻¹⁰ to 17.2×10 ⁻¹⁰	(Simal et al., 2005)
Mango slices	Infinite slab	4.97×10 ⁻¹⁰ to 10.83×10 ⁻¹⁰	(Akoy, 2014)
Parsley	Infinite slab	6.44×10 ⁻¹²	(Akpınar, 2006b)
Plum	Sphere	1.02×10 ⁻⁸ to 5.47×10 ⁻⁹	(Jazini and Hatamipour, 2010)
Pumpkin	Cylinder	4.08×10 ⁻⁸ to 2.35×10 ⁻⁷	(Guiné et al., 2011)
Tomato slices	Slap	1.31×10 ⁻⁹	(Sacilik et al., 2006)

The equations below are solutions for the diffusivity of moisture in different component geometries.

1.1) Slab (Plate).

This product geometry has been used extensively to assess the moisture diffusivity of fruits and vegetables, as shown in Table 2. The solution for the second distribution of Fick's Law using slab geometry and the initial limit terms laid out above for different fruits and vegetables can be represented as follows:

$$MR = \frac{(M - M_e)}{(M_i - M_e)} = \frac{8}{\pi^2} \sum_{n_t=0}^{\infty} \frac{1}{(2n_t + 1)^2} \exp\left(\frac{-(2n_t + 1)^2 \pi^2 Dt}{4(h^*)^2}\right) \quad \text{Eq. (2)}$$

However, in practice (for a long drying period) only the first term of the series is often applied. Thus, Equation 1 becomes

$$MR = \frac{(M - M_e)}{(M_i - M_e)} = \frac{8}{\pi^2} \exp\left(\frac{-\pi^2 Dt}{4(h^*)^2}\right) \quad \text{Eq. (3)}$$

Equation 3 can further be simplified and expressed in a logarithmic form (Doymaz, 2005; Hii and Ogugo, 2014; Kadam et al., 2011; Murthy and Manohar, 2012; Rayaguru and Routray, 2012; Sacilik et al., 2006; Saxena and Dash, 2015).

$$\ln(MR) = \ln\left(\frac{8}{\pi^2}\right) - \left(\frac{\pi^2 Dt}{4(h^*)^2}\right) \quad \text{Eq. (4)}$$

where D is the effective moisture diffusivity in m^2/s , h^* is the half thickness of slab (m), and n_t is the number of terms (a positive integer). Equation 2, 3, and 4 have been used in estimating the moisture diffusivity of basil leaves, pumpkin, tomato, carrot, and green bean as presented in Table 2.

1.2) Infinite slab.

This product configuration, along with the slab geometry, is the most commonly used in determining the diffusivity of moisture for fruit and vegetables. The solution of Fick's second law of diffusion for long drying of infinite slab geometry content is sometimes interpreted as identical to that of slab geometry in most research (Akoy, 2014; Akpinar, 2006b; Omolola et al., 2014; Simal et al., 2005)

$$MR = \frac{(M_t - M_e)}{(M_i - M_e)} = \frac{8}{\pi^2} \sum_{n_t=0}^{\infty} \frac{1}{(2n_t + 1)^2} \exp\left(\frac{-(2n_t + 1)^2 \pi^2 Dt}{4(h^*)^2}\right) \quad \text{Eq. (5)}$$

Equation 5 can further be expressed as

$$\ln(MR) = \ln\left(\frac{8}{\pi^2}\right) - \left(\frac{\pi^2 Dt}{4(h^*)^2}\right) \quad \text{Eq. (6)}$$

where D is the moisture diffusivity in m^2/s , h^* is the half thickness of slab (m), and n_t is the number of terms (as a positive integer). This geometry has been used in estimating the moisture diffusivity of banana, kiwifruit, parsley, and mango (Table 2).

1.3) Sphere

This product configuration is the third most commonly used to measure diffusivity of moisture for fruit and vegetables. The solution of Fick's law of diffusion for spherical geometry for a long drying time can be presented as follows:

$$MR = \frac{(M_t - M_e)}{(M_i - M_e)} = \frac{6}{\pi^2} \sum_{n_t=0}^{\infty} \frac{1}{(n)^2} \exp\left(\frac{-n_t^2 \pi^2 Dt}{R^2}\right) \quad \text{Eq. (7)}$$

Equation 7 can further be expressed as

$$\ln(MR) = \ln\left(\frac{6}{\pi^2}\right) - \left(\frac{\pi^2 Dt}{R^2}\right) \quad \text{Eq. (8)}$$

where R is the equivalent radius of the fruit or vegetables.

Equation 7 and 8 have been applied in estimating the moisture diffusivity of green peas and plum (Table 2).

1.4) Cylinder.

This concept is seldom used to measure the diffusivity of moisture in fruit and vegetables. The solution of Fick's equation (Equation 1) for determining the diffusivity of fruit and vegetables with cylindrical geometry may be given as follows (Guiné et al., 2011) as

$$MR = \frac{(M_t - M_e)}{(M_i - M_e)} = \sum_{n_t=1}^{\infty} \frac{4}{b_{n_t}^2} \exp\left(\frac{-b_{n_t}^2 Dt}{r^2}\right) \quad \text{Eq. (9)}$$

Equation 9 can be expressed in a simple form as

$$\ln(MR) = \ln\left(\frac{4}{b_1^2}\right) - \left(\frac{b_1^2 Dt}{r^2}\right) \quad \text{Eq. (10)}$$

where r is the cylinder radius. From Table 2, Equation 9 and 10 have been used to estimate the moisture diffusivity of pumpkin.

2) Thin-layer drying model

Thin layer drying is typically used to dry as one layer of sample particles or slices (Akpınar et al., 2006). Due to its thin nature, the thermal conductivity can accurately be presumed to be consistent, and the thin layer drying is ideal for lumped parameter designs. Table 3 shows some chosen thin-layer fruit and vegetable, drying models.

Table 3 Thin-layer models for the drying of fruits and vegetables.

Model name	Model	Reference
Lewis	$MR = \exp(-kt)$	(Wang et al., 2007b)
Page	$MR = \exp(-kt^n)$	(Doymaz, 2004)
Modified Page	$MR = \exp(-kt)^n$	(Wang et al., 2007b)
Henderson and Pabis	$MR = a \exp(-kt)$	(Doymaz, 2004)
Logarithmic	$MR = a \exp(-kt) + c$	(Kaur and Singh, 2014)
Two-term model	$MR = a \exp(-k_0t) + b \exp(-k_1t)$	(Henderson, 1974)
Diffusion	$MR = a \exp(-kt) + (1 - a) \exp(-kat)$	(Akpınar, 2006a)
Wang and Singh	$MR = 1 + at + bt^2$	(Wang et al., 2007b)
Quadratic equation	$MR = at^n + bt^{n-1} + \dots + d$	(Srinivasa et al., 2004)
Simplified Fick's diffusion	$MR = a \exp(-c(t/L_c^2))$	(Wang et al., 2007b)
Midilli et al model	$MR = a \exp(-kt^n) + bt$	(Akpınar, 2006a)

These models are also used to classify drying fruits and vegetables, as seen in Table 3. They can be divided into three categories based on their competitive advantages and disadvantages as well as their permutations. Theoretical, semi-theoretical, and scientific versions are included. The semi-theoretical and empirical models are the most extensively used forms of thin-layer models (Akpınar, 2006a; Doymaz, 2007; Guiné et al., 2011; Özdemir and Onur Devres, 1999; Panchariya et al., 2002). These model categories consider the exterior friction between the material and ambient air to the moisture transfer process, have more detailed outcomes, better simulate drying process activities, and make fewer predictions because of their dependency on research observations. For dryer engineers and designers, these variants have emerged as the most beneficial (Brooker et al., 1992). They are, however, only applicable within the context of the drying process. On the other hand, theoretical models make too many assumptions, resulting in a large number of errors (Bruce, 1985; Henderson, 1974), thereby restricting their use in dryer development.

Typically, the semi-theoretical structures are derived from the second Fick's Law solutions and integration of its more basic forms. The semi-theoretical and some observational models view the transport processes and demonstrate a better fit with

the empirical results (Janjai et al., 2011). The empirical and semi-theoretical structures have comparable features. The major problems faced by the analytical models are that they rely primarily on experimental data and have little data about heat and mass transfer in the drying process (Erbay and Icier, 2010). These models are commonly used for estimating drying kinetics because of the features of semi-theoretical and observational models and the high moisture content properties of several fruits and vegetables.

2.1.5 Closed-loop control system

A control system is the integration of factors that comprise a system structure that produces a system response that is required. The rationale for system analysis is the framework given by linear system theory, which suggests that the elements of a system have a cause-effect relationship. As seen in Figure 9, apart, or operation, to be managed can be depicted visually. The input-output relationship is the process's cause-and-effect link, which consequently reflects the input signal processing to produce the desired output signal. As seen in Figure 10, an open-loop control (OPC) device utilizes a controller and an actuator to achieve the intended reaction. An OPC system is a system without feedback. It utilizes an actuating device to control the process directly without using feedback.

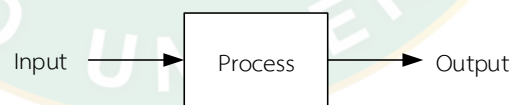


Figure 9 Process to be controlled.

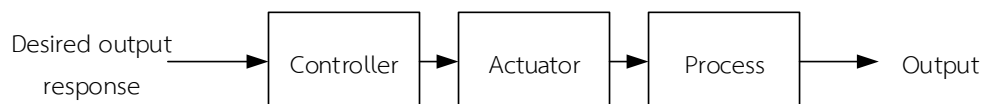


Figure 10 Open-loop control system (without feedback).

A closed-loop control (CLC) system uses another measure of the actual output to relate the actual output with the preferred output response, unlike an OPC system. Measurement of output is termed a feedback signal. Figure 11 displays a primary CLC method. The feedback control system is a control system that seeks to preserve a specified relationship between one system variable and another by matching the functions of both variables and using the variance as a control mechanism. For a precise sensor, the calculated output is a reasonable estimate of the actual output of the device.

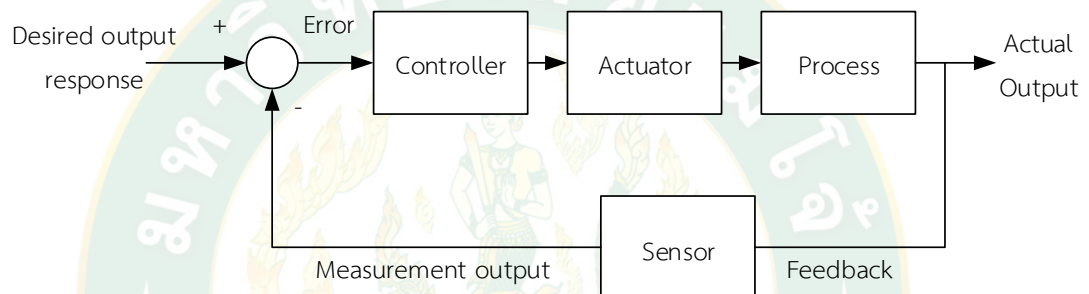


Figure 11 CLC system (with feedback).

The role of the specified relationship between output and reference input to simulate the performance is dictated by a feedback control system. The discrepancy between the output of the process under control and the comparison input is always enhanced and employed to improve the process such that the variance is constantly decreased. In general, the variance between the expected outcome and the actual output is proportional to the error that the controller then changes. The output of the controller allows the operation to be modulated by the actuator to minimize error. For instance, the temperature controlling in the hot-air oven as shown in Figure 12.

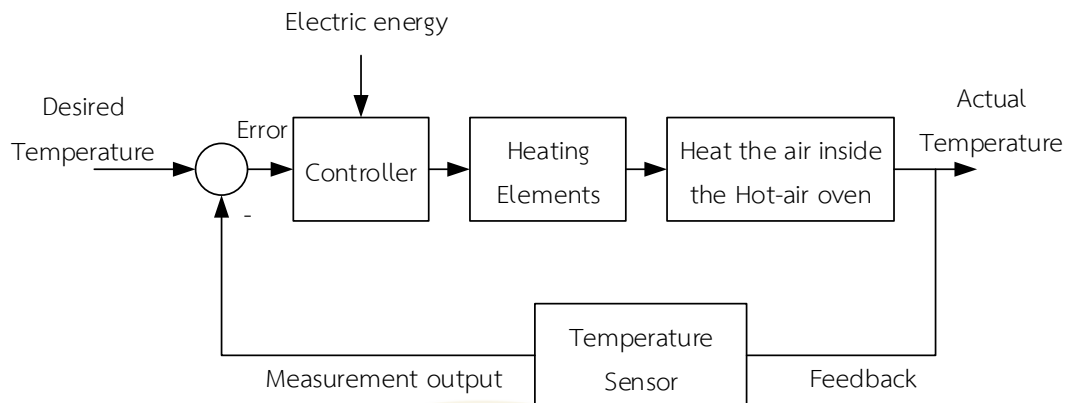


Figure 12 Closed-loop temperature control system of the hot-air oven.

A temperature sensor (input device) continuously screens the air temperature inside the oven and sends a signal back to the controller for comparison with the desired temperature and calculated the error ($\text{Error} = \text{Required Temperature} - \text{Actual Temperature}$), and then the controller sends the output signal for adjustment to the heater to minimize the error, as seen in Figure 12. For instance, the controller's temperature will be raised if the current temperature is lower than the ideal temperature. Similarly, the heating mechanism will be interrupted if the temperature is greater than the ideal temperature to lower the temperature and retain the temperature until the current temperature is equal to the target temperature. The effect of the error signal was directly attributed to the variance between the desired temperature and the actual temperature of the air within the hot-air furnace. The CLC system can also manage any system disruptions or adjustments in circumstances that can limit its potential to achieve the intended mission. For instance, if the door of the oven is open, the heat is released. Each time the feedback sensor observes the temperature variation, the controller rectifies the problem by keeping the temperature steady inside the set threshold's parameters or sending an alarm signal to the user.

CLC systems have a number of benefits over OPC systems. The primary benefit of the CLC system is its capacity to lower the sensitivity of the system to external

forces. Further, CLC systems are much more effective in the case of non-linearities. Nevertheless, the architecture of CLC systems involving numerous physical components is sophisticated since there are uncertainties, i.e., non-linearities, in enabled devices. Based on this, the researcher aimed to incorporate these elements (control system framework) to be clear and usable. The conventional block diagram is therefore significant in the study and development of control systems.

1) Control system design

The control system design process is illustrated in Figure 13.

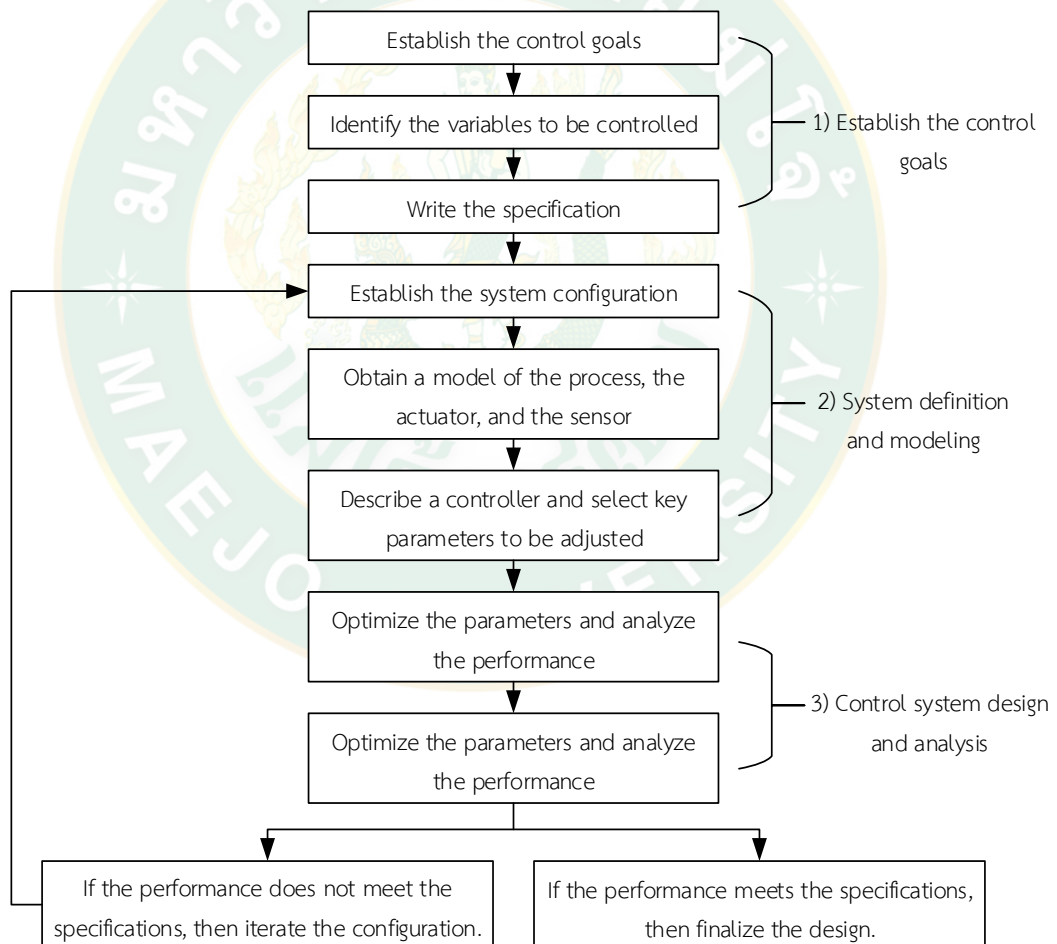


Figure 13 The control system design process (Drof and Bishop, 2017).

According to the model of Drof and Bishop (2017), establishing the system objectives, System specification and modeling, Control system design, and analysis are the seven core building blocks that make up the design process.

1.1) Establishing the system goals

The first step of designing the controls system is establishing the goal to control the process, for example, controlling the hot-air oven temperature, as mentioned in the previous section (Figure 12). The next step is to define the parameters that we want to monitor. The third step is to record the parameters in terms of the precision that we need to achieve. This required control precision would contribute to identifying the sensor for the calculation of the regulated parameter. The design requirements help explain how the PLC framework can work.

1.2) System definition and modeling

First of all, it is essential to set up a system that will achieve the desired control results. As shown in Figure 2.11, this device configuration will usually include a sensor, the mechanism under control, an actuator, and a controller. Identifying a candidate for the actuator is the next phase. From Figure 2.12, the process definitely will determine this, but the actuation chosen must be capable of effectively modifying the process's output. If the regulation of the temperature inside a hot-air oven is required, a heater is chosen to act as the actuator (Figure 2.12). In this event, the temperature sensor must accurately measure the temperature and generate a model for individual components.

1.3) Control system design and analysis

The next thing is to find a controller, which usually comprises a summing amplifier that matches the expected reaction to the real response and then forwards the error-measuring signal to the amplifier. Changing the device parameters in order to produce optimal efficiency is the final step in the design process. Formalize the configuration and record the effects if the control system optimizes the efficiency. Otherwise, an enhanced configuration may be developed, and an upgraded actuator

and sensor can be chosen. Then repeat the design phase until the criteria have been reached or until the criteria are too demanding and can be relaxed.

In conclusion, it can be summarized that the following is the controller's conceptual framework: Considering a suitable controller or determine there is not one provided a model of the device to be controlled (namely its sensors and actuators) and a set of design objectives. The feedback controller's design is an iterative and non-linear process. Control design strategy, controller design configuration (i.e., what sort of controller shall be required), and efficient controller tuning techniques are all important aspects of a successful design.

2.1.6 Uncertainty of measurement

Uncertainty of measurement refers to apprehension about a measurement's outcome. Measurement uncertainty is defined as a “parameter, associated with the result of a measurement, that characterizes the dispersion of the values that could reasonably be assigned to the measured quantity,” according to the “Guide to the expression of uncertainty in measurement” or “GUM” (ISO, 2008). The proper estimation of measurement uncertainty is central to the efficiency and cost control of calculations. The study of uncertainty enables deeper awareness of the relative value of different amounts of measurement effects. Using an uppercase letter U meaning “uncertainty”, the uncertainty of the measurement result y is generally indicated by U_y though U_y is used as well in notation. If U_y is the uncertainty of the measurement result y gained by using a measurement approach to a calculated value with an unspecified value Y , it may be expressed as:

$$Y = y \pm U_y \quad \text{Eq. (11)}$$

An equivalent expression allowed by the GUM is

$$y - U_y \leq Y \leq y + U_y \quad \text{Eq. (12)}$$

The evaluation of uncertainty of measurement was summarize as shown in Figure 14 and the details were described below.

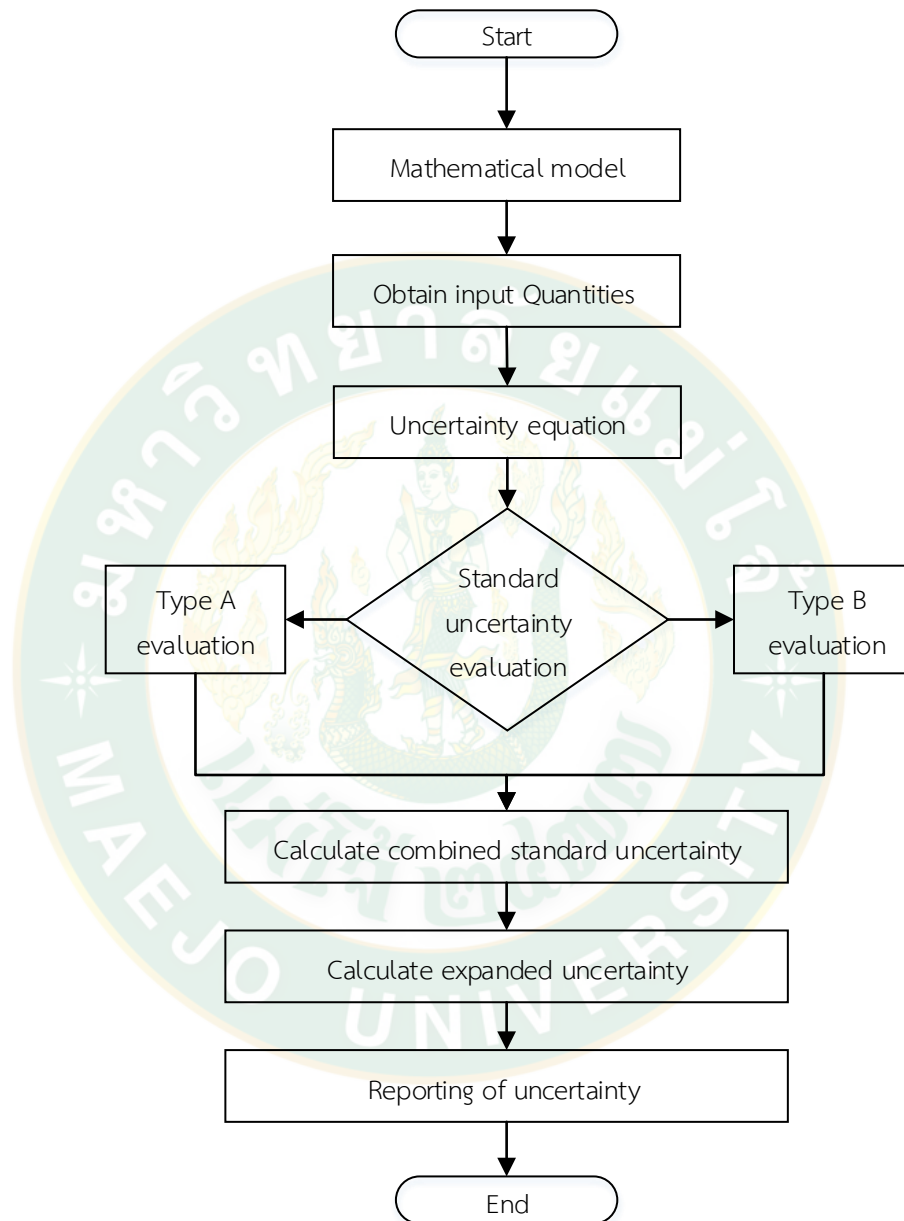


Figure 14 Flowchart of summary for evaluating uncertainty of measurement.

1) Modeling the measurement

The output of measured quantity Y is usually determined from N input quantities, ie. X_1, X_2, \dots, X_N through a function f :

$$Y = f(X_1, X_2, \dots, X_N) \quad \text{Eq. (13)}$$

Comprising corrections and correction factors for organized influences, the input quantities X_1, X_2, \dots, X_N may be considered calculated quantities that depend on other quantities, thus causing a complex functional relationship f . Each quantity that contributes a significant component of ambiguity to the measurement outcome is included in the function f . Both corrections and corrective considerations are contained. In order to eradicate any insufficiency, if the function f does not model the calculation to the degree defined by the necessary precision of the measurement outcome, supplementary input quantities must be used in the function f . The set of input quantities X_1, X_2, \dots, X_N can be sorted as:

a) In the existing measurement, quantities with values that are uncertainties are established directly. These values and uncertainties may be extracted, for instance, from a single measurement, repetitive assessments, or analysis based on experience, and may include the calculation of adjustments to instrument readings and corrections for impact values such as atmospheric temperature, barometric pressure, and humidity.

b) Quantities whose measurements and inconsistencies are found in calculations from external references, including quantities correlated with calibrated measuring specifications, approved test products, and sample details derived from guides.

Employing input estimates x_1, x_2, \dots, x_N for the values of the N input quantities X_1, X_2, \dots, X_N an estimate of the measured quantity Y , denoted by y , is obtained from Equation (13). The output estimate y , which is the outcome of the quantity, can be expressed as:

$$y = f(x_1, x_2, \dots, x_N) \quad \text{Eq. (14)}$$

Estimated standard deviation associated with each input estimate x_i , denoted by $u_{x,i}$, is used to describe the estimated standard deviation correlated with the output estimate or measurement result y , denoted by u_y . As mentioned below, each standard uncertainty $u_{x,i}$ is obtained from either a “Type A” or “Type B” evaluation.

2) Evaluation of standard uncertainty

The variability in the outcome of the calculation usually includes multiple elements, which can be divided into two types per the methodology used to determine their statistical measures, which are 'Type A' and 'Type B' of the traditional uncertainty assessment.

2.1) Type A

Type A Standard Uncertainty Assessment is based on any appropriate statistical approach used in the study of a set of observations. An aspect of the Type A standard uncertainty measurement is the product of a random effect. The Gaussian or Standard Error Law lays the foundation for an empirical analysis of explanatory variables. The ideal existing estimation of the anticipated value of a quantity q that differs randomly is the arithmetic mean \bar{q} . Typically, the arithmetic means for n_t independent examinations can be expressed as:

$$\bar{q} = \frac{1}{n_t} \sum_{s=1}^{n_t} q_s \quad \text{Eq. (15)}$$

The experimental standard deviation $s(q_s)$ is used to estimate the distribution of q .

$$s(q_s) = \sqrt{\frac{1}{n_t-1} \sum_{s=1}^{n_t} (q_s - \bar{q})^2} \quad \text{Eq. (16)}$$

The experimental standard deviation of the mean $s(\bar{q})$ is used to estimate the spread of the distribution of the means.

$$s(\bar{q}) = \frac{s(q_s)}{\sqrt{n_t}} \quad \text{Eq. (17)}$$

The quantity determined from n_t independent repeated observations, the Type A standard uncertainty $u_{x,i}$ and the degrees of freedom ν_i is:

$$u_{x,i} = s(\bar{q}) \quad \text{Eq. (18)}$$

$$\nu_i = n_t - 1 \quad \text{Eq. (19)}$$

The degrees of freedom ν_i should always be given when Type A evaluation of uncertainty components are documented.

2.2) Type B

Processes other than the statistical analysis of a series of observations are used to obtain the Type B evaluation of standard uncertainty. Scientific judgment by all pertinent data obtainable is the common approach used, which could comprise:

- a) previous measurement data
- b) experience with, or general knowledge of the behavior and property of relevant materials and instruments
- c) manufacturer's specification
- d) data provided in calibration and other reports and
- e) uncertainties assigned to reference data taken from data book

The quoted uncertainty must be changed to a standard uncertainty when reflecting Type B uncertainty. By allocating the quoted uncertainty with a factor contingent on the probability distribution, the quoted uncertainty can be changed to standard uncertainty.

2.2.1) Rectangular distribution

When the uncertainties are specified by maximum bound within which all values are equally probable, rectangular distribution is employed. As seen in Figure 15, standard uncertainty is calculated by dividing the half-interval “a” by $\sqrt{3}$.

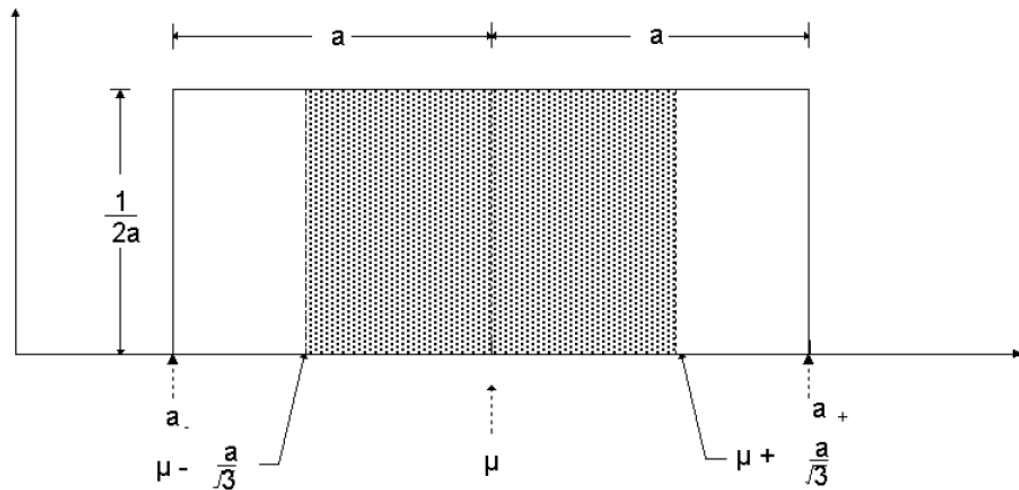


Figure 15 Rectangular distribution.

2.2.2) Triangular distribution

When it is identified that most of the values tend to be near the center of the distribution, triangular distribution is the more suitable option. As revealed in Figure 16, the standard uncertainty is calculated by dividing the half-interval 'a' by $\sqrt{6}$.

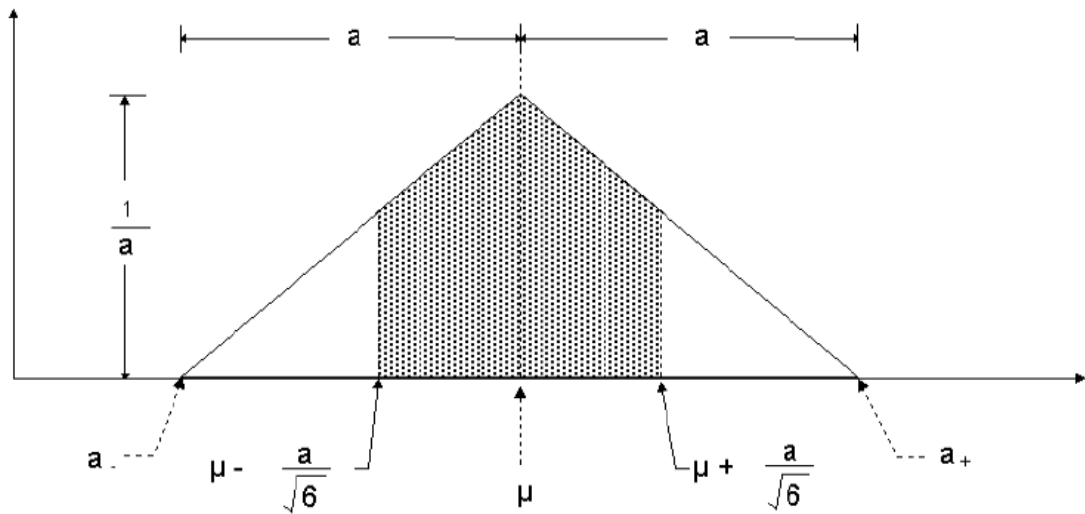


Figure 16 Triangular distribution.

2.2.3) Normal or Gaussian distribution

This allocation form can be inferred for an ambiguity that determines a confidence interval with a confidence level of 95% or 99%. As revealed in Figure 17, the standard uncertainty is gained by dividing the quoted uncertainty by the suitable factor for such an allocation (see Tables 4 and 5 concerning factor selections).

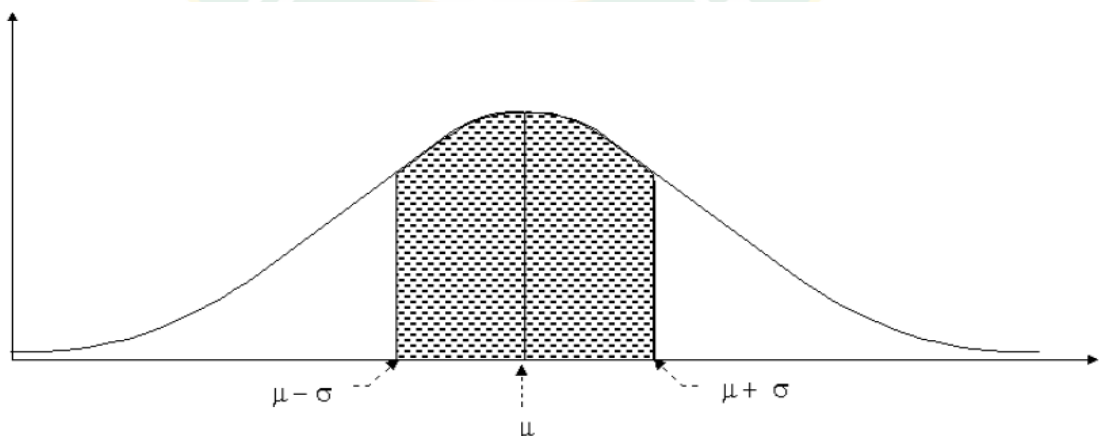


Figure 17 Gaussian distribution.

The rectangular distribution is a good default model in case of no other details. Nonetheless, suppose it is agreed that the value of the sum of concern is near to the center of the boundaries. In that case, the triangular or normal distribution might be a better model. The probability distributions for Class B instability are derived from earlier probability distributions. It is implicitly presumed that the probability distribution is well-defined. In certain cases, the degree of freedom for such standard uncertainty can be calculated to be inestimable. This is a fair assumption since it is common practice to select a category B uncertainty such that the probability of the quantity in question falling beyond the uncertainty band is extremely low (refer to section 4.1 Coverage factor).

3) Combined standard uncertainty

The standard uncertainty, $u_{x,i}$ linked with each input estimate x_i (see Section 1 on "Modeling the Measurement") is used to define the projected standard deviation correlated with the output estimate or measurement result y , labeled the combined standard uncertainty and denoted by u_y . In cases where all input variables are linearly separable, their mutual distributions of probability are derivatives of their specific distributions of probability. The combined standard uncertainty u_y is the positive square root of the combined variance u_y^2 expressed as:

$$u_y = \left(\sum_{i=1}^N u_{x,i}^2 \right)^{1/2} \quad \text{Eq. (20)}$$

4) Expanded uncertainty

Several applications demand a measure of uncertainty that expresses an interval about the measurement result y , within which the value of the measure and Y can be positively declared to remain, though the combined standard uncertainty $u_c(y)$ may be employed to articulate the uncertainty of measurement outcomes. Indicated by symbol U_y and acquired by multiplying u_y by a coverage factor, the measure of uncertainty proposed to achieve this requisite is called expanded

uncertainty. Accordingly, $U_y = k_c u_y$ can positively state that $y - U_y \leq Y \leq y + U_y$, frequently expressed, as $Y = y \pm U_y$.

Existing international practice dictates providing a confidence level of roughly 95% (95.45%). k_c differs with effective degrees of freedom when level of confidence is fixed. In numerous cases, k_c equal to 2 may be employed where operative degree of freedom is moderately large, better or equal to 30. It is required to acquire the value of k_c using the t-distribution table in cases where effective degree of freedom is minute (Tables 4 and 5). The calculation of effective degrees of freedom is follow section 4.1 Coverage factor.

4.1) Coverage factor

Approximating the coverage factor value necessitates considering the uncertainty of u_y , which is described by the efficient degrees of freedom, v_{eff} of u_y . For instance, if v_{eff} is less than 11, supposing that the uncertainty of u_y is insignificant and taking $k_c = 2$ may be insufficient if an enlarged uncertainty $U_y = k_c u_y$ that describes an interval having a level of confidence close to 95 % is essential for a particular function. It is doubtful in this case as well as in similar cases where eff n of u_y is relatively small and an interval having a level of confidence close to a specified level is essential, that the uncertainty of u_y would be deemed insignificant. Rather, the minimal value of v_{eff} , and consequently the uncertainty of u_y , would likely be considered when establishing k_c . The four-step process for calculating k_c can eb expressed as follows:

a) Obtain y and u_y .

b) Estimate the effective degrees of freedom v_{eff} of u_y from the Welch-Satterthwaite formula:

$$v_{eff} = \frac{u_y^4}{\sum_{i=1}^N \frac{u_{x,i}^4}{v_i}} \quad \text{Eq. (21)}$$

where all of the $u_{x,i}$ are mutually statistically independent, v_i is the degrees of freedom of $u_{x,i}$ and

$$v_{eff} \leq \sum_{i=1}^{n_t} v_i \quad \text{Eq. (22)}$$

Type A evaluation yields the degrees of freedom of a typical uncertainty $u_{x,i}$, where $x_i = X_i$ and $u_{x,i} = s_{x,i}$ is $v_i = n_t - 1$. If m parameters are evaluated by fitting a curve to n_t data points using the least squares method, the degrees of freedom for the standard uncertainty of each parameter are $n_t - m$.

The degrees of freedom associated with a standard uncertainty $u_{x,i}$, derived from a Type B evaluation with lower and upper limits a_- and a_+ , are established such that the possibility of the quantity in question resting beyond these limits is extremely small. It was discovered that the degrees of freedom were v_i . If not, the equation below can be used to define the degrees of freedom, $v_i \rightarrow \infty$, that are to be applied to a standard uncertainty, $u_{x,i}$, obtained from a Type B evaluation:

$$v \approx \frac{1}{2} \left[\frac{u_{x,i}^2}{\sigma^2[u_{x,i}]} \right] \approx \frac{1}{2} \left[\frac{\Delta u_{x,i}}{u_{x,i}} \right]^{-2} \quad \text{Eq. (23)}$$

The measure in large brackets is the relative uncertainty of $u_{x,i}$, which is a subjective value for a Type B assessment. Experience and knowledge of the measurement procedures can be used to find this value.

c) Acquire the t-factor $t_p(v_{eff})$ for the requisite confidence level of p from a table of values for $t_p(v)$ from the t-distribution table, (Table 4) Interpolate or truncate v_{eff} to the subsequent lower integer if v_{eff} is not an integer, which is typical.

d) Take $k_c = t_p(v_{eff})$ and calculate $U_y = k_c u_y$

Table 4 The t-distribution table.

Degrees of freedom (ν)	Fraction p in percent					
	68.27	90	95	95.45	99.00	99.73
1	1.84	6.31	12.71	13.97	63.66	235.8
2	1.32	2.92	4.30	4.53	9.92	19.21
3	1.20	2.35	3.18	3.31	5.84	9.22
4	1.14	2.13	2.78	2.87	4.60	6.62
5	1.11	2.02	2.57	2.65	4.03	5.51
6	1.09	1.94	2.45	2.52	3.71	4.90
7	1.08	1.89	2.36	2.43	3.50	4.53
8	1.07	1.86	2.31	2.37	3.36	4.28
9	1.06	1.83	2.26	2.32	3.25	4.09
10	1.05	1.81	2.23	2.28	3.17	3.96
11	1.05	1.80	2.20	2.25	3.11	3.85
12	1.04	1.78	2.18	2.23	3.05	3.76
13	1.04	1.77	2.16	2.21	3.01	3.69
14	1.04	1.76	2.14	2.2	2.98	3.64
15	1.03	1.75	2.13	2.18	2.95	3.59
16	1.03	1.75	2.12	2.17	2.92	3.54
17	1.03	1.74	2.11	2.16	2.90	3.51
18	1.03	1.73	2.10	2.15	2.88	3.48
19	1.03	1.73	2.09	2.14	2.86	3.45
20	1.03	1.72	2.09	2.13	2.85	3.42
25	1.02	1.71	2.06	2.11	2.79	3.33
30	1.02	1.70	2.04	2.09	2.75	3.27
35	1.01	1.70	2.03	2.07	2.72	3.23
40	1.01	1.68	2.02	2.06	2.70	3.20
45	1.01	1.68	2.01	2.06	2.69	3.18
50	1.01	1.68	2.01	2.05	2.68	3.16
100	1.005	1.660	1.984	2.025	2.626	3.077
∞	1.000	1.645	1.960	2.000	2.576	3.000

5) Reporting of the results

In stating the uncertainty of measurement results, the following information would be provided.

- a) the measurement result,
- b) the expanded uncertainty,
- c) the level of confidence used in defining the interval of the expanded uncertainty, and
- d) the coverage factor, k_c used in defining the interval of the expanded uncertainty.

In this research, the uncertainty of measurement was used to verify the accuracy of the measuring systems and moisture calculation of the CLC system. The error was acceptable within the range of 5%.

2.2 Literature review

2.2.1 Microwave freeze-drying characteristics and effect on product quality

In the MFD process, the relationship linking material temperatures, microwave power levels, material thickness, vacuum pressure and moisture content is also important factors that influence the efficiency of the MFD process and the product quality of the end result. These relationships among factors will ultimately affect the product quality and drying rate as would be seen in the literature following:

According to Abbasi and Azari (2009), the study used an onion slice as a model to demonstrate the capabilities of the MFD technique. The results show that the effects of vacuum speed, microwave strength, and thickness were almost identical for microwave drying with and without vacuum. The rate of dehydration is very rapid in the early stages of MFD, owing to the high moisture content and, as a result, a higher amount of absorbed electromagnetic energy. As the process proceeds, the rate of dehydration decreases due to lower moisture content and

absorbed electromagnetic energy (Ozkan et al., 2007; Sharma and Prasad, 2001). Furthermore, the dehydration phase intensified with increasing microwave power levels at a constant thickness, most likely due to the mass transfer rate and the vapor pressure differential between the central and external sections of the slices (Maskan, 2000; Wang and Sheng, 2006; Wang and Xi, 2005). It should be noted, however, that high microwave power intensities were not ideal for dehydration because they caused the substance to burn. Thinner slices dried in slightly shorter periods and had a higher rate of dehydration, owing to a higher rate of mass transfer; according to the results, according to the reports on carrots and mushrooms, this is accurate (Giri and Prasad, 2007; Wang and Xi, 2005). Despite the fact that the MFD process had an effect that was almost identical to microwave drying with and without vacuum, unexpectedly, the MFD of onion slices dehydrated in a much shorter time, with no shrinkage, no discernible color change, and a completely porous structure similar to that of a fresh onion slice. MFD is a fast, convenient, reliable, and cost-effective dehydration technique that can be used to dehydrate a variety of foods. The quality properties of slices produced by this method were also totally comparable and competitive with those produced by commercial FD, with a processing time savings of more than 96 percent and huge energy and capital investments.

Wang et al., 2009 studied the influences of microwave power, material thickness, material weight and material temperature on drying characteristics and sensory quality of instant vegetable soup by using MFD. The experimental was divided into 4 parts as follows: the effect of microwave power, materials thickness, material weight and material temperature. In the first part, the study on the influences of microwave power, found that after increased microwave power, the drying rate increased, and the drying time reduced. Form the overall results of the satisfaction survey on product quality, it was found that products at 225, 450 and 675 W of microwave power received high scores, and the lowest scores was given to product at 900 W microwave power. In the second part, the study on the influences of material thickness, found that the material with more thickness need more drying

time than the material with less thickness. From the overall results of the satisfaction survey on product quality, it was found that the lowest score was given to the product with 5 mm material thickness. On the other hand, 25 mm material thickness was found to have poor score as well. The appropriate thickness from this experiment was 10 to 20 mm, which received high scores of satisfactions. In the third part, the study on the influences of the material weight, found that 150 grams of material weight used shortest drying time, but received the lowest scores from the satisfaction survey on product quality. On the other hand, product weighted 450 grams received highest scores from the satisfaction survey on product quality. The microwave power should be adjusted to suit the material weight without exceeding 1.0 to 1.5 W/g for product drying. In the final part, the study on the influences of the maximum temperature of material, found that at the 40°C temperature, the product required more drying time than the product at 50°C to 70°C temperatures. However, the product at 40°C received the highest scores from the satisfaction survey on product quality. On the other hand, product at 70°C temperature required short drying time, but also received the lowest overall score from the satisfaction survey on product quality.

Duan et al., 2010b studied MFD process done on sea cucumber (*Stichopus japonicus*) compared to hot-air drying process and FD processes. Moreover, Duan et al., 2010b also studied the relationship between plasma discharge and microwave power at various vacuum pressures and initial moisture content conditions to study the possibility of plasma discharge during MFD process. The study revealed that FD uses a long time for processing and requires more energy consumption, but does maintain the product quality of sea cucumbers. While it uses much less energy, hot-air drying results in poor product quality. MFD used less drying time and energy consumption than FD about 30-40% but provided a good product quality such as structure color and nutrients similar to FD. Energy consumption is the highest at 200W microwave power, followed by 1.6 and 2.3 W/g. Improved product efficiency is accomplished by using a microwave power range of 2 W/g, but the lowest energy consumption was achieved at a microwave power of 2.3 W/g given the short process

durations. Moreover, corona discharge testing found that a pressure range from 100 to 200 Pa could easily initiate corona discharge in the MFD process. When the cavity pressure was about 150 Pa, the critical discharge microwave power was the lowest, notwithstanding the moisture content. In addition, the result ensures that a pressure range from 50 to 100 Pa have no corona discharge occurs.

According to the research of Wang et al. 2010b, the study focused on exploring potatoes as the model material to investigate the microstructural variations of potato slices in the MFD and FD procedures with and without blanching. Raw potato slices were soaked in a 0.5 percent calcium chloride formulation for 10 minutes before drying in order to investigate the effect of calcium treatment on the microstructure of potato tissue. To examine the microstructural changes in blanched potato tissue during the drying period, the slices were blanched in boiling water for 5 minutes. After blanching, the material was cooled and deposited in the freezer. The MFD procedure was carried out using a microwave power of 1.6 W/g. The researchers discovered that the temperature differences between bleached and unbleached potatoes for the same drying process were similar, though the MFD stage dried 37 percent faster than the FD stage. Furthermore, the results of the microstructural analysis showed that in the MFD and FD systems, the majority of differences in the microstructure of both unbleached and bleached potatoes occurred during the pre-frozen and sublimation phases. Moreover, during the desorption phases, there were no significant changes in the cell wall. The polyhedral cells in raw potatoes were stable and well-organized, with a stiffening of the cell wall after Ca^{2+} soaking. Blanching also causes starch gelatinization. White potato cells that were standard and bloated were easier to freeze than unbleached cells. As a result, the microstructural changes in the whitened dried samples were greater than in the unbleached samples. When efficient performance is considered, the results showed that neither the MFD nor the FD methods lost significant amounts of vitamin C, sugar, or starch. The rehydration ability of dried potatoes was improved by Ca^{2+} treatment, but bleaching was more effective in improving the rehydration performance. Calcium

ions therapy and bleaching were effective methods for avoiding shape changes during MFD.

In the research of Jiang et al., 2011, drying properties of microwave freeze-drying (MFD) and microwave vacuum drying (MVD) of restructured banana and potato chips of varying proportions and microwave strength were examined. According to the results, increasing both microwave power and drying time decreases MFD drying time, which agrees with Soysal, 2004. Higher potato content results in a faster drying rate for restructured chips. The overall drying time was also shorter for potatoes with a higher potato content than for others. One explanation for this activity is that higher moisture content, which can lead to more ice crystal formation, can create more channels in dry areas, allowing vapor to escape more easily. The dielectric properties of the drying materials are another important factor that influences the drying rate. Between the samples handled with 2 W/g and 3 W/g microwave fuel, the MFD drying time varied by up to one hour. MFD samples outperformed MVD samples in terms of rehydration ratio. The best rehydration ratio is achieved at a microwave power level of 3 W/g. The color difference meter data, on the other hand, indicated that 3 W/g microwave power would slightly char samples. The most important variations between the MFD and MVD chips, as opposed to the MFD, were in their texture and shape; the hardness of MVD samples was three times that of MFD samples. In terms of drying rate, MVD is faster than MFD, but the overall product quality of MVD samples is lower than that of MFD samples.

Jiang et al., 2013 conducted the study to compare the energy usage of FD and MFD methods for making banana chips. The MFD process was found to save up to 35.7 percent energy and 40 percent drying time as compared to the conventional FD process. During the secondary drying stage, the heating power becomes a critical factor that has a direct impact on the overall energy consumption. The overall energy consumption decreases from 35.75 MJ (10.79 kWh) to 29.17 MJ (8.63 kWh) and 27.25 MJ (8.09 kWh) after changing the heating capacity in the secondary drying stage of FD from 400 W to 500 W and 600 W, respectively. Additionally, the drying

time can be decreased from 600 minutes (400 W) to 480 minutes (500 W) and 420 minutes (420 W) (600 W). When the microwave power in the secondary drying stage is increased from 1.0 W/g to 1.5 W/g, the MFD overall energy consumption is around 18.12 MJ (5.56 kWh), and the drying period is decreased from 360 minutes to 270 minutes. As a result, rising the heat power in the MFD process's secondary drying stage was found to reduce energy consumption and drying time. Furthermore, color data shows that FD samples can produce more brilliant color than MFD samples, and that the darker color was caused by high power from the heating plate and microwave source. The findings clearly demonstrated that microwave heating drying would be an efficient method for reducing the drying time and cost of the conventional FD process, which could be useful to industrial-scale production.

The browning mechanism of button mushrooms during the MFD phase was investigated by Duan et al., 2016 Microwave freeze-drying (MFD) was used on dry button mushrooms to achieve faster drying and better product quality. MFD mushrooms have a higher color degradation than FD mushrooms, despite the fact that they produce similar product consistency. By considering the whiteness and browning degree for describing the browning kinetics of button mushrooms during the MFD process, two drying methods were used to investigate the browning behaviors of button mushrooms during MFD. It was discovered that rising microwave power while lowering pressure sped up the drying process. The moisture content significantly influenced the browning rate. At high microwave power, the browning rate was rapid in the early stages of the MFD process, implying that a high moisture content could result in a high browning rate. At the same drying conditions, the browning kinetics of button mushrooms were significantly associated with the moisture content. This implied that during the MFD process, mushroom browning behavior regulation should be based on moisture content change tendency. During the MFD button mushrooms, both non-enzymatic browning and enzymatic browning can occur. The effect of enzymatic browning, on the other hand, is more important and should be regulated during MFD. To avoid enzymatic browning during MFD button mushrooms, low microwave power should be used at the start of the

process. In the meantime, to minimize non-enzymatic browning, low microwave power should be used at the end of MFD. As a result, if the microwave power can change based on the changing moisture content during the MFD process, the MFD process efficiency and product quality will be increased.

Cao et al., 2018a studied on the effect of microwave freeze drying on quality and energy supply in drying of barley grass. The results showed that MFD is superior to FD for MFD decreased drying time as well as in the MFD of banana (Jiang et al., 2014), sea cucumber (Duan et al., 2010b), instant vegetable soup (Wang et al., 2009), potato (Wang et al., 2010b), and cabbage (Duan et al., 2007a). Microwave heat output of the MFD operation helps to increase the sublimation of ice relative to the touch heat of the FD phase. In comparison to FD, the moisture content on MFD fell significantly. Microwave heat output of the MFD process helps to increase the sublimation of ice relative to the touch heat of the FD process. In comparison to FD, the moisture content on MFD fell significantly. In comparison, the temperature in MFD is higher than in FD at the main stage. This could be proportional to the volumetric heat of the microwave energy, which reduces heat transfer time. In the secondary stage, high microwave power levels increased the temperature of desorption to accelerate the drying process, thus reducing the energy consumption. The MFD process can reduce the drying time and energy consumption about 40% while obtained the product quality similar to FD process. From the results of product quality and energy consumption, it can conclude that MFD process is a better method to dry barley grass compared to the FD process. However, at highest microwave power used in this research (2 W/g) the quality of the product is unacceptable. Cao et al., 2018a found that high microwave heat (2 W/g) could contribute to product charring in a short period, posing a threat to the nutrition and consistency of the products during the final drying phase. This is apparent from the high value of L^* and the low green value of a^* .

From the above literature, it can conclude that the MFD can reduce the drying time and energy consumption of FD by about 30-40%. Increasing microwave power

could minimize drying time more so than reduced microwave power. Conversely, higher microwave capacity contributed to low product quality. Moreover, the pre-treatment of MFD, such as blanching and dipping the sample in Ca^{2+} before the MFD phase, can enhance the MFD product's quality. However, it increases the expense of the procedure and makes the MFD process more complicated. Thus, enhance the MFD process efficiency with no pre-treatment is challenging for further research, such as controlling the drying conditions during the MFD process based on the material properties changing, which reviews in the next section. In addition, it can conclude that the cavity pressure should be applied within the range of 50–100 Pa to avoid the corona discharge, which can lead to material burn and can damage the magnetrons during the MFD process. Moreover, the measuring system of moisture content should be developed to continuously monitor and collect the moisture content data in real-time, which could be used in further research because it is the important factor linking with controlling the MFD process and the product quality. In addition, the microwave power at different phases of the MFD process should be optimized based on energy efficacy and product quality.

2.2.2 Microwave freeze-drying with microwave dynamic loading scheme

Generally, in the MFD process, a fixed level of microwave power is used throughout the entire microwave drying process. The high microwave power can reduce the drying time but provide low product quality. In contrast, the low microwave power can maintain the best product quality but took a long drying time which consumes energy. Thus, if the MFD process's drying conditions were optimized, the efficiency of the MFD process would be enhanced and provided the best product quality. However, In the past decade years, it has a few works in the literature that apply a dynamic microwave loading scheme based on the material properties changing to enhance the efficiency of the MFD process as following:

Duan et al., 2012 investigated the effects of moisture content and temperature on the dielectric properties of apple slices and proposed a microwave power loading scheme for MFD of apple slices based on the calculated dielectric properties to

prevent plasma discharge under high vacuum. Two microwave power loading designs were used to examine the features of MFD apple slices. Using 3 W/g for 2 hours, 2.5 W/g for 2.5 hours, and 1.5 W/g for 1.5 hours with 300 g materials weight, one design was assessed based on the alteration in dielectric properties, while the other design was assessed at a fixed microwave power of 2.5 W/g. MFD procedures were carried out at 60 Pa cavity and -40°C cold trap temperature. MFD was found to have used about 60% shorter drying time than FD. Since much of the free water had been withdrawn and the critical power at the end of the MFD process was minimal, the temperature at the end stage rose steadily during the sublimation process. Consequently, comparatively low power is suggested in the final stage to conserve energy. Moreover, when compared fixed microwave power loading scheme with changed microwave power loading scheme based on dielectric properties, found that there was no difference drying rate but changed microwave power loading scheme can provide a better product quality and has no significant difference from the FD.

Ren et al., 2015 agreed with Duan et al., 2012 that it is better to use a step-down microwave power loading scheme to enhance the quality of product when mushrooms were microwave freeze-dried. A step-down microwave loading program (1.5 kW for 1 hour, 1 kW for 2 hours, 0.6 kW for 3 hours, and 0.4 kW for 2 hours) was conducted to examine the impact of the altered microwave loading system on the MFD method. It was found that microwave power has a major influence on drying time, and the drying time could clearly be decreased by enhanced microwave power. Varying microwave influences had a negligible impact on the temperature of the specimens at the sublimation point. Under various microwave power loading programs, however, the water loss rate of the materials showed evident improvement. One potential explanation was that in this point, much of the free water sublimated, and much of the frozen water in mushrooms accumulated microwave energy. Consequently, enhancing the drying rate is possible by utilizing moderately high microwave power in this phase. When reducing moisture level to less than 50% wet basis, a fixed microwave power scheme (1 kW and 2 kW) led to a high temperature increase rate and the highest microwave power (2 kW) takes a

shortest drying time while the temperature of the step-down microwave power loading was gradually increase and takes a longest drying time. As a results of product quality analysis, the step-down microwave power loading can reduce the shrinkage of the dried product and obtained the good product quality with the highest score of color (L^*), crispness and rehydration ratio. On the other hand, microwave power at 2kW has lowest crispness, highest hardness, and more shrinkage compared to other two treatments. This was because the porous structure inside the samples was destroyed.

Liu et al. (2017) studied mushrooms and employed a dynamic microwave loading scheme which responded to changes arising in the porosity during the process of MFD in order to achieve faster drying times while maintaining a high level of product quality. The complex technique for microwave loading was constructed according to the action of porosity shift in the MFD phase of mushrooms and the curves of porosity shift, the process conditions and the outcomes of dried product quality. The dynamic microwave loading strategy was design based on the porosity change behavior was applied to mushrooms MFD process, and the porosity change curves, drying process and the dried product quality results. The dynamic microwave loading strategy was design by applied microwave power 3 W/g at the beginning of the drying process for 5 hours to reduce the drying time with no effect to the open-pore porosity and the product quality, then changed the microwave power to 2 W/g for 1.5 hour to maintain the quality of the product, after that the microwave power to 4 W/g until the drying process is finished to reduce drying time with little pore structure collapsing. The findings reveal that the measurements of the open-pore porosity of the modified microwave power do not vary substantially from the 2W/g microwave power. The adjusted power showed the maximum values of the open-pore porosity and the weakened structure ratio was just 14.68% and requires the drying period relative to the 2 W/g fixed microwave power, the drying time of the adjusted microwave power loading approach. Also, the vitamin C content of specimens receiving an adjusted microwave power loading technique was far higher compared to dried samples under fixed 2 W/g microwave power.

Li et al. (2019) was studied on the microwave-assisted pulse-spouted bed FD of Chinese yam by employing a multi-stage variable microwave power loading device that was designed to reduce gas discharge dependent on the dielectric characteristics of yam. The experiment was performed using a pilot scale microwave-assisted, pulse-proof bed freezer they created. The analysis demonstrated that the microwave power loading scheme was built on the basis of the evolving dielectric microstructures separated into five phases. In stage 1, the microwave was cut off at the pre-drying stage in the first half hour to sublimate any surface ice crystals by heat transfer. Because of the low dielectric loss factor of the frozen sample, the microwave power of 650 W was chosen in stage 2 and the length was 1.5 hours, culminating in weak electromagnetic field coupling of the sample. Microwave energy for ice crystal sublimation was absorbed by the samples at a low rate. Due to the dielectric constant and loss factor posing a strong upward trend due to the usable water content for the microwave in the sample increased and comparatively high (>60 percent) in stage 3, the microwave power was set at 1300 W for 3.5 hours. This implied that the coupling potential between electromagnetic field sample and microwave increased, the materials could absorb a significant amount of microwave radiation. In the fourth step, due to the dielectric constant, the microwave power lowered to 650 W for 1 hour and the loss factor lowered as the moisture content lowered. In order to prevent corona discharge and minimize energy consumption, microwave power can also be limited. Owing to the reduced dielectric constant and loss factor initiated by the low moisture content of the sample, the drying phase was controlled at 390 W for half an hour at the end of drying (stage 5). The coupling of the electromagnetic microwave field and the corona discharge could have been weakened, so that safe microwave power loading was minimal. The results in terms of the drying time, and energy consumption and product quality of the microwave assisted pulse-spouted bed FD by using a microwave power loading scheme were compared with the FD show that the microwave assisted pulse-spouted bed FD by using a microwave power loading scheme can shortened the drying time by up to 48.3% with the advantage of rapid drying, and accordingly reduced the total energy consumption by 34.4% while provided the quality of the product similar to FD.

Even though, the above literature showed the comprehensive study that the dynamic microwave loading approach based on changing material properties would dramatically enhance product quality on the basis of preserving an appropriate drying period. However, in some cases, it still needs a longer drying time than the fixed microwave power, which led to increasing the operation cost. Moreover, the changing of material properties during the MFD process did not monitor in real-time, and the process control was not a real-time control. Further, the temperature of the drying sample is usually not controlled. Increasing the temperature of the sample to an unpleasantly high level can cause product charring at the last stage (Cao et al., 2018a). These may cause the efficiency of the drying process and the product quality not to be as good as expected. Thus, the development of automatic dynamic process control focusing on reducing the drying time and energy consumption while maintaining the best product quality to enhance the efficiency of the MFD process is challenging for further research.

2.2.3 Microwave freeze-drying kinetics

Mathematical models such as Newton's model, Page's model, the Henderson and Pabis model, the Midilli et al.'s model, Diffusion approximation, and Logarithmic model have been widely applied to describe and predict the drying kinetics of microwave-assisted combination drying methods such as, Sutar and Prasad, 2007 was found that the Page model showed high correlation with microwave power density at constant pressure in the studies of microwave vacuum drying of carrot slices. Moreover, there have a few research report that Midilli et al. showed the best performance in simulation the experimental drying kinetics in the study of microwave drying of hawthorn fruit (Amiri Chayjan et al., 2015), Black pepper (Amarasinghe et al., 2018) and potato (Azimi-Nejadian and Hoseini, 2019). These works show that the higher microwave power could be increased the drying rate and reduced the drying time, but high microwave led to pool quality of products. On the other hand, low microwave power could be obtained the best quality of product but required the long drying time and consumed the energy consumption. Thus, it is the challenging

to optimize the microwave power based on the drying rate to reduce the drying time and energy consumption while maintain the best product quality for increasing the drying performance. For the drying kinetics of MFD, there is a research work in the past decade years about using the mathematical model to describe the drying kinetics of the MFD process as follow:

Ambros et al., 2018 studied the dying behavior of bacterial granules during the MFD process. This work was conducted by using the pilot-scale microwave freeze dryer. The study found that the modified Page and Diffusion approach model could adequately describe the dying behavior of bacterial granules during the MFD process with the high r^2 and low $RMSE$ and X^2 . The drying time of the drying process is reduced by increasing power and vacuum pressure. The shortest drying time was provided at microwave power 3 W/g with vacuum pressure 2 mbar. However, when considered the survival rate and the membrane integrity of the bacterial granules. The lowest microwave power at 1.5 W/g provided the best survival rate (100%) and the membrane integrity of about 80-90%. The drying rate of all microwave power levels is not significantly different under different vacuum pressure at the initial stage of drying. However, the microwave power level of 2 and 3 W/g, plasma, occurs intermittently after the process starts at all pressure levels. This was because the sample could absorb a small amount of microwave energy as the rigid structure of the ice crystals was not easily excitable. As soon as the ice started to sublime, the arcing stopped. Thus, microwave power of 1.5 W/g should be applied in the initial stage to avoid the plasma discharge and reduce the energy consumption and increase the microwave power to 3W/g to increase the drying rate. In the later stage of drying, the microwave power should be reduced following the decrease in water content to avoid the plasma discharge and obtain the best product quality.

As the reviewing and discussion about this work, the drying kinetics would be useful for understanding the MFD profiles and their characteristics to improve the efficiency of the CLC system and optimize the MFD to maximize the quality of the products. If the focus on the drying kinetics were intended to select appropriate

drying conditions and to control the processes of MFD, a better understanding of the drying rate would help in developing a CLC system to enhance the MFD process.

Besides the above literature, it has not been found the research work which applied used mathematical models to describe and predict the drying kinetics of the MFD process. However, a study of the drying kinetics would be useful for understanding the MFD profiles and their characteristics to improve the efficiency of the CLC system and optimize the MFD to maximize the quality of the products. The studies on MFD of cabbage by Duan et al. (2007) and MFD of onion slices by Abbasi and Azari (2009) have proven that the findings from drying kinetics could be used as the basis for the optimization of the MFD process, such as increasing the microwave power in the first stage of MFD was able to increase the drying rate, and decreasing the microwave power in last stages of MFD was able to maintain the product quality as well as Ambros et al. in 2018. Moreover, moisture diffusivity was another index to indicate the efficiency of the MFD process. Past studies in the literature have also shown effective diffusivity in the MFD process due to the altered appearance of the drying material, e.g., porosity and shrinkage of the sample. The higher microwave power yielded a pore formation and moisture diffusivity of the samples. It is possible that as the moisture content inside the samples was heated up by the microwave energy, the vapor inside the solid matrix of the samples generated the vapor pressure. This created the pressure gradient between the internal vapor pressure and vacuum pressure in the surroundings of the samples. This pressure gradient was responsible for the moisture transportation (Datta and Anantheswaran, 2001), which caused the increase in moisture diffusivity during the drying process (Feng et al., 2001; Narjes et al., 2018; Sharma and Prasad, 2001; Wang et al., 2007a). However, the high levels of microwave power led to increasing the vapor pressure inside the pores structure and increased the pressure for opening the pores, which causes the matrix collapse in the carrot slices. The collapse of the pore structure leads to reducing the number of the pore, causing the shrinkage of the samples. Thus, using drying kinetics and moisture diffusion were proposed in this research to develop the CLC system, which explained the phenomena of the MFD process in each stage. If the focus on

the drying kinetics and moisture diffusion were intended to select appropriate drying conditions and to control the processes of MFD, a better understanding of the drying rate would help in developing a CLC system to enhance the MFD process.

2.3 Summary of literature review

From the above literature review, it could be determined that a multi-stage microwave loading scheme is an effective technique if it is necessary to improve the MFD process. Even so, the literature on the subject of a multi-stage microwave loading scheme is relatively sparse. However, it is evident that the MFD can replace FD because it dramatically reduces the drying time and energy consumption by roughly 40% while producing the same product quality similar to FD. The important factors that influence the MFD and quality of products are the relationships among microwave power levels, materials temperature, and moisture content of the materials. The relationships are also associated with the drying rate and product quality. Suppose the MFD conditions during the drying process is controlled properly with a better understanding the MFD profiles and their characteristic. In that case, it can increase the drying performance and quality of products.

The increasing microwave power level and material temperature reduce drying time and energy consumption. However, they may produce low product quality because a high microwave power level might lead to material burn and hardening of the product cell wall. Moreover, the rehydration ratio and preservation rate of nutrients is likely to decline as well. While using a low microwave power level, overall product quality is likely to be better than at a high microwave power level. In addition, the increasing and decreasing of microwave power level should be correlated with the moisture content of materials by the vacuum pressure level at 100 Pa to avoid the possibility of plasma discharge, which may lead to the magnetrons being damaged, the material being burnt, and microwave energy being excessively consumed. Thus, the researcher proposes the concept to control the MFD conditions by measuring material temperature and calculating content moisture for processing and controlling the drying environment during the MFD process by using the closed-loop control (CLC) system. Higher microwave power with material

temperature should be applied in the sublimation drying phase to reduce drying time. In the desorption drying phase, the CLC system then decreased microwave power levels in relation to moisture content to avoid plasma discharge and obtain better quality. From this concept, the researcher expects to design the control strategy and develop the CLC system that can control the MFD condition to produce the dried food materials with high quality. Figure 18 shows the conceptual overviews of the MFD with the CLC systems. The researcher expects that the MFD with CLC systems could improve the efficiency of the FD and the general MFD process by reducing the energy consumption and drying time while obtaining the product quality similar to FD.

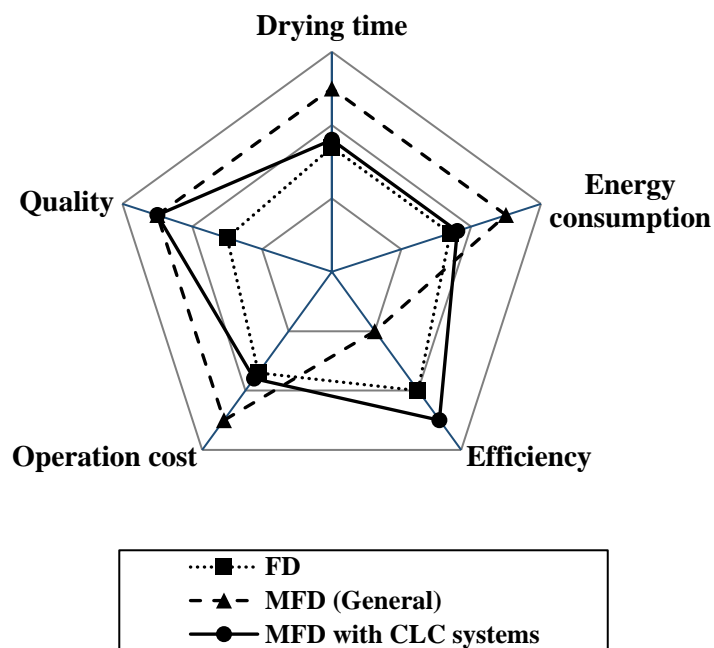


Figure 18 Conceptual overview of CLC system for MFD.

CHAPTER 3

RESEARCH METHODOLOGY

In this research, the researcher divided the works into three parts as shown in Figure 19.

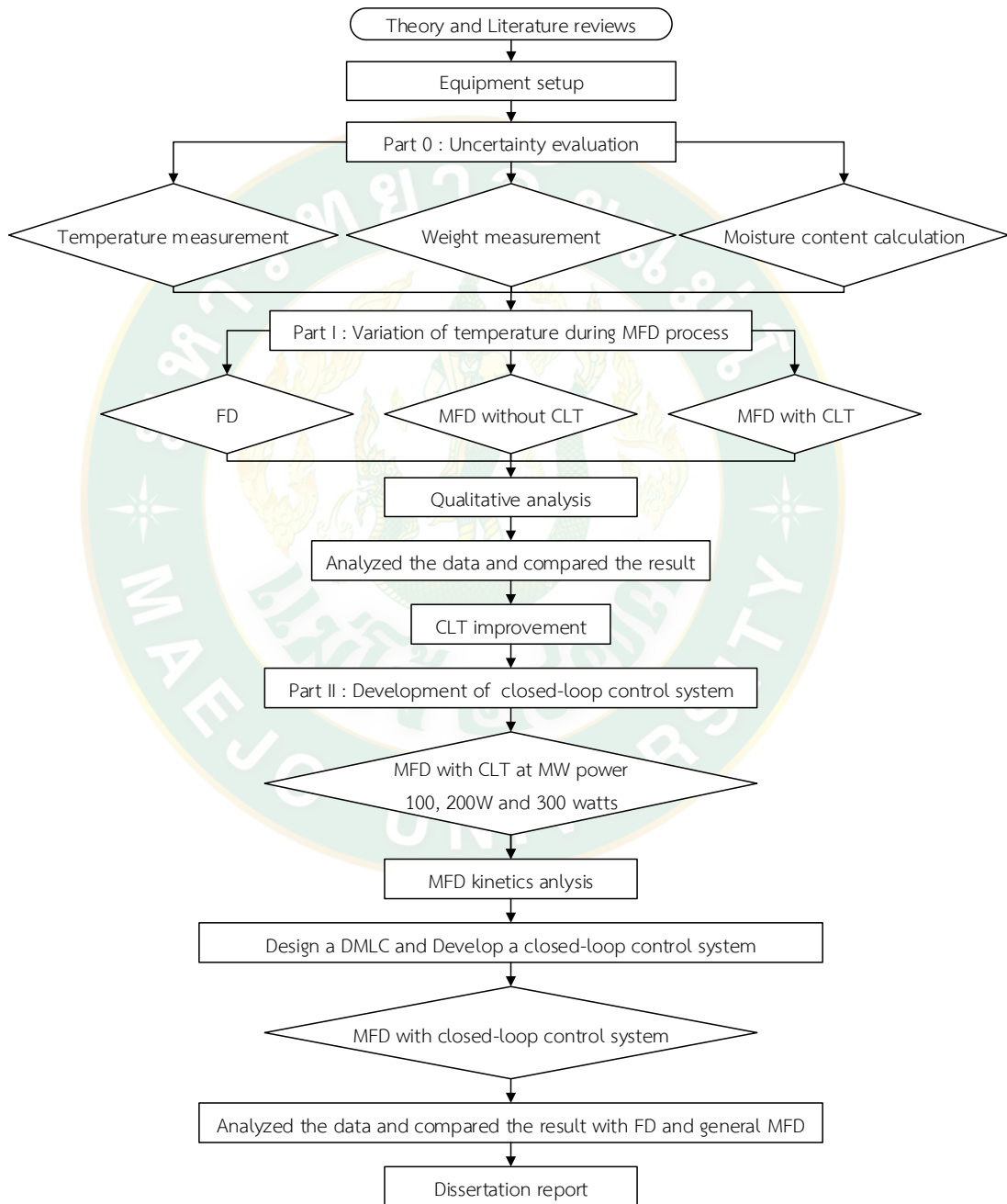


Figure 19 Research diagram and framework.

From Figure 19, this research consisted of three-part. Part 0 is the uncertainty of measurement systems, and the calculation of moisture content was evaluated to verify the accuracy of the temperature measurement, weight measurement, and moisture content calculation. Part 1 is the study of the temperature variation during MFD using a closed-loop temperature control system (CLT) to improve temperature variations and study its effects on the product quality. Experimentation was conducted using three drying methods, namely FD, MFD without CLT, and MFD with CLT. The product's quality was analyzed in terms of color, texture, rehydration ratio, and energy consumption. In Part 2, the closed-loop control (CLC) system was developed. The development process consisted of two sections: the MFD experiment to develop the DMLC and the implementation of the CLC with the DMLC on the MFD process. The qualitative of products was analyzed for the evaluation of the CLC-MFD efficiency. The details of the research methodology were described below.

3.1 Sample preparation

The carrot used in this experiment was obtained from local markets in Thailand. The sample was stored at a temperature of 4°C ($\pm 0.5^{\circ}\text{C}$) before the MFD experiments. The carrots were trimmed, scraped, washed, and sliced into a 10 mm thickness with a 35 mm diameter to prepare the samples. The samples were washed and slightly shaken to remove excess water, slightly shaken to remove the excess water, and frozen in the refrigerator at -35°C ($\pm 0.5^{\circ}\text{C}$) for eight hours (Figure 20).



Figure 20 Fresh carrots slices.

3.2 Design of microwave freeze dryer

The laboratory-scale microwave freeze dryer was design based on a dimension similar to that of a household microwave oven. Figures 21 and 22 present the 3D model and the schematic diagram of the microwave freeze dryer used in this research. The dryer consisted of five main components, e.g., MFD drying chamber, PLC system, refrigeration system, cold trap, and vacuum system. During the MFD operation, the frozen carrot slices were placed onto a rotating tray inside the MFD cavity. A load cell model Snug 3 (Jadever Scale Co., Ltd, Taiwan) was placed inside the MFD cavity underneath the tray to monitor the sample's real-time weight loss. To collect the carrot's temperature at its center-point, an optical fiber temperature probe size of 3 mm in diameter model SR-G (Fuzhou Skyray Opto-electronic Technology Co. Ltd., China) was used to ensure the non-interference of the temperature measurement with the electromagnetic field in the MFD cavity. The signal from the temperature probe was converted by a signal converter. The output signals from both the load cell and temperature signal converter were sent to the PLC system attached to a personal computer for moisture content calculation, temperature collection, and process control regulation.

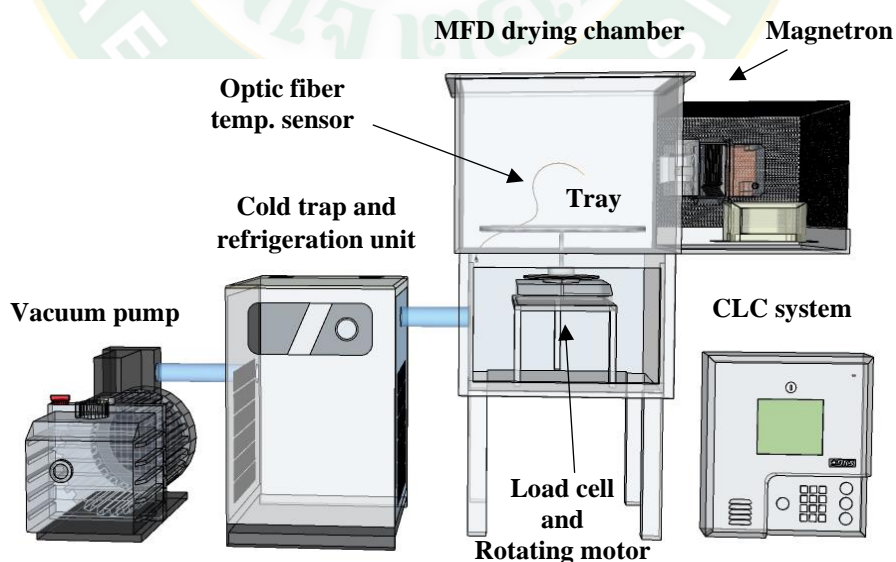


Figure 21 3D model of laboratory-scale microwave freeze dryer.

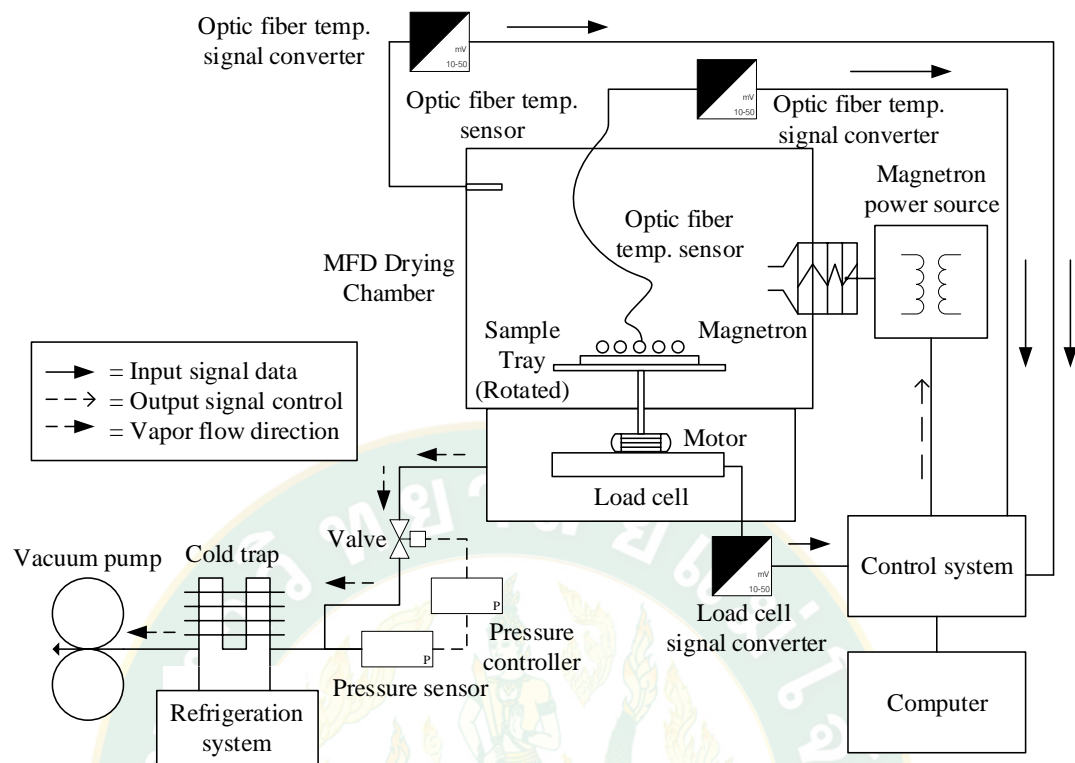


Figure 22 Schematic diagram of laboratory-scale microwave freeze dryer.

During the MFD process, vapor, either from sublimation or evaporation, was generated inside the MFD cavity. This vapor was sucked out from the cavity by the vacuum pump and condensed inside the cold trap under a temperature of -40°C . The cold trap temperature is typically below -40°C , cooled by the refrigeration system to condense the vapor during the MFD process. This stops water vapor from accessing the vacuum pump, which could impair the pump operations. To achieve the MFD sublimation, vacuum pressure was applied at a constant pressure of 100 Pa, maintained by the vacuum pump during the MFD process. The vacuum mechanism comprises a separate vacuum pump linked to and fixed to the drying chamber by an airtight condenser. A magnetron at a frequency of 2.4 GHz capable of 0-900 W was attached to the MFD cavity. The magnetron converts electric energy to microwave energy. Microwave energy generated in the magnetron is guided through a waveguide to arrive at the drying chamber. The materials absorbed microwave energy and converted to heat for the sublimation. This magnetron was connected to the PLC

system and was regulated to achieve the MFD process with a drying strategy programmed for optimum energy consumption and final carrot's quality. The researcher has developed the dryer, measurement system, control system, and software for the control system from the design of the microwave freeze dryer. The details were described in Chapter 4 in the section of Equipment setup for Microwave freeze dryer.

3.3 Hardware design for closed-loop control system

The designing goal of the CLC system was to control the MFD process by adjusting the microwave power levels based on the changing temperature and moisture content of the materials during the MFD process. The temperature of the materials can detect by using the optical fiber temperature sensor system, which can be used in the electrical field as in the literature (Cao et al., 2018a; Duan et al., 2012; Liu et al., 2017; Ren et al., 2015; Wang et al., 2009). The moisture content of the materials could be calculated by using Equation 24.

$$M_r = M_i - \left[\left(\frac{W_{in} - W_r}{W_{in}} \right) \times 100 \right] \quad \text{Eq. (24)}$$

where M_r is the real-time moisture content, M_i is the initial moisture content, W_{in} is the initial materials weight, and W_r is the real-time materials weight.

From Equation 24, the initial moisture content and the weight of the initial material is the pre-set values, and the weight of the real-time material during the MFD process can be detected by using the load cell. Thus, the CLC system's hardware design should consist of the real-time temperature measurement system, the real-time materials weight detection system, the output control for control the microwave power, and the central processing unit to control the systems. The schematic diagram of the CLC system hardware was shown in Figure 23.

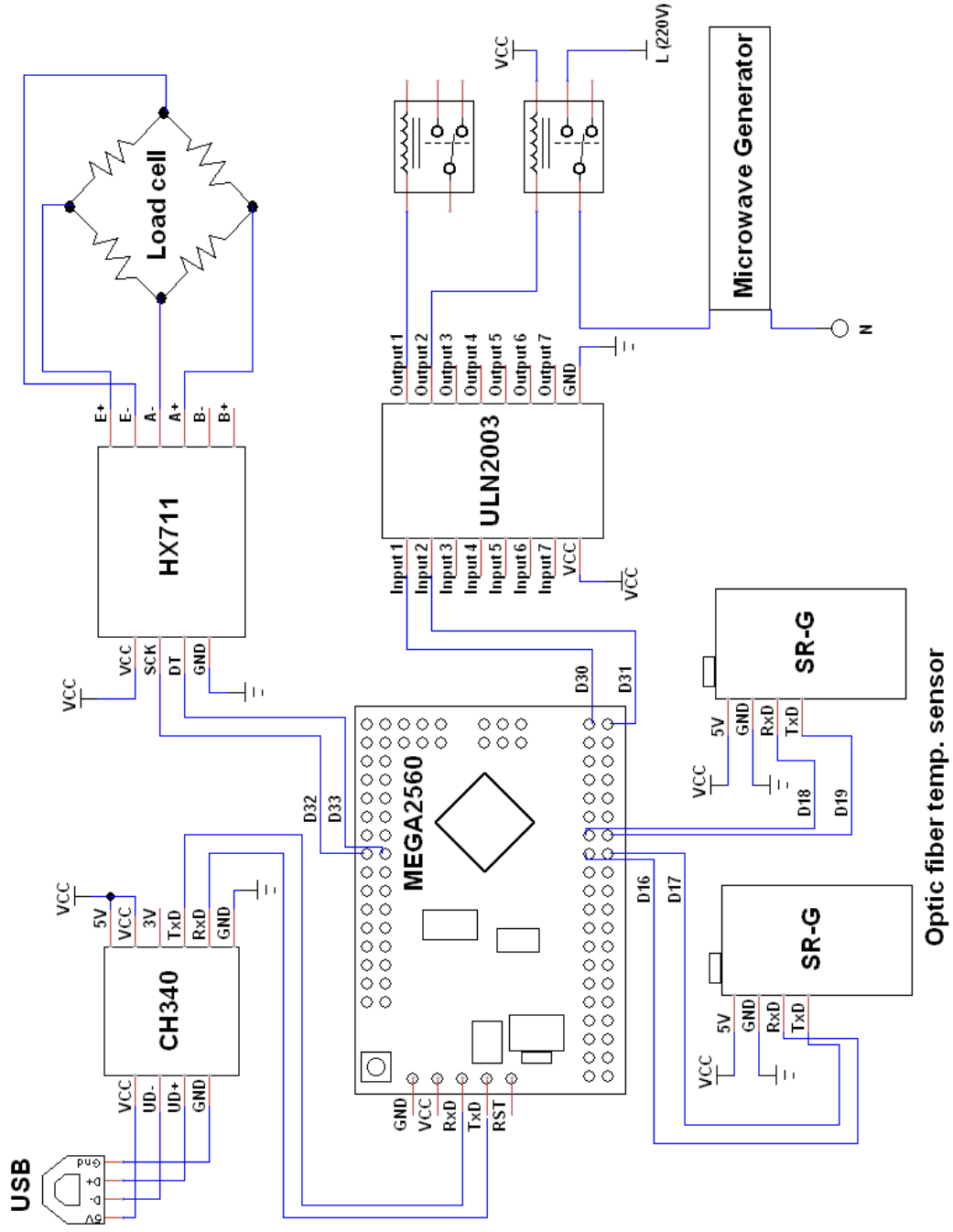


Figure 23 The schematic diagram of the CLC system hardware.

From Figure 23, The optic fiber temperature sensor model SR-G (Fuzhou Skyray Opto-electronic Technology Co. Ltd., China) and a load cell model Snug 3 (Jadever Scale Co., Ltd., Taiwan) detected the temperature and materials weight during the MFD process. The analog signal from the temperature probe and load cell was converted to the digital signal by signal converter model SR-G and HX711 (Avia Semiconductor Ltd., China). The output signals from both the temperature and load cell signal converter were sent to the central processing unit, which was embedded with the micro-controller model Atmega2560 (Microchip Technology Inc., USA) to calculate the moisture content and the regulation of the process control. The output signal from the central processing unit was used to control the microwave power levels through the relay driver model ULN2003 (STMicroelectronics SA., Switzerland) to control the on/off of the magnetron. The PLC hardware was attached to a personal computer through the universal serial bus (USB) port using the USB to serial port converter model CH340 (Jiangsu Haoheng Co. Ltd., China) to collect the data of the temperature, material weight, and moisture content of the materials.

In the first part of this research, the researcher used the PLC system to monitor the material's temperature and moisture content. The researcher used only temperature control with feedback to control the final state materials temperature. However, after the logic process control for MFD called dynamic microwave logic control (DMLC) was developed in the second part of this research, it was embedded into the PLC system for the regulation of the MFD process control to enhance the performance of the MFD process.

3.4 Part 0: Uncertainty of the measurement system

3.4.1 Uncertainty of temperature measurement

The temperature was one of the key parameters in the DMLC, especially the temperature of the carrot slices. In this research, the optical fiber temperature sensor (OFT) model SR-G (Fuzhou Skyray Opto-electronic Technology Co. Ltd., China) was used to detect the temperature of carrot slices and feedback to the PLC system for controlling the temperature of carrot slices in the final stage of the MFD process.

Thus, evaluating the uncertainty of the temperature measurement system is integral to confirm that the temperature control system was accurate and suitable to use with the CLC system. The uncertainty of the temperature measurement was evaluated by considering the effect of the temperature reading, the uncertainty base on its calibration data, the OFT resolution, and the effect of the vacuum pressure inside the drying chamber. The uncertainty measurement of the OFT system according to the GUM is described as the following subtopic.

1) Mathematical model

The mathematical model for the temperature measurement of the OFT (T_x) is given by:

$$T_x \cong T_{rd} + \Delta T_{cb} + \Delta T_{res} + \Delta T_{vc} \quad \text{Eq. (25)}$$

where T_{rd} is the temperature reading of the OFT, ΔT_{cb} is the temperature of the OFT reading error based on its calibration data, ΔT_{res} is the temperature reading error due to the resolution of the OFT, and ΔT_{vc} is the temperature reading error of the OFT, which was affected by the vacuum pressure.

2) Uncertainty equation

The combined standard uncertainty of the temperature measurement, $u_{T,x}$ is given by:

$$u_{T,x} \cong \sqrt{[u_{T,rd}^2 + u_{\Delta T,cb}^2 + u_{\Delta T,res}^2 + u_{\Delta T,vc}^2]} \quad \text{Eq. (26)}$$

where $u_{T,rd}$ is the standard uncertainty of the temperature reading, $u_{\Delta T,cb}$ is the standard uncertainty of the OFT based on its calibration data, $u_{\Delta T,res}$ is the standard uncertainty of the OFT resolution, and $u_{\Delta T,vc}$ is the standard uncertainty of OFT, which was affected by the vacuum pressure inside the drying chamber.

3) Standard uncertainty evaluation

3.1) Type A evaluation

3.1.1) The standard uncertainty of the temperature reading, $u_{T,rd}$ was evaluated by setup the equipment as show in Figure 24.

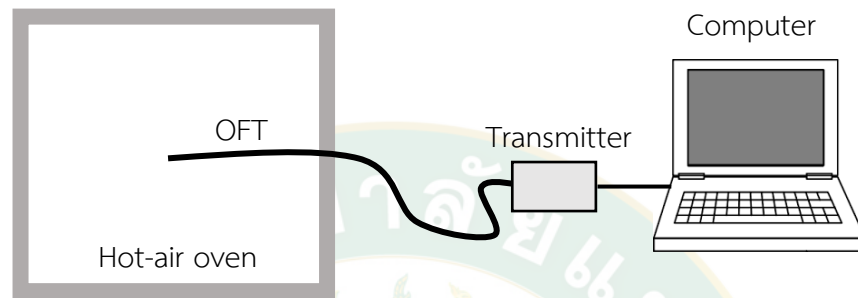


Figure 24 Temperature measurement equipment setup.

In Figure 24, the OFT was used to measure the temperature inside a temperature chamber of hot-air oven model UNB-100 (Mettler, GmbH & Co., Germany). Its controller controlled the temperature of the air inside the chamber. The OFT has measured the temperature of the chamber in the range of 30-50°C. When the temperature chamber indicator reached the target temperature, the readings are taken after a stabilization time of half an hour then the ten measurements are taken. The OFT system signal gave the resolution of temperature at 0.1°C with its accuracy of $\pm 1^\circ\text{C}$. The data of temperature inside the chamber was transmitted to the computer for data collection. These data were used to calculate the standard uncertainty of temperature reading as follow in Equation 27 and 28.

$$\text{Mean value, } \bar{T} = \frac{1}{n_t} \sum_{i=1}^{n_t} T_i \quad \text{Eq. (27)}$$

where T_i are the temperature which measured by the OFT.

The standard uncertainty of the temperature reading is assigned by using the standard deviation of the mean, which was defined as follows:

$$u_{T,rd} = s(\bar{T}) = \frac{s(T_i)}{\sqrt{n_t}} \quad \text{Eq. (28)}$$

3.2) Type B evaluation

3.2.1) The standard uncertainty of OFT based on its calibration data, $u_{\Delta T, cert}$ was evaluated by:

$$u_{\Delta T, cb} = \frac{u_{cb,t}}{\sqrt{3}} \quad \text{Eq. (29)}$$

where $u_{cb,t}$ is the uncertainty of the OFT corrected from the calibration certificate of the OFT, which was equal to $\pm 1^\circ\text{C}$.

3.2.2) The standard uncertainty of the OFT resolution, $u_{\Delta T, res}$ was assigned by using the half limit of the resolution of the OFT. As assuming a rectangular distribution, the standard uncertainty of the OFT resolution can define as follows:

$$u_{\Delta T, res} = \frac{(Resolution/2)}{\sqrt{3}} \quad \text{Eq. (30)}$$

where the resolution of the OFT was 0.1°C

3.2.3) The standard uncertainty of OFT, which was affected by the vacuum pressure inside drying chamber, $u_{\Delta T, vc}$ was assigned by estimated the value and evaluated by:

$$u_{\Delta T, vc} = \frac{(u_{vc, es})}{\sqrt{3}} \quad \text{Eq. (31)}$$

where $u_{vc,es}$ is the estimated uncertainty of the OFT, which was affected by the vacuum pressure, is equal to $\pm 1^\circ\text{C}$.

4) Effective degree of freedom

The effective degrees of freedom of the combined standard uncertainty of the temperature measurement, $v_{T,eff}$ was evaluated using the Welch-Satterthwaite formula (Equation 32):

$$v_{T,eff} = \frac{(u_{T,x})^4}{\frac{u_{T,rd}^4}{v_{T,rd}} + \frac{u_{\Delta T,cb}^4}{v_{T,cb}} + \frac{u_{\Delta T,res}^4}{v_{T,res}} + \frac{u_{\Delta T,vc}^4}{v_{T,vc}}} \quad \text{Eq. (32)}$$

5) Expanded uncertainty

Form the result of the effective degrees of freedom for the combined standard uncertainty. The coverage factor k_c was obtained from the “t” distribution table (Table 4) at the appropriate degrees of freedom and confidence level. The expanded uncertainty was calculated by:

$$U_T = k_c u_{T,x} \quad \text{Eq. (33)}$$

3.4.2 Uncertainty of weight measurement

Weight was another essential parameter embedded in the DMLC system in order to calculate the real-time moisture content. The correct calculation of real-time moisture content with the accurate weighing system can lead to the correct decision in the DMLC regulation during the MFD process. In order to evaluate the uncertainty of weight measurement. A load-cell model Snug 3 (Jadever Scale Co., Ltd, Taiwan) was placed in the chamber and connected to the signal converter and computer for data collection, as shown in Figure 25. The load-cell system signal gave the resolution of weight at 0.01 g. The weighing system's uncertainty was determined by the standard weight for balance in the range of 0–150 g under 100 Pa vacuum pressure. The data of the standard weight was transmitted to the computer for data collection. These data are used to evaluate the uncertainty of weight measurement.

The uncertainty of the weight measurement was evaluated by considering the effect of the weight reading, the uncertainty base on its calibration data, the load-cell resolution, the effect of the vacuum pressure inside the drying chamber, and the effect of the rotation tray. The uncertainty measurement of the weight system according to the GUM is described as the following subtopic.

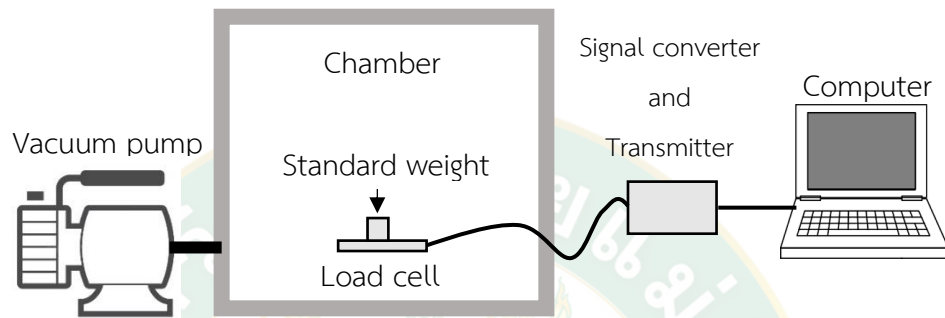


Figure 25 Weight measurement equipment setup.

1) Mathematical model

The mathematical model for the weight measurement, W_x was given by:

$$W_x \cong W_{rd} + \Delta W_{cb} + \Delta W_{res} + \Delta W_{vc} + \Delta W_{rot} \quad \text{Eq. (34)}$$

where W_{rd} is the weight reading of the load-cell, ΔW_{cb} is the weight reading error of the load-cell based on its calibration data, ΔW_{res} is the weight reading error due to the resolution of the load-cell, ΔW_{vc} is the weight reading error of the load-cell, which was affected by the vacuum pressure, and ΔW_{rot} is the weight reading error of the load-cell, which was affected by rotating the tray.

2) Uncertainty equation

The combined standard uncertainty of the weight measurement, $u_{W,x}$ is given by:

$$u_{W,x} \cong \sqrt{[u_{W,rd}^2 + u_{\Delta W,cb}^2 + u_{\Delta W,res}^2 + u_{\Delta W,vc}^2 + u_{\Delta W,rot}^2]} \quad \text{Eq. (35)}$$

where $u_{W,rd}$ is the standard uncertainty of the weight reading, $u_{\Delta W,cb}$ is the standard uncertainty of the load-cell base on its calibration data correction, $u_{\Delta W,res}$ is the standard uncertainty of the load-cell resolution, $u_{\Delta W,vc}$ is the standard uncertainty of load-cell, which was affected by the vacuum pressure inside the drying chamber, and $u_{\Delta W,rot}$ is the standard uncertainty of load-cell which was affected by rotating the tray.

3) Standard uncertainty evaluation

3.1) Type A evaluation

3.1.1) The standard uncertainty of the weight reading under the vacuum pressure 100 Pa, $u_{W,rd}$ was assigned by using Equation 34 and 35.

$$\text{Mean value, } \bar{W} = \frac{1}{n_t} \sum_{i=1}^{n_t} W_i \quad \text{Eq. (36)}$$

where W_i are the weight which measured by the load-cell.

The standard uncertainty of the weight reading under vacuum pressure 100 Pa is assigned using the standard deviation of the mean, which was defined as follows:

$$u_{W,rd} = s(\bar{W}) = \frac{s(W_i)}{\sqrt{n_t}} \quad \text{Eq. (37)}$$

3.2) Type B evaluation

3.2.1) The standard uncertainty of load-cell base on its calibration data, $u_{\Delta W,cb}$ was evaluated by:

$$u_{\Delta W,cb} = \frac{u_{cb,w}}{\sqrt{3}} \quad \text{Eq. (38)}$$

where $u_{cb,w}$ is the standard uncertainty of the load-cell corrected from the calibration certificate of the load-cell, which was equal to ± 0.1 g.

3.2.2) The standard uncertainty of the load-cell resolution, $u_{\Delta W, res}$ was assigned by using the half limit of the load-cell resolution. As assuming a rectangular distribution, the standard uncertainty of the load-cell resolution can define as follows:

$$u_{\Delta W, res} = \frac{(Resolution/2)}{\sqrt{3}} \quad \text{Eq. (39)}$$

where the resolution of load-cell was 0.01 g.

3.2.3) The standard uncertainty of the load-cell, which was affected by the vacuum pressure inside the drying chamber, $u_{\Delta W, vc}$ was assigned by the estimated value. As assuming a rectangular distribution, the standard uncertainty of the load-cell, which was affected by the vacuum pressure inside the drying chamber, can define as follows:

$$u_{\Delta W, res} = \frac{(u_{vc, es})}{\sqrt{3}} \quad \text{Eq. (40)}$$

where $u_{vc, es}$ is the estimated uncertainty of the load-cell, which was affected by the vacuum pressure, equal to ± 0.2 g.

3.2.4) The standard uncertainty of the load-cell, which was affected by rotating the tray, $u_{\Delta W, rot}$ was assigned by the estimated value. As assuming a rectangular distribution, the standard uncertainty of the load-cell, which was affected by rotating the tray, can define as follows:

$$u_{\Delta W, rot} = \frac{(u_{rot, es})}{\sqrt{3}} \quad \text{Eq. (41)}$$

where $u_{rot,es}$ is the estimated uncertainty of the load-cell, which was affected by rotating the tray, equal to ± 0.2 g.

4) Effective degree of freedom

The effective degrees of freedom of the combined standard uncertainty of the weight measurement ($v_{w,eff}$) was evaluated by using the Welch-Satterthwaite formula (Equation 42):

$$v_{w,eff} = \frac{(u_{W,x})^4}{\frac{u_{\Delta W,rd}^4}{v_{W,rd}} + \frac{u_{\Delta W,cb}^4}{v_{W,cb}} + \frac{u_{\Delta W,res}^4}{v_{W,res}} + \frac{u_{\Delta W,vc}^4}{v_{W,vc}} + \frac{u_{\Delta W,rot}^4}{v_{W,rot}}} \quad \text{Eq. (42)}$$

5) Expanded uncertainty

Form the result of the effective degrees of freedom for the combined standard uncertainty of the weight measurement. The coverage factor k_c was obtained from the “t” distribution table (Table 4) at the appropriate degrees of freedom and level of confidence. The expanded uncertainty was calculated by:

$$U_W = k_c u_{W,x} \quad \text{Eq. (43)}$$

3.4.3 Uncertainty of moisture content calculation

The real-time moisture content of carrot slices during the MFD process was calculated from Equation 44.

$$M_r = M_i - \left[\frac{(W_{in} - W_r)}{W_{in}} \times 100 \right] \quad \text{Eq. (44)}$$

where M_r is the real-time moisture content, M_i is the initial moisture content, W_{in} is the initial materials weight and W_r is the real-time materials weight.

The uncertainty of the real-time moisture content calculation (U_{MC}) was calculated by Equation 45.

$$U_{MC} = 2U_{W,in} + U_{W,r} \quad \text{Eq. (45)}$$

where $U_{W,in}$ is the uncertainty of the initial weight measurement and $U_{W,r}$ is the uncertainty of the real-time weight measurement.

3.5 Part I: Variation of temperature during microwave-freeze drying process experiment

3.5.1 Experimental procedure

In this study, the temperature variation during MFD using closed-loop temperature control (CLT) was investigated to improve temperature variations and study its effects on the product quality. Experimentation was conducted using three drying methods: FD, MFD without CLT, and MFD with CLT, respectively.

FD: The experiment was conducted using a freeze dryer (Model Scanvac Coolsafe 110-4, Labogene ApS, Denmark). The cooling system was set at -40°C . One hundred grams of the sample with 10 mm material thickness were dried at 100 Pa constant vacuum pressure until the sample moisture content was reduced to 6% (wet basis). The material temperature was monitored but not controlled.

MFD without CLT: The experiment was conducted using a laboratory-scale Microwave freeze dryer which the researcher developed. The experiment was conducted at a fixed microwave power of 100 W. The cooling system was set at -40°C . One hundred grams of the sample with 10 mm material thickness were dried at 100 Pa constant vacuum pressure until the moisture content was reduced to 6% (wet basis). The material temperature was monitored but not controlled. The microwave was controlled with the on/off duty cycle operation of the magnetron.

MFD with CLT: The experiment was conducted using a laboratory-scale Microwave freeze dryer which the researcher developed. The experiment was conducted by applying a microwave power of 100 W with CLT at a constant

temperature of 40°C by using the CLT. The temperature of the cooling systems was set at -40°C. One hundred grams of the sample with 10 mm material thickness were dried at a constant vacuum pressure of 100 Pa until the sample moisture content was reduced to 6% (wet basis).

All experiments were carried out in triplicate to obtain the average material temperature and moisture content. In all the treatment conditions, the dried samples were stored in aluminum foil bags and sealed for further qualitative analysis. The temperature curve and drying curve of the material was analyzed using the average temperature and moisture content.

3.6 Part II: Development of closed-loop control system for microwave freeze-drying

3.6.1 Logic design of a closed-loop control system

A logic design of the closed-loop control (CLC) system for MFD was developed (Figure 26). Firstly, the input values for the desired final state material temperature (T_m) 40°C, holding temperature (T_h) 1°C, initial moisture content (M_i) 92%, the final moisture content (M_f) 6%, and microwave power levels for the process control of DMLC were manually inputted into the CLC system. Once the logic started, the stage of the MFD process was determined by the DMLC. The DMLC collected the carrot's weight and real-time temperature (T_r) during the MFD process to calculate the real-time moisture content (M_r) according to the mode of the increase or decrease in temperature. Simultaneously, the DMLC adjusted the level of the microwave power depending on the carrot's moisture content and drying rate as it sends the feedback of its T_r . In the initial drying stage, where the T_r was less than the lower setting point ($T_m - T_h$), the temperature increasing mode was selected for the MFD operation to raise the carrot's temperature. During the interval, the temperature sensor was sensing the carrot's temperature and then sending the feedback to the CLC system to select the appropriate control mode. When the real-time temperature (T_r) reached the upper limit ($T_m + T_h$), the control mode switched to a decreasing mode to avoid temperature overshooting and sample burning. In the final stage, the

final temperature of the carrot was controlled at the endpoint of $40\pm 1^{\circ}\text{C}$ to maintain the color and nutrients in the carrot slices (Gamboa-Santos et al., 2013). The adjustment and loop-setting of the microwave power levels in relation to the moisture content was accomplished automatically by the DMLC until the carrot reached a final moisture content of $6\pm 1\%$.



3.6.2 Microwave freeze-drying experiment

To develop the DMLC, the MFD experiment was performed to obtain the drying characteristics of the carrot and followed by a two-part analysis. In the first part, the MFD without DMLC was performed by drying 100 ± 0.1 g of carrot slices at fixed microwave power levels of 100 W, 200 W, and 300 W at a constant pressure of 100 Pa. The real-time temperature and weight were collected and used for the calculation of the real-time moisture content. As the MFD progressed, the temperature of the carrot slices increased over time but was held at $40\pm 1^\circ\text{C}$ to maintain their quality. The MFD process continued until the real-time moisture content of the carrot slices reached $6\pm 1\%$ (termination point of the process). The experiment was performed in triplicate. The drying curve and drying rate of the carrot were analyzed for drying efficiency, quality, and phases of drying to be used in the succeeding part.

The second part of the MFD experiment was to compare the drying of carrot slices between MFD with DMLC and MFD without DMLC. After the data from the first part were analyzed, the drying strategy was identified. The logic coding was then developed and embedded into the DMLC program. The MFD with DMLC was performed by drying 100 ± 0.1 g of carrot slices under 100 Pa vacuum pressure using selective microwave power levels, real-time moisture content, and temperature following the designated drying strategy. As MFD with DMLC progressed, the temperature of the carrot slices increased over time but was held at 40°C to maintain their quality. The MFD process continued until the real-time moisture content of the carrot decreased to $6\pm 1\%$ (termination point of the process). The experiment was conducted in triplicate. MFD with and without the DMLC was evaluated and compared based on their drying efficiency, energy consumption, and resulting product quality.

The MFD process was also compared with the conventional FD process serving as the control. A freeze-dryer with an established cooling system of -40°C (Model Scavac Coolsafe 110-4, Labogene ApS, Denmark) was utilized for the FD. Ten-millimeter-thick carrot slices weighing 100 ± 0.1 g was dehydrated at a continuous

vacuum pressure of 100 Pa until the moisture content was lowered to $6\pm 1\%$ (wet basis). Both the moisture content and temperature were observed but not regulated.

3.6.3 Microwave freeze-drying characterization

For the MFD characterization, the kinetics models were analyzed. The moisture content of the material was expressed in a wet basis, and the moisture ratio (MR) was determined using Equation 46.

$$MR = \frac{M_t - M_e}{M_i - M_e} \quad \text{Eq. (46)}$$

where MR is the moisture ratio, M_i , M_t are the initial moisture content and moisture content at time t (%wet basis), respectively, and M_e is the equilibrium moisture content (% wet basis). The mathematical modeling of the MFD kinetics was determined using the semi-theoretical mathematical models were selected, namely, Newton's model (McMinn et al., 2005), Page's model (Amiri Chayjan et al., 2015), the Henderson and Pabis model (Ghazanfari et al., 2006), the Midilli et al.'s model (Midilli et al., 2002), Diffusion approximation, and Logarithmic model (Yaldız and Ertekyn, 2001) as presented in Table 5.

Table 5 Mathematical models used for fitting the experimental data.

Model name	Model equation
Newton	$MR = \exp(-kt)$
Page	$MR = \exp(-kt^n)$
Henderson and Pabis	$MR = a \exp(-kt)$
Logarithmic	$MR = a \exp(-kt) + bt$
Midilli et al.	$MR = a \exp(-kt^n) + bt$
Diffusion approach	$MR = a \exp(-kt) + (1 - a) \exp(-kbt)$

In Table 5, the drying rate constant (k) and the equation constants (a , b and n) were determined by the non-linear regression method. The goodness of fit of the mathematical modeling of the MFD kinetics to the experimental data was calculated by utilizing statistical parameters, which also consisted of the coefficient of determination (r^2), sum of squared error (SSE) and root mean square error ($RMSE$) (Torki-Harchegani et al., 2016), as shown in Equations 47, 48 and 49. The obtained drying rate constant (k) and fitting parameter were used for the comparison of the MFD kinetics.

$$r^2 = 1 - \frac{\sum_{i=1}^{n_t} (MR_{exp.i} - MR_{pre.i})^2}{\sum_{i=1}^{n_t} (MR_{exp.i} - \overline{MR})^2} \quad \text{Eq. (47)}$$

$$SSE = \frac{1}{n_t} \sum_{i=1}^{n_t} (MR_{exp.i} - MR_{pre.i})^2 \quad \text{Eq. (48)}$$

$$RMSE = \left[\frac{1}{n_t} \sum_{i=1}^{n_t} (MR_{exp.i} - MR_{pre.i})^2 \right]^{0.5} \quad \text{Eq. (49)}$$

3.6.4 Estimation of moisture diffusivity

While undertaking the MFD process, the moisture transfer was calculated using a simple diffusion model founded on Fick's second law. By using slab body assumption for the carrot slices, the moisture transfer was obtainable. This being (1) the preliminary moisture is equally allocated on the complete mass of the sample, and (2) the outward opposition and contraction are insignificant throughout the dehydration process. Assuming that the carrot slices were considered as an unlimited slab, as they were thicker (10 mm) than the diameter (35 mm) (Demirhan and Özbek, 2011; Nguyen and Price, 2007), the authors applied Fick's second law of diffusion. (Crank, 1975) provided an equation for analyzing the diffusion to show the continuous moisture diffusivity (D). This is shown in Equation 5 as follows (Amiri Chayjan et al., 2017; Crank, 1975; Süfer et al., 2017):

$$MR = \frac{8}{\pi^2} \exp\left(\frac{-\pi^2 Dt}{L^2}\right) \quad \text{Eq. (50)}$$

where, D is the moisture diffusivity (m^2/s), L is the thickness of the carrot slices (m), and t is the drying time(s). Equation 50 was simplified into a logarithmic form and evaluated numerically for the Fourier number, $F_0 = D \cdot t/L^2$ in Equation 51 and further calculated for moisture diffusivity (D). Thus, Equation 50 could be re-written into Equations 51-53 as follows (Sharma and Prasad, 2004; Younis et al., 2018):

$$\ln(MR) = \ln \frac{8}{\pi^2} - \pi^2 F_0 \quad \text{Eq. (51)}$$

$$F_0 = -0.10124 \ln(MR) - 0.02134 \quad \text{Eq. (52)}$$

$$D = \frac{F_0 L^2}{t} \quad \text{Eq. (53)}$$

3.7 Qualitative and statistical analysis

3.7.1 Color analysis

The color of the carrot slices was measured using a spectrophotometer model MiniScan XE Plus (Hunter Associates Laboratory, Inc., USA). The spectrophotometer was calibrated with the certified standard white and black plate. The configuration of the light source was D65/10°. To measure the color, the sample was randomly snap flashed on the carrot's surface. The color parameters were reported in the CIE L*-a*-b* scale where L* indicated the lightness, and a* (green to red) and b* (blue to yellow) indicate the chromatic elements.

3.7.2 Texture analysis

The texture characteristics of the dried carrot were assessed with a texture analyzer model TA-XT2 (Stable Micro System Ltd., UK) using a 2 mm-cylindrical penetration probe. The probe penetrated through the sample at a speed of 2 mm/s. The trigger force and penetration distance were set to 20 g and 50%, respectively. A

force-time curve was analyzed using Texture Exponent 32 software (Stable Micro System Ltd., UK). The hardness of the carrot was assessed by the maximum force required to rupture the dried carrots. The crispness of carrot slices was characterized by the number of peaks with the threshold values of 30 g force, while the larger number of peaks resulting in higher crispness (Raikham et al., 2013). Three different samples were tested for each MFD treatment, and the average of the hardness and crispness were reported.

3.7.3 Rehydration ratio

The MFD samples were evaluated for their rehydration capacity, determined by soaking 3 grams of dried sample in 300 ml of distilled water at a temperature of 25°C for one minute. Following this, the sample was taken out of the water, the excessive water was siphoned, and the rehydrated sample checked for any differentiation in the weight. The proportion of the rehydration sample was evaluated by the rehydrated weight per dried sample.

3.7.4 Shrinkage ratio

The shrinkage of the carrot slices was defined by Equation 54, where d_f and d_i refer to the diameter of the dried and fresh carrot slices, respectively. The higher the value, the more severe was the shrinkage of the dried carrot.

$$\%Shrinkage = \frac{(d_i - d_f)}{d_i} \times 100 \quad \text{Eq. (54)}$$

3.7.5 Energy consumption

For the MFD process, the energy consumption was measured using the energy used for the microwave system, a cold trap system, and a vacuum pump. For the FD process, the energy consumption involved only the energy used for the cold trap and vacuum pump since the heating element of the FD was minimal and therefore negligible. The energy consumption was measured using a power meter model

PZEM-061 (Ningbo Peacefair Electronic Co., Ltd., China). The reading from the power meter of kWh was converted to MJ where 1 kWh = 3.6 MJ.

3.7.6 Specific moisture extraction rate

The specific moisture extraction rate (*SMER*), defined by the ratio of the amount of moisture removed ($kg_{moisture}$) per kilowatt-hour (*kWh*) energy consumption, is the parameter used to indicate the efficiency of the energy consumption of the drying process. The *SMER* was determined by using Equation 55 (Chua et al., 2002; Prasertsan and Saen-saby, 1998).

$$SMER = \frac{\text{Amount of moisture removed}}{\text{Total energy consumption}}, \left(\frac{kg_{moisture}}{kWh} \right) \quad \text{Eq. (55)}$$

3.7.7 Statistical analysis

The data were analyzed for the Analysis of Variance (ANOVA) on SPSS 24.0 (SAS Institute Inc., USA). Duncan's new multiple range test was utilized to compare the mean, and the results showed that the data had significant differences at a p-value < 0.05.

CHAPTER 4

RESULTS AND DISCUSSION

4.1 Equipment setup for Microwave freeze dryer

In this research, the laboratory-scale microwave freeze dryer, which was developed, consists of the five main components, e.g., MFD drying chamber, CLC system, refrigeration system, cold trap, and vacuum system, as shown in Figure 27.

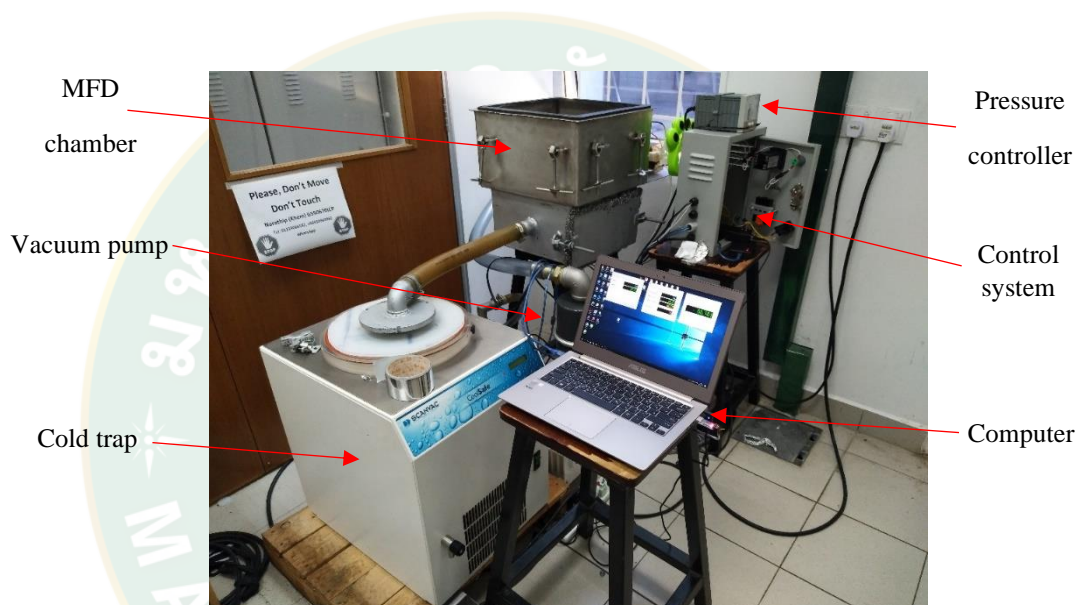


Figure 27 Laboratory-scale microwave freeze dryer setup.

During the MFD process, vapor, either from sublimation or evaporation, was generated inside the MFD cavity. This vapor was sucked out from the cavity by a rotary oil-sealed vacuum pumps (Model Alcatel 2033SD, Pfeiffer Vacuum Technology AG, Germany) and condensed inside the cold trap under a temperature of -40°C , cooled by the refrigeration system to condense the vapor during the MFD process. This can stop water vapor from accessing the vacuum pump, which could impair the pump operations. The vacuum pressure applied at a constant pressure of 100 Pa during the MFD process, maintained by the vacuum pump, attached with pressure controller model AGP-M-NW16 (Edwards Limited, UK). The vacuum mechanism

comprises a separate vacuum pump linked to and fixed to the MFD drying chamber by an airtight cold trap.

Figure 28 shows the MFD drying chamber, which was developed based on the commercial household microwave oven. The MFD drying chamber dimension was 500 mm width, 500 mm length, and 450 height. The material of the MFD drying chamber is stainless steel 304, which can reflect microwaves. This material can help the microwaves distribute evenly and can avoid the arcing. The 6 mm thickness of the MFD drying chamber wall was selected to resist the high vacuum pressure during the MFD process. Moreover, the cover of the MFD drying chamber was sealed with the flexible stainless-steel tubing to avoid microwave leakage and the rubber gasket to seal the cover when the vacuum pump was working. The microwave leakage was detected by microwave leakage detector model MD-2000 (Less EMF, USA). During the experiment, the microwave did not leak from the MFD drying chamber, indicating that the flexible stainless-steel tubing can prevent the microwave leakage.

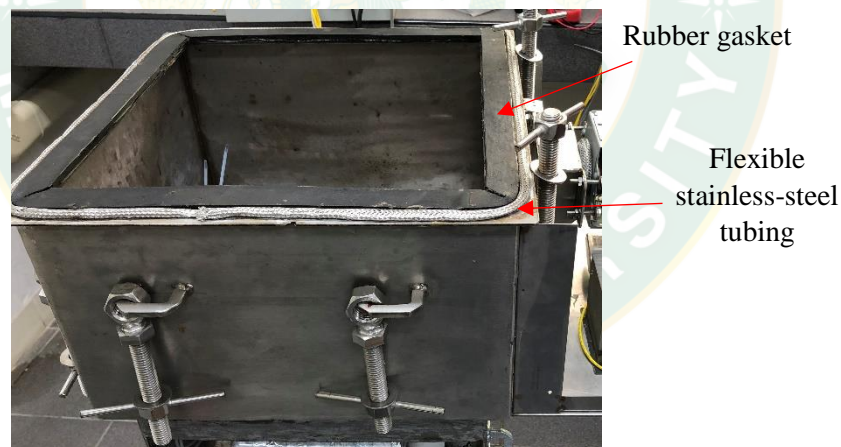


Figure 28 Microwave freeze-drying chamber.

Figure 29a shows the component of a microwave generation system which consists of a magnetron, waveguide, transformer, and cooling fan. A transformer transforms the 220V input voltage to about 2,200V to supply the magnetron. A magnetron at a frequency of 2.4 GHz capable of 0-900 W was attached to the MFD cavity. A magnetron converted the electrical energy into a microwave and conveyed

it to the MFD cavity by a rectangular waveguide. The waveguide dimension was 50 mm width, 90 mm length, similar to the commercial household microwave oven. During the magnetron generate microwave, it also generated heat. If the magnetron is overheating, it would affect the efficiency of the microwave generation and damage the equipment. Thus, the fan is installed to cool the magnetron and transformer. In addition, the microwave generation system was covered with stainless steel sheets with a small ventilation hole of 2 mm (diameter) as in the Figure 29b to avoid microwave leakage and the electrometric field generated from the magnetron and transformer, which can interfere with the electronic component and the control system. The microwave leakage was detected by microwave leakage detector model MD-2000 (Less EMF, USA). During the experiment, the microwave did not leak from the microwave generation system.

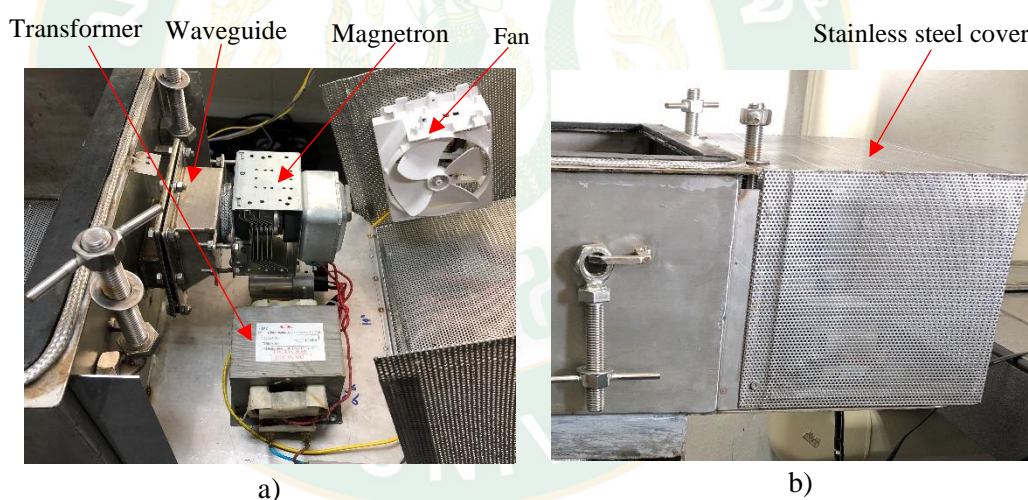


Figure 29 Microwave generation system.

- a) A component of microwave generation system
- b) Microwave generation system with stainless steel cover

Figure 30 shows the installation of the load-cell, tray, and rotating motor. A load cell model Snug 3 (Jadever Scale Co., Ltd, Taiwan) was placed inside the cavity underneath the tray to monitor the sample's real-time weight loss. The rotating motor is installed on the top of the load-cell connected with the tray. This motor is

a synchronous motor used in the commercial microwave oven, which has lightweight and almost no vibration. The motor rotated the tray with speed at four rounds per minute. The rotating tray help microwaves radiate to the samples evenly. The tray is made from a mica sheet which is microwave transparent materials and has lightweight. A stainless-steel sheet with a small ventilation hole of 2 mm (diameter) was installed between the tray and the motor to prevent microwaves and electric fields from disturbing the load cell's signal, leading to the signal beating and causing the weight reading error.

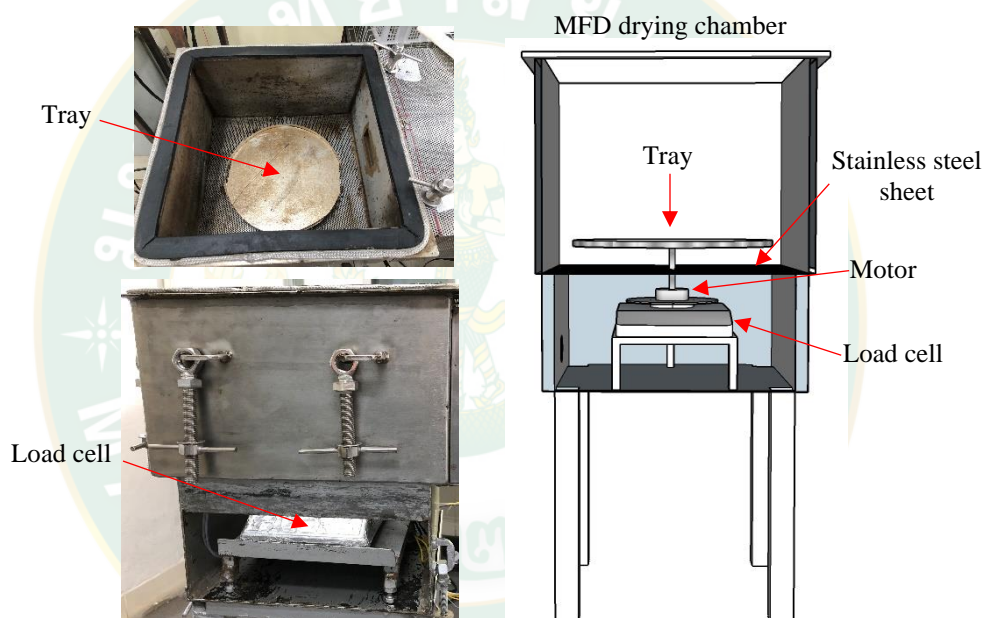


Figure 30 Installation of the load-cell, tray, and the rotating motor.

Figure 31 shows the hardware of the control system. During the MFD process, the sample's temperature was detected and used in the CLT system to control the final state of the MFD process. To collect the sample's temperature at its center-point, an optical fiber temperature probe size of 3 mm in diameter model SR-G (Fuzhou Skyray Opto-electronic Technology Co. Ltd., China) was used to ensure the non-interference of the temperature measurement with the electromagnetic field in the MFD cavity. In addition, a load cell model Snug 3 (Jadever Scale Co., Ltd, Taiwan)

was used to detect the sample's real-time weight loss during the MFD process. The signal from the temperature probe and the load cell was converted by a signal converter. The output signals from both the load cell and temperature signal converter were sent to the central processing unit, embedded with the microcontroller model Atmega2560 (Microchip Technology Inc., USA) for the moisture content calculation and process control regulation. The output signals used to control the magnetron were sent from the central processing unit to the relay to control the on/off cycle for adjusting the microwave power levels and control the material temperature in the final state of the MFD process. To verifying the accuracy of the measuring systems and moisture content calculation, the uncertainty of the measurement system and moisture content calculation was evaluated as in Part 0. During the MFD-DMLC process, the MFD with an embedded DMLC and the CLC system software was found to work correctly during the MFD process of carrot slices. The CLC system can detect the material temperature and material weight accurately. It can calculate the moisture content in real-time, and the process regulation works smoothly with no logical error control during the drying process.

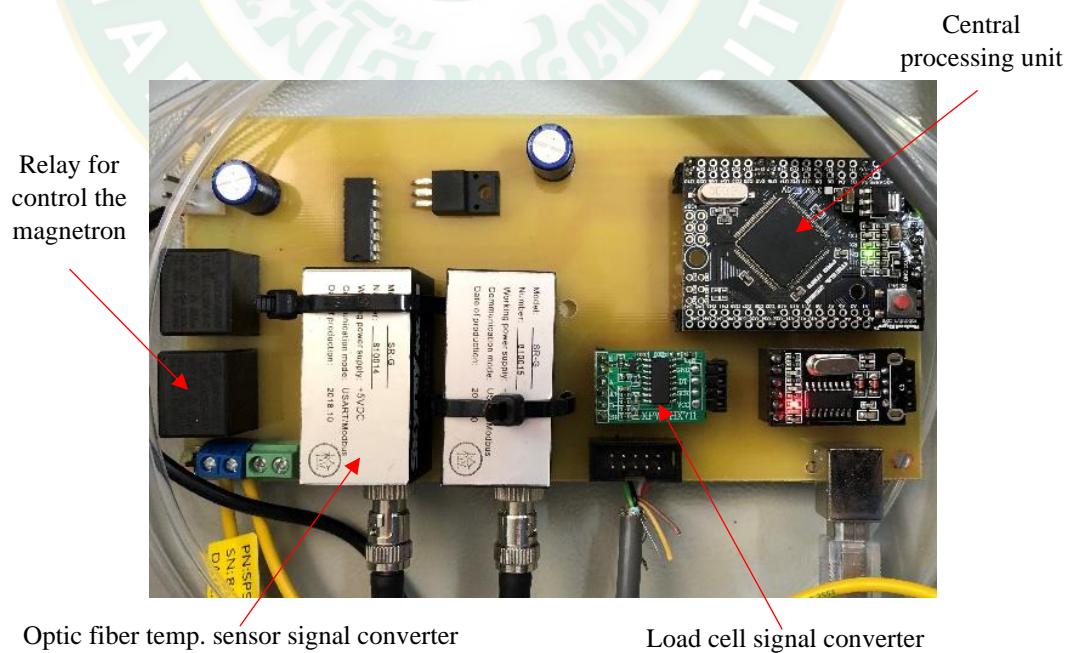


Figure 31 A control system hardware.

Figure 32 shows the software for displaying and configuring the process control strategy for the CLC system. This software was developed to support the CLC system, displaying and recording the sample's temperature, sample weight, microwave power, and moisture content. In addition, this software supported the configuration of the microwave power levels and the process control strategy for the DMLC. This software was developed using Microsoft visual studio 2019 with the visual basic language. The software processing diagram was shown in Figure 33, and the details are described below.

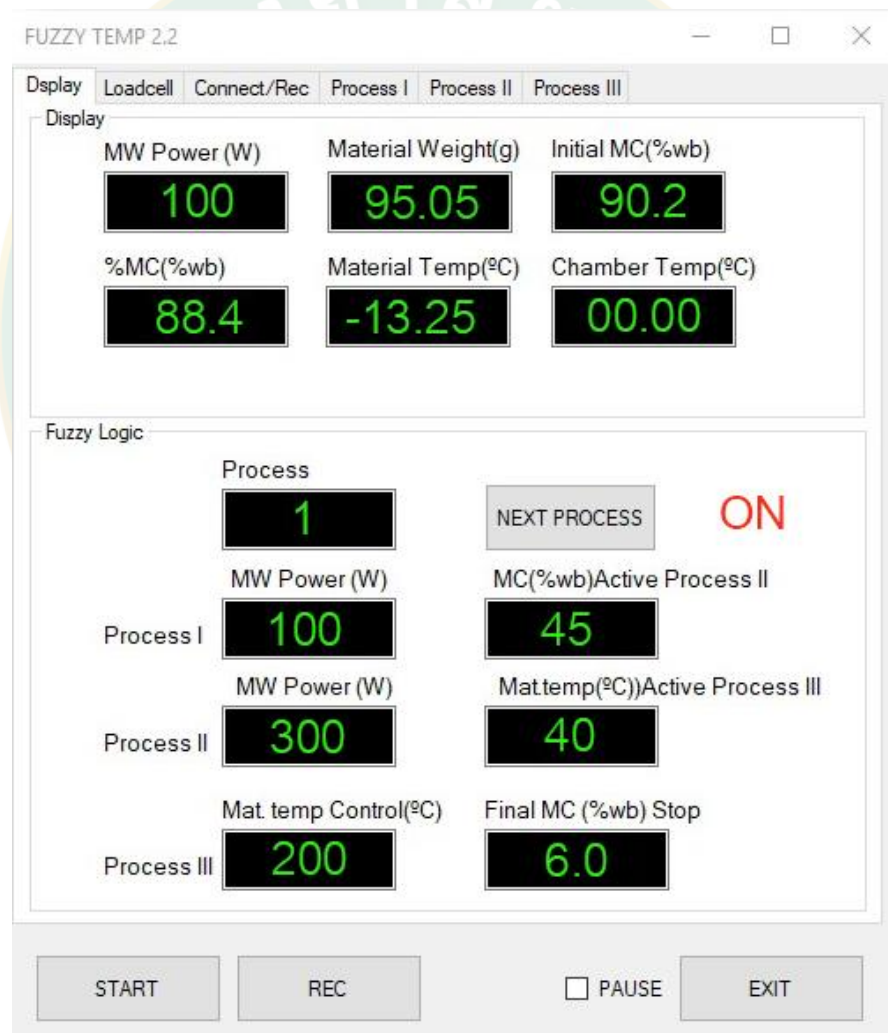


Figure 32 User interface of CLC system software.

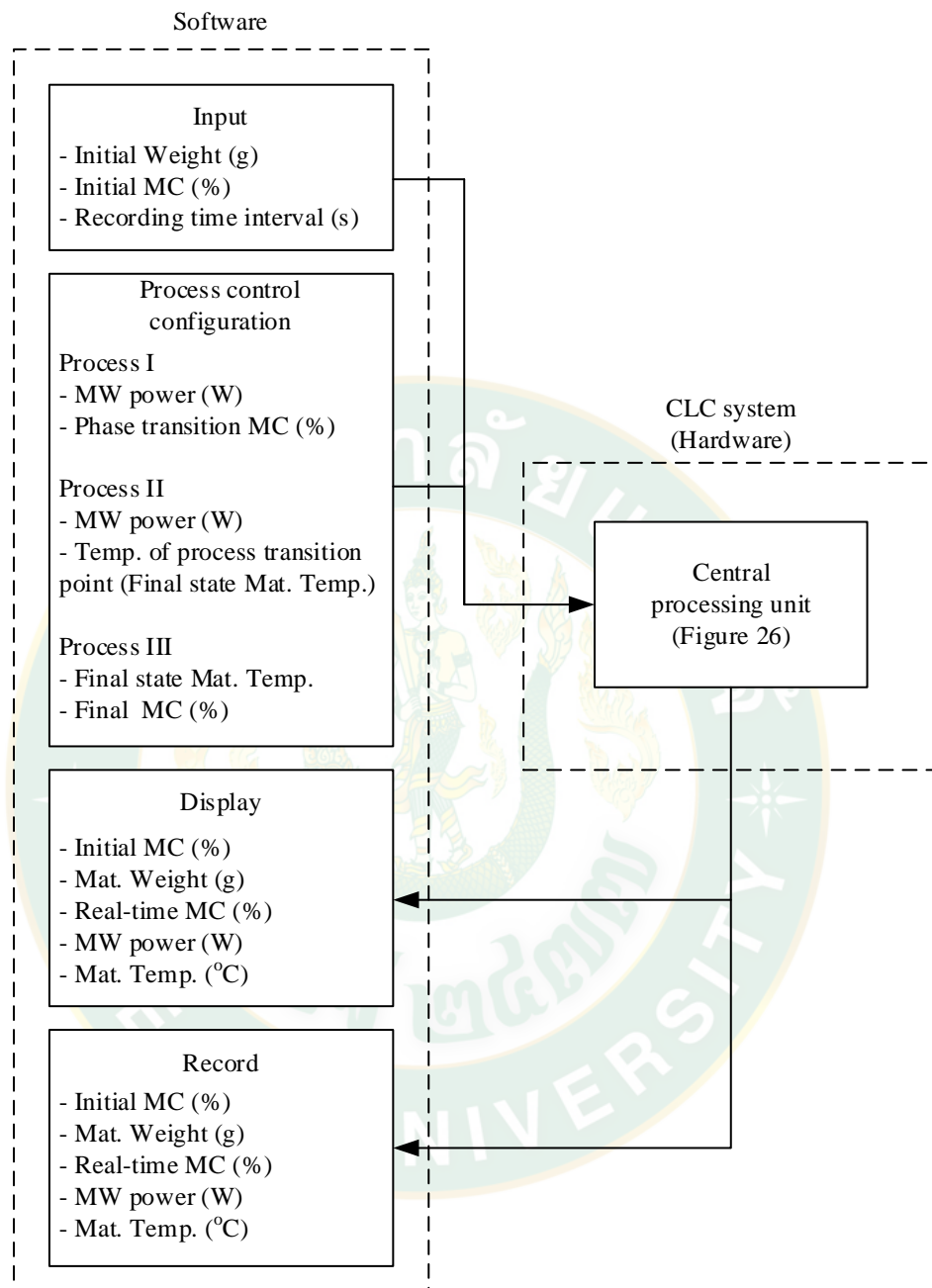


Figure 33 A software processing diagram.

From Figure 33, The input values of initial weight and moisture content were feed to the CLC system through the software for moisture calculation following Equation 24. During the MFD process, the material temperature, material weight, and moisture content were sent to the computer for display and recording the data

through the software. The record data consists of material temperature, material weight, moisture content, and microwave power levels. The average data was used to analyze the characteristic of the MFD process and design the DMLC. Moreover, this software was design for the process control configuration of the DMLC. It can input the desired values and send them to the PLC system for regulating the MFD process. This software can work properly with the PLC hardware and display the data in real-time. It helps the operation of the PLC system was more flexible and convenient.

4.2 Part 0: Uncertainty of the measurement system and moisture content calculation

4.2.1 Uncertainty of temperature measurement

According to the GUM, the uncertainty of temperature measurement results was evaluated by considering the effect of the temperature reading, the uncertainty based on its calibration data, the OFT resolution, and the impact of the vacuum pressure inside the drying chamber. The results of the standard uncertainty following Equation 25 to 31 were shown in Table 6.

Table 6 Uncertainty budget table for the uncertainty of temperature measurement calculation.

Source of uncertainty	Type	Uncertainty value (°C)	Probability distribution	Degree of freedom	Coverage factor
$u_{T,rd}$	A	0.05	-	9	-
$u_{\Delta T,cb}$	B	0.5	Normal	∞	2
$u_{\Delta T,res}$	B	0.03	Rectangular	∞	1.732
$u_{\Delta T,vc}$	B	0.58	Rectangular	∞	1.732

Equation 32 is used to determine the combined uncertainty of temperature measurement using the standard uncertainty from Table 6. The combined uncertainty of temperature calculation was $\pm 0.77^\circ\text{C}$, according to the results. For the combined normal uncertainty of temperature calculation, the effective degrees of

freedom are believed to be infinity (Equation 3.9). At a confidence level of about 95%, this results in a coverage factor of k_c equal 2 (Table 4). As a result of Equation 31, the temperature measurement uncertainty from a full-scale range of 30 – 50°C is 1.5°C or 3.9 percent.

Even though the MFD process requires temperature as one of the parameters to control the loop setting, the process's error due to uncertainty of temperature measurement may significantly affect the MFD process. However, the later results in this research show no significant effect of temperature difference on the quality of the product. It is possible that MFD process was not sensitive to the temperature fluctuation of 2°C; thus, the process gave approximately the same results of product quality, not being affected by the uncertainty of temperature measurement. Thus, the temperature measurement system with the uncertainty of temperature measurement of $\pm 1.5^\circ\text{C}$ is acceptable for use in the CLC system.

4.2.2 Uncertainty of weight measurement

According to the GUM, the results of the uncertainty of weight measurement were evaluated by considering the effect of the weight reading, the uncertainty base on its calibration data, the load-cell resolution, the effect of the vacuum pressure inside the drying chamber, and the effect of the rotation tray. The results of the standard uncertainty following Equation 36 to 41 as shown in Table 7.

Table 7 Uncertainty budget table for uncertainty of weight measurement calculation.

Source of uncertainty	Type	Uncertainty value (g)	Probability distribution	Degree of freedom	Coverage factor
$u_{W,rd}$	A	0.057	-	9	-
$u_{\Delta W,cb}$	B	0.050	Normal	∞	2
$u_{\Delta W,res}$	B	0.003	Rectangular	∞	1.732
$u_{\Delta W,vc}$	B	0.115	Rectangular	∞	1.732
$u_{\Delta W,rot}$	B	0.115	Rectangular	∞	1.732

The standard uncertainty in Table 7 was used to calculate the combined uncertainty of weight measurement as following Equation 35. The result shows that the combined uncertainty of weight measurement was ± 0.174 grams. The effective degree of freedom for the combined standard uncertainty of weight measurement, $u_{W,x}$ was assumed to be infinity (Equation 40). This gives a coverage factor k_c equals 2 (Table 4) at a level of confidence of approximately 95%. Therefore, the uncertainty of weight measurement according to Equation 43 is ± 0.347 grams or 0.8% from a full-scale range of 0 – 150 grams.

During the MFD process with the CLC system, material weight is the one parameter used to calculate the moisture content of the materials. The error of the moisture content calculations may lead to the error of the MFD process control. However, the later result in the uncertainty of moisture content calculation (section 4.1.3) shows good results, which can confirm that the weight measurement system with the uncertainty of weight measurement of ± 0.347 grams is acceptable for use in the CLC system.

4.2.3 Uncertainty of moisture content calculation

The real-time moisture content was used to control the loop setting for the CLC system during the MFD process and detected the final moisture content of the materials. During the MFD process, the real-time moisture content calculation was calculated from the real-time material weight detected by the weight measurement system. The calculation of the uncertainty of real-time moisture content was evaluated based on the uncertainty of weight measurement. The result shows that the uncertainty of real-time moisture content calculation according to Equation 45 is $\pm 1\%$ (wet basis). The error of the process control due to moisture content calculation uncertainty may significantly affect the MFD process. However, the later results in terms of product quality are approximately the same in each experimental treatment's repetition. This can be indicated that the weight measurement system and moisture calculation process can work properly and did not affect the research results under the uncertainty of weight measurement of ± 0.347 grams and the uncertainty of real-time moisture content calculation of $\pm 1\%$ (wet basis). Thus, the

moisture content calculation process based on real-time materials weight was acceptable for use in the PLC system.

4.3 Part I: Variation of temperature during microwave freeze-drying process

4.3.1 Effect of temperature variation during microwave freeze-drying process

Figure 34-36 presents variations of temperature of the carrot slices versus moisture content during FD, MFD, and MFD with CLT of carrot slices at the microwave power of 100W and the terminal temperature of 40°C. The results show that the traditional FD process requires a longer drying time (16.5 hours) due to the low heat transfer rate inside the samples at low vacuum pressure (Ceballos et al., 2012), while MFD with and without CLT requires a shorter drying time (9 hours) due to the rapid heating in materials through the use of microwave energy. The volumetric-heat generation inside the samples involves two mechanisms: dipole rotation and ionic conduction. These mechanisms occur simultaneously, as the electrical oscillation induces the ions to align the ions within the electromagnetic field. The electromagnetic energy in this process is converted to kinetic energy and absorbed in all parts of the sample at the same time. (Song et al., 2018; Varith et al., 2007). Thus, microwaves can accelerate the freeze-drying process.

In Figure 34-36, both MFD with and without CLT process clearly show two phases: sublimation and desorption phase, as well as in the MFD of banana (Jiang et al., 2014), sea cucumber (Duan et al., 2010b), instant vegetable soup (Wang et al., 2009), potato (Wang et al., 2010b), and cabbage (Duan et al., 2007a). The first, the sublimation phase, exhibits a gradual increase in temperature. The second, the desorption phase, comprises an initial sharp increase followed by a slower increase in sample temperature until the terminal moisture content is achieved. During the sublimation phase, the ice sublimates until the moisture content drops to approximately 22±1% (wet basis). After that, the sample temperature increases sharply until it reaches the final state temperature, which indicates the onset of the desorption phase. Thus, the moisture content of 22±1% (wet basis) can be regarded

as the transition moisture content and denotes the end-point of sublimation and the onset of the desorption phase.

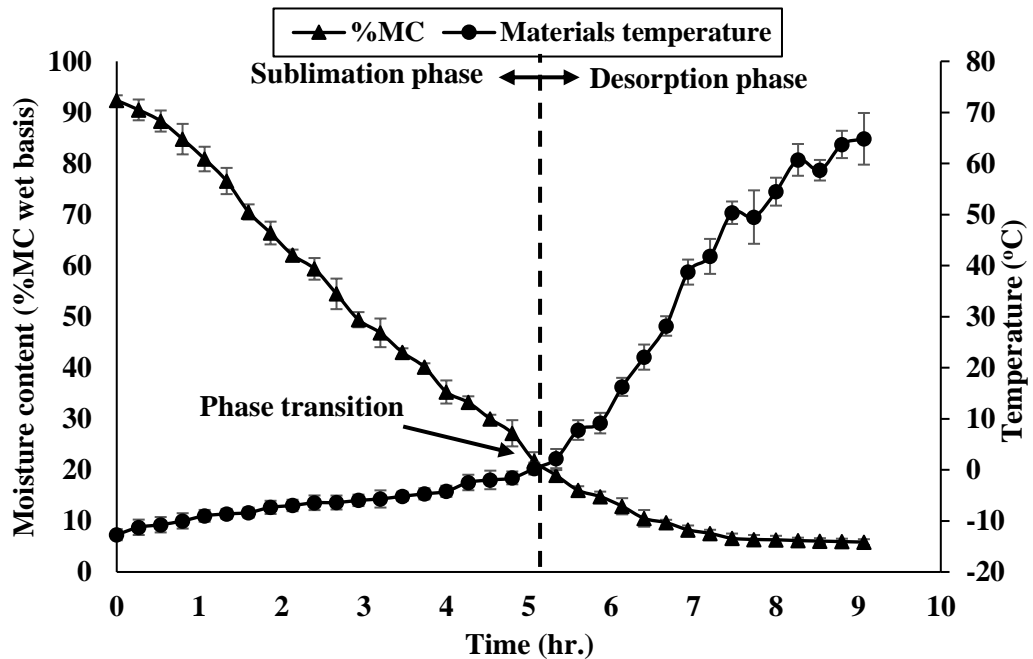


Figure 34 Moisture content and temperature of carrot slices from MFD process.

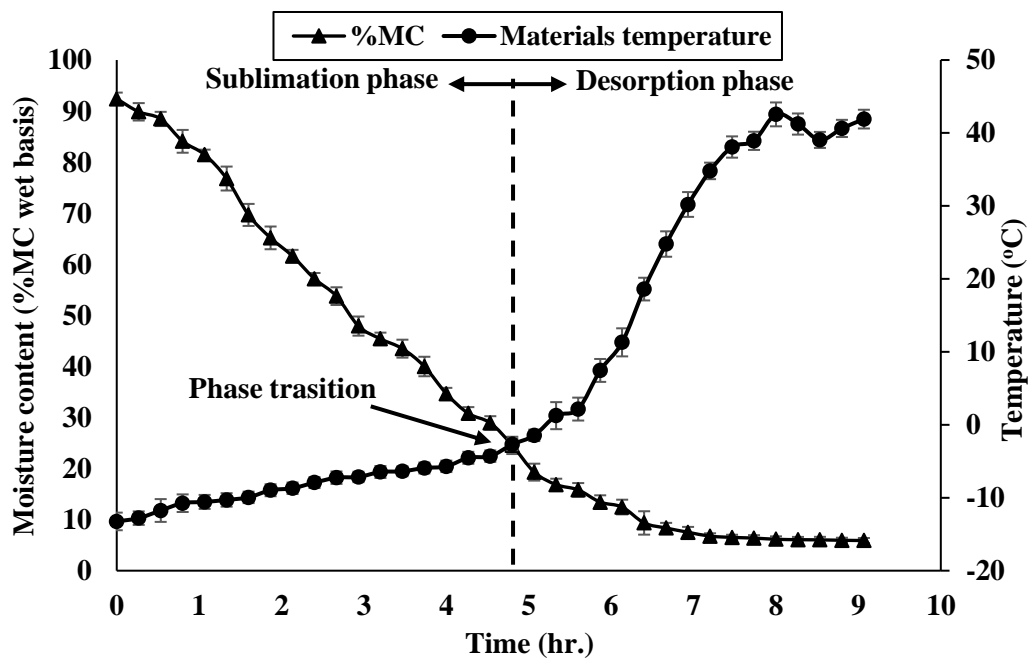


Figure 35 Moisture content and temperature of carrot slices from MFD process with CLT.

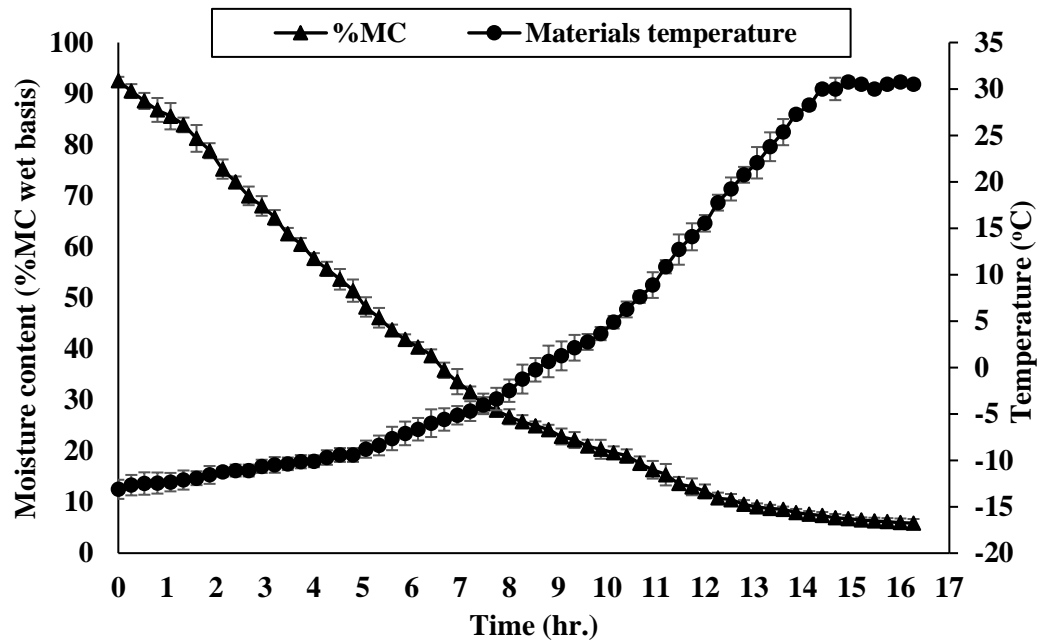


Figure 36 Moisture content and temperature of carrot slices from FD process.

In the sublimation phase, the ice absorbs a small amount of microwave energy at the beginning since the water molecules in the ice are locked by hydrogen bonds in a crystal structure (Tanaka and Sato, 2007). These bonds inhibit the water molecules from rotating, which results in a low dielectric permittivity of ice. This phenomenon causes an initial slow increase in material temperature. In this phase, the MFD characteristic of the MFD with CLT is not different from the MFD without CLT. At the onset of the desorption phase when the moisture content is reduced below the transition moisture content of $22\pm 1\%$ (wet basis), the product temperature exhibits an initial sharp increase that later flattens out until it reaches the final state temperature. It is possible that the majority of ice may have already sublimed in this phase and only non-frozen water remains inside the carrot. The non-frozen water can then absorb the energy generated from the microwave in the desorption phase better than in the sublimation phase due to the increased effectiveness of the dipole rotation and oscillation of ions.

In the desorption phase, the temperature of the carrot slices dried with MFD without CLT increases continuously until the end of the process. Due to a high-temperature variation and the overshooting temperature in this process, the products became charred and showed a burning spot, which leads to low product quality. In the MFD with CLT process, however, the variation in the temperature of the carrot slices in the desorption drying phase is less than that occurring in the processing of MFD without CLT. This results in a more-desired quality of the final products.

4.3.2 Control of temperature variation in microwave freeze-drying with closed-loop temperature control system process

When the CLT was implemented in the MFD process by using feedback temperature control to maintain a constant final product temperature of 40°C, the temperature variation in the sample was reduced. Figure 37 compares the temperature profile of MFD with CLT to that of MFD without CLT at a microwave power of 100W using an on/off cycle during the sublimation and desorption phases. For both methods, the on/off cycle continued until the desired moisture content of the carrot slices was achieved. In MFD without CLT process the temperature of the material increased continuously from the 7th hours of drying time to the end. The sample temperature reached over 60°C between the 8th - 9th hours of drying time. At this stage, the temperature fluctuation was in a range of 40 - 70°C, i.e. 30° fluctuation. With this high and wide-range temperature variation, the charring of the carrot slices and the burning spot were observed, which negatively affected the quality of the final product. In contrast, the MFD with CLT provided better control of the temperature variation, which was in a range of 33 - 45°C or 12° fluctuation. This accounted for 60% improvement in temperature control efficiency. With better temperature variation control using CLT, the product quality was better than that obtained from the MFD without CLT.

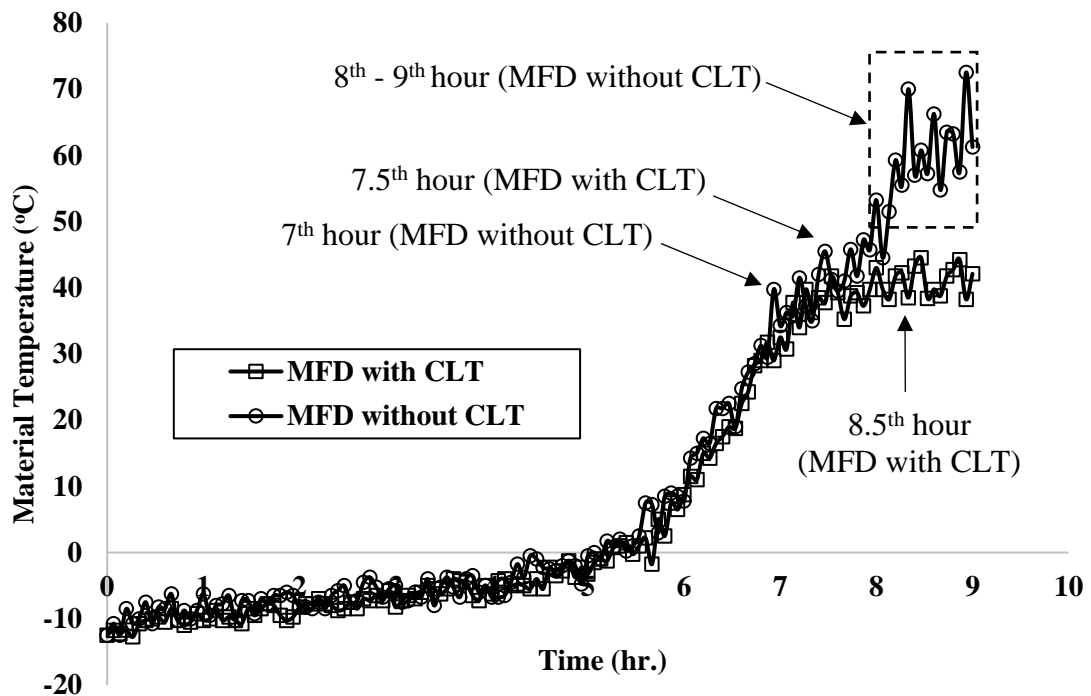


Figure 37 Temperature profile of carrot slices in MFD with CLT compared to MFD without CLT at 100W microwave power.

It should be noted that the results were still less effective in the desorption phase, even though the on/off cycle of the magnetron was well controlled to maintain the product temperature in the sublimation phase. With the closed-loop temperature control system, as the magnetron was turned on, the carrot temperature increased and overshoot the desired final temperature of 40°C. At the 7.5th hours of drying time with the CLT, the temperature reached 46°C in most cases. In some treatments, the feedback signal in the CLT requested the magnetron to be “off”. However, the physical duty cycle was still in the “on” status and could not be turned off until the cycle finished. As the magnetron was still in the “on” cycle, the sample temperature increased continuously and overshoot. On the other hand, when the duty cycle was “off” but the feedback signal in the CLT requested “on”, the magnetron remained off until the cycle finished. This caused the sample temperature to decrease continuously and undershoot (Figure 37 at the 8.5th hours). Thus, even though the CLT can control the temperature fluctuation better within a

temperature of 12°C compared to 30°C the MFD without CLT, a more efficient feedback control to minimize temperature fluctuation is of interest in the future. From this work, it seems that the on/off duty cycle provides good control of the magnetron at the sublimation stage with a temperature fluctuation range of 5°C. Thus, it is suggested that further development of the process control for MFD should involve the control system being divided into two stages. For the sublimation stage, the microwave power on/off cycle should be designated. For the second stage of desorption, the coupled feedback CLT without microwave power on/off cycle is proposed to achieve a better temperature control.

4.3.3 Improvement of closed-loop temperature control system

The CLT was improved by dividing the process control into two stages. For the sublimation stage, the microwave power on/off cycle was designated. For the second stage of desorption, the coupled feedback CLT without microwave power on/off cycle is proposed to achieve better temperature control. In the second stage, when the temperature of the material reached 40°C, the CLT was in the decreasing mode. In decreasing mode, the microwave power always off until the temperature of the material drops below 40°C, then the control system was changed to the temperature increasing mode. In this mode, the magnetron was turned on continuously until the temperature of the material reached 40°C and then changed to decreasing mode. This procedure was continuing until the end of the drying process. Figure 38 shows materials temperature after the temperature reached 40°C and the CLT was started. The material temperature was controlled at 40°C by a CLT with continuous microwave power on. The fluctuation of materials temperature was reduced ostensibly from a temperature fluctuation range of 12°C reduced to 2°C or about 80% improvement in temperature control efficiency. It provided smooth control over the CLT with microwave power on/off cycle until the end of the process.

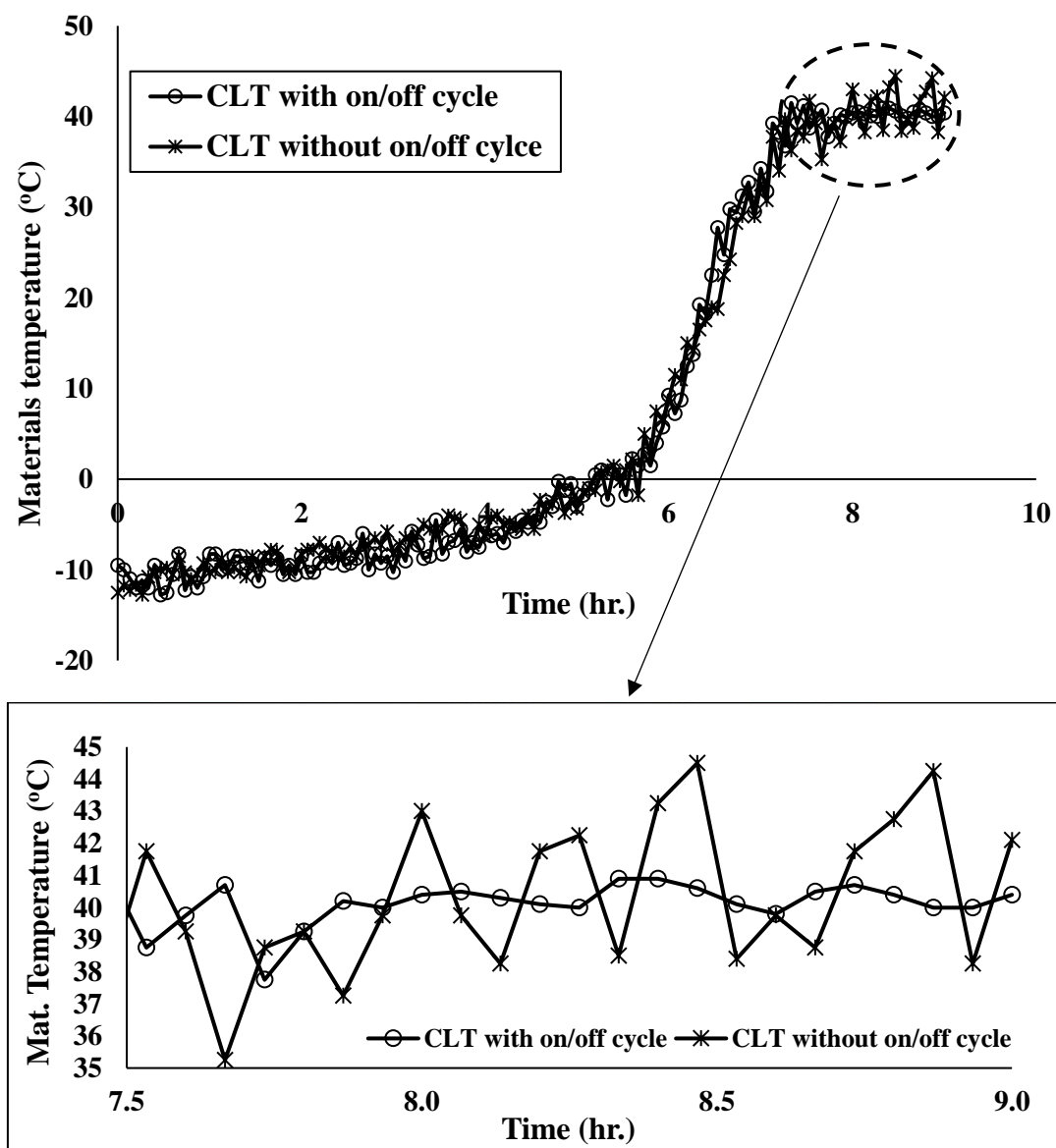


Figure 38 Carrot slices temperature controlled by CLT with and without on/off cycle.

4.3.4 Quality of products and energy consumption

The overall color of the carrot dried using MFD with CLT was not significantly different ($p \geq 0.05$) from that using freeze-drying, nor was there any significant difference in the rehydration ratio, crispness, or hardness, as shown in Table 8. In comparing the energy consumption, both the MFD with and without CLT consumed about 40% less energy than the FD due to a significant reduction in drying time. However, MFD without CLT yielded a less desired product quality due to

temperature overshooting during the end of the desorption phase, which resulted in a significant decrease in L* and an increase in a* and b* values, as indicated by the darker color of the carrot slices. It also resulted in the charring of the carrot sample and the burning spot was observed, which negatively affected the quality of the final product.

Table 8 Product quality and energy consumption obtained from different drying methods.

	FD	MFD without CLT	MFD with CLT
Product quality			
L*	64.69 ± 2.79 ^a	45.76 ± 2.78 ^b	61.79 ± 3.99 ^a
a*	25.16 ± 3.06 ^a	31.46 ± 3.51 ^b	26.84 ± 2.23 ^a
b*	29.79 ± 1.46 ^a	38.11 ± 3.26 ^b	32.95 ± 5.84 ^a
Crispness	15.44 ± 0.97 ^a	11.22 ± 0.93 ^b	14.89 ± 0.97 ^a
Hardness (N)	7.69 ± 0.47 ^a	8.25 ± 0.31 ^b	7.75 ± 0.32 ^a
Rehydration ratio	5.66 ± 0.12 ^a	5.39 ± 0.28 ^a	5.46 ± 0.53 ^a
Energy consumption (MJ)	70.98 ± 0.48 ^a	46.40 ± 0.41 ^b	45.85 ± 0.24 ^b

Note: Values followed by the same superscript letters within the same row are not significantly different from each other ($p \geq 0.05$).

The effects of temperature variation from the different drying processes can be physically observed, as shown in Figure 39. The removal of water during the drying process affects the appearance of the final product as rapid water loss causes the hardness of the sample to increase. The samples were observed to retain their initial shapes with minor shrinkage in all drying methods due to the fact that the removal of moisture content from the sample occurred under low vacuum pressure, low temperature, and low microwave power. These observations are in good agreement with the findings in other studies (Duan et al., 2010b; Wang et al., 2010b; Zhang et al., 2012). However, Figure 39c shows the carrot sample's charring due to the overshooting temperature and a high fluctuation of the material temperature

during the MFD without CLT, leading to unacceptable product quality. Thus, controlling the final state material temperature is necessary for the MFD process to obtain the best product quality.

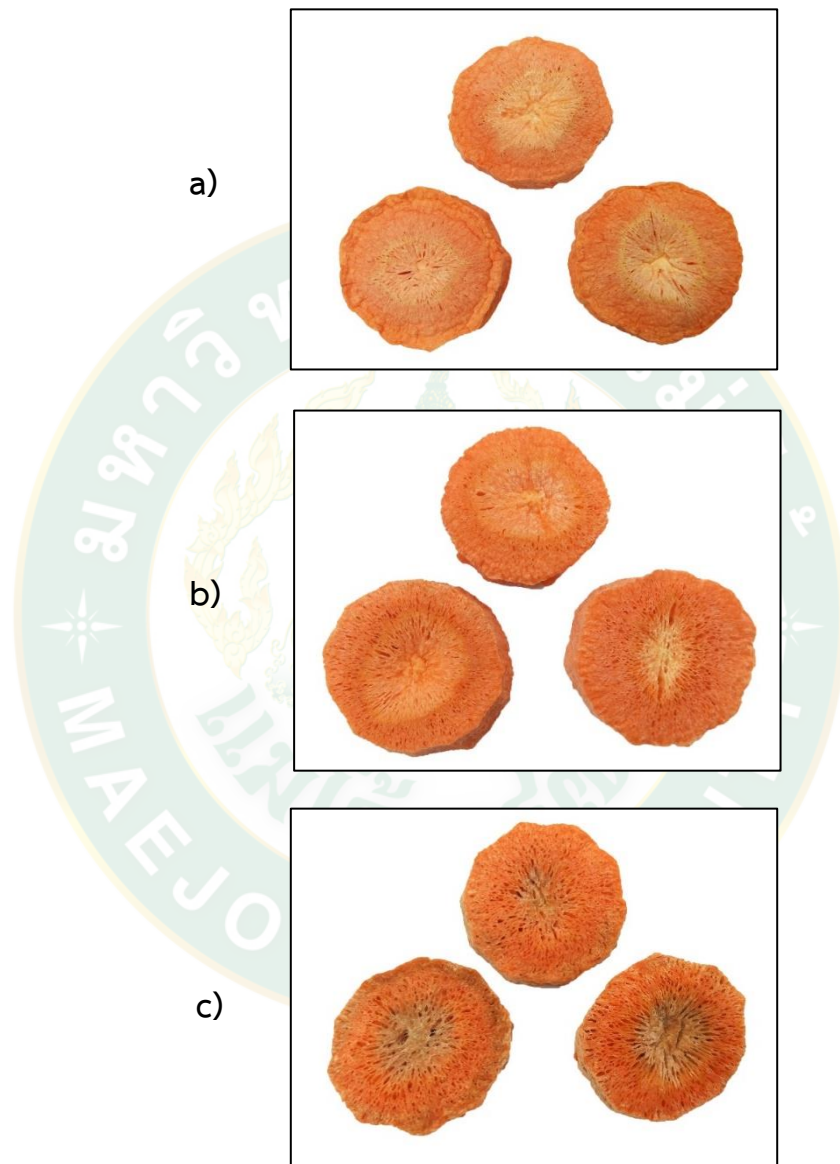


Figure 39 Dried carrot slices from different drying methods

a) FD; b) MFD with CLT; c) MFD without CLT.

4.4 Part II: Development of closed-loop control system for microwave freeze-drying

4.4.1 MFD drying characteristics and kinetics

In the MFD process of the carrot slices, there were two stages of drying: namely, the sublimation and desorption phases, as well as in the MFD of banana (Jiang et al., 2014), sea cucumber (Duan et al., 2010b), instant vegetable soup (Wang et al., 2009), potato (Wang et al., 2010b), cabbage (Duan et al., 2007a), and carrot slices (Sujinda et al., 2020). In the sublimation phase, the moisture content of the carrot slices gradually decreased until it reached approximately $21\pm 1\%$ (wet basis) (Figure 40). This phase took place slowly, as the ice was being sublimed. Later in the desorption phase, the moisture content decreased below $21\pm 1\%$ at which point the temperature of the carrot slices increased faster than that in the sublimation phase. The moisture content in the carrot slices in this phase remained in a liquid form, possibly as nonfrozen water, and was to be vaporized. During sublimation, the temperature of the carrot slices did not significantly change with the different microwave powers. A small amount of heat was produced inside the sample due to fixed water molecules within the ice. These fixed water molecules prevented the ion or dipole rotation and led to low dielectric permittivity in the ice (Tanaka and Sato, 2007). This phenomenon caused an initial slow increase in the material temperature. Once the drying process continued until the moisture content dropped below $84\pm 1\%$, a gradual increase in temperature was observed. As soon as the moisture content decreased below the transition phase at $21\pm 1\%$ moisture content, the desorption phase started. In the desorption phase, the carrot's temperature increased sharply until it reached the 40°C limit. It was possible that most of the ice was already sublimed at the onset of this phase and only nonfrozen water remained inside the carrot. This allowed the carrot to absorb the microwave energy in the desorption phase better than in the sublimation phase due to better dipole rotation and ions oscillation (Sujinda et al., 2020).

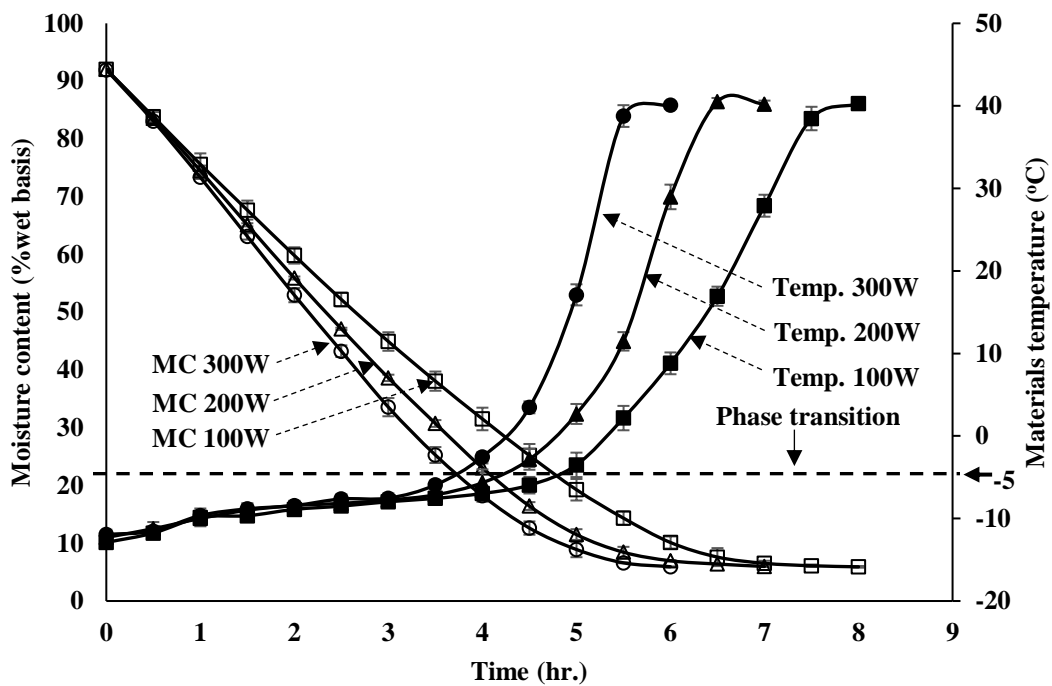


Figure 40 Moisture content (MC) and temperature profiles (Temp.) of carrot slices in MFD under various microwave power settings.

Figure 40 showed that before drying, the initial moisture content of carrot slices was approximately $92 \pm 0.5\%$ percent wet basis (mean \pm std.). The drying characteristics of the carrot slices were significantly affected by the drying microwave power levels, as predicted. The moisture content gradually decreased over time, and as the temperature rose, the drying time decreased. Microwave power of 100 W (8 hr.) and 300 W (3 hr.) recorded the longest and shortest drying times, respectively (6 hr.). At microwave power of 300 W, 200 W, and 100 W, respectively, it took 6, 7, and 8 hours to reduce the moisture content of carrot slices from 92 ± 0.5 percent (wet basis) to a final 6 ± 0.1 percent (wet basis), as shown in Figure 40. The drying time of MFD with a power of 300 W was approximately 15% and 25% faster than MFD with a power of 200 W and 100 W, respectively. Microwave power levels were found to be the most important factor affecting drying kinetics, as observed in other studies (Wang et al., 2009; Wang et al., 2010b; Jiang et al., 2014). As a result, a higher microwave power resulted in a faster drying rate, and the moisture content

decreased faster. This is attributable to an improvement in dipole rotation and ions oscillation in the carrot slices, resulting in faster removal of water from the slices.

Table 9 Statistical analysis of the drying kinetic models at different microwave power.

Model name	Power (W)	k ($\times 10^{-6} \text{ min}^{-1}$)	a	b ($\times 10^{-4}$)	n	SSE	$RMSE$	r^2
Newton	100	465.3	-	-	-	0.0031	0.0554	0.980
	200	534.8	-	-	-	0.0035	0.0592	0.981
	300	585.2	-	-	-	0.0040	0.0636	0.980
Page	100	232.2	-	-	1.398	0.0003	0.0170	0.994
	200	386.6	-	-	1.440	0.0005	0.0151	0.995
	300	413.0	-	-	1.468	0.0002	0.0127	0.996
Henderson and Pabis	100	403.6	1.0811	-	-	0.0022	0.0474	0.975
	200	581.7	1.0874	-	-	0.0025	0.0502	0.976
	300	637.4	1.0873	-	-	0.0030	0.0541	0.974
Logarithmic	100	428.5	1.0811	0	-	0.0022	0.0474	0.978
	200	503.6	1.0833	0	-	0.0009	0.0307	0.989
	300	637.4	1.0872	0	-	0.0029	0.0541	0.974
Midilli et al	100	286.0	0.9707	0.133	1.500	0.0002	0.0188	0.997
	200	344.3	0.9760	0.136	1.512	0.0002	0.0140	0.998
	300	410.0	0.9851	0.130	1.512	0.0001	0.0105	0.997
Diffusion approach	100	266.7	1.3779	0.152	-	0.0007	0.0265	0.993
	200	306.5	1.3772	0.164	-	0.0010	0.0323	0.990
	300	295.5	1.3801	0.154	-	0.0009	0.0304	0.992

The statistical parameters of the chosen model were shown in Table 9. The three statistical parameters SSE , $RMSE$, and r^2 . The r^2 was used to compare the fitting of the six thin-layer drying models to experimental results. All of the selected models had r^2 values greater than 0.95, indicating a good fit with the experimental data in all drying conditions (Doymaz and İsmail, 2011). The r^2 values ranged from

0.974 to 0.998, *SSE* values between 1×10^{-4} and 4×10^{-3} , and *RMSE* values from 0.0105 to 0.0636. These results indicate that the tested drying models accurately predict the thin-layer drying of carrot slices. Generally, the Midilli et al. model gave the highest r^2 and the lowest *SSE* and *RMSE* values (Table 9). Thus, the Midilli et al. model could be selected to represent the thin-layer drying characteristics of carrot slices. The Midilli et al. model showed the best fit for the overall experimental data with the high values of r^2 and the lowest *SSE* and *RMSE*. Moreover, when calculated separately for the sublimation phase and desorption phase, the Midilli et al. model also showed the best fit to the most experimental data. The drying rate constant (k) and the coefficients for drying curves fitting of the carrot slices was shown in the Table 10. From the result, it was found that the value of the drying rate constant (k) increased significantly ($p < 0.05$) with the increasing microwave power, which implied an increase in the drying rate as well.

However, the k values of the desorption phase were lower than those of the sublimation phase at the same power as shown in Table 10. Since the layer of ice was already removed and a dry layer was formed, it became an obstacle for the removal of the water causing mass transfer resistance at the surface. Moreover, only non-frozen water or bound water remains inside the carrot in the desorption phase, which consumes a large portion of energy and takes time to remove the water. Consequently, the drying rate decreased as the k values of the desorption phase were lower than that of the sublimation phase. It was noted that the k values of the desorption phase between the microwave power of 200W and 300W were not significantly different ($p \geq 0.05$). Thus, in the desorption phase, the microwave power of 200W was selected to be apply in the development of the DMLC to minimize the energy consumption for the MFD of the carrot slices.

Table 10 The drying rate constant and coefficients for drying curves fitting of the carrot slices from Midilli et al. model.

Drying Phase	Microwave power (W)	k ($\times 10^{-6} \text{ min}^{-1}$)	a	b ($\times 10^{-4}$)	n	RMSE	r^2
Overall	100	286.0 ± 5.0^a	0.9707	0.133	1.500	0.0188	0.997
	200	344.3 ± 8.0^b	0.9760	0.136	1.512	0.0140	0.998
	300	410.0 ± 7.8^c	0.9851	0.130	1.512	0.0105	0.997
Sublimation	100	530.6 ± 21.4^a	0.9774	0	1.378	0.0088	0.997
	200	628.7 ± 17.9^b	0.9863	0	1.393	0.0072	0.998
	300	780.9 ± 27.4^c	0.9950	0	1.379	0.0062	0.998
Desorption	100	136.5 ± 2.9^a	2.0848	1.053	1.716	0.0028	0.996
	200	155.2 ± 1.9^b	2.3787	1.453	1.751	0.0007	0.995
	300	152.6 ± 2.0^b	2.0233	1.342	1.749	0.0013	0.997

Note: Different superscripts a, b, c indicated significant differences among treatments within each drying phase at $p < 0.05$.

4.4.2 Moisture diffusivity (D)

The moisture diffusion (D) in Equation 53 was further elaborated in terms of apparent moisture diffusion (D_{APP}) at a given time in the MFD process and averaged the moisture diffusion (D_{AVG}) in each phase of the MFD process. Figure 33 shows the apparent moisture diffusivity (D_{APP}) of the MFD carrot slices in the full range of the moisture contents. During the MFD process, the D_{APP} of the carrot varied at different levels of microwave power. As the moisture content decreased, the D_{APP} increased as an inverse-Sigmoidal shape that was similar to the findings by Sharma and Prasad (2004). As such, the higher microwave power yielded a higher D_{APP} of the carrot slices. It is possible as the moisture content inside the carrot slices was heated up by the microwave energy, the vapor inside the solid matrix of the carrot slices generated the vapor pressure. This created the pressure gradient between the internal vapor pressure and vacuum pressure at the surroundings of the carrot surface. This pressure gradient was responsible for the moisture transportation (Datta and

Anantheswaran, 2001), which caused the increase in the moisture diffusivity during the MFD process.

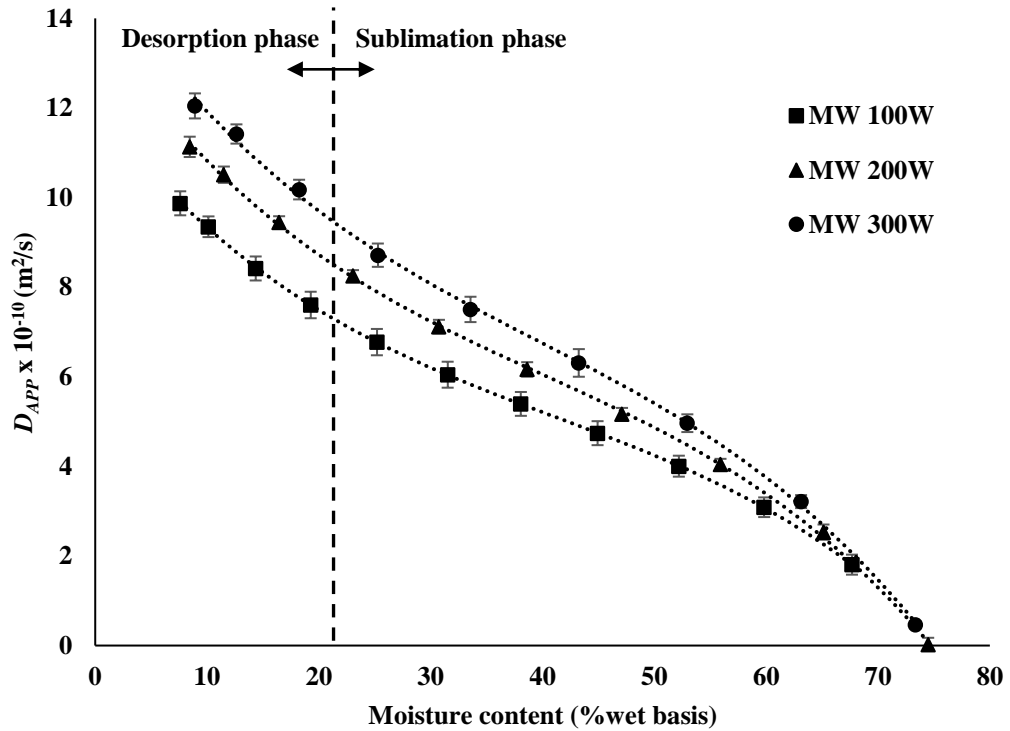


Figure 41 The apparent moisture diffusivity (D_{APP}) of carrot during MFD process at different microwave power levels.

The apparent moisture diffusivity was found to be a function of moisture content. A third-order polynomial relationship was correlate to describe the variation in D_{APP} with moisture content of carrot slices and is given as:

$$D_{APP} = A + BM_t + CM_t^2 + DM_t^3 \quad \text{Eq. (54)}$$

where, D_{APP} is the apparent moisture diffusivity (m^2/s), M_t is the moisture content at time t ($\text{kg water}/\text{kg dry matter}$) and A ; B ; C ; D are coefficient of regression equation for MFD of carrot slices in different drying conditions are presented in Table 11. The high values of r^2 are indicative of the good fit of the empirical relationship to

represent the variation in apparent moisture diffusivity with moisture content of carrot slices during MFD process under different drying conditions.

Table 11 Regression coefficient and r^2 of apparent moisture diffusivity during the MFD.

Drying condition	Regression coefficient				r^2
	A	B	C	D	
100 W	0.9815	-0.2222	0.0248	-0.0012	0.9992
200 W	1.1998	-0.3063	0.0378	-0.0020	0.9992
300 W	1.4626	-0.4008	0.0530	-0.0028	0.9985

Table 12 displayed the measured average moisture diffusivity (D_{AVG}) values for the various microwave power levels. At microwave powers of 100 W, 200 W, and 300 W, the average moisture diffusivity values were 6.406×10^{-10} , 7.404×10^{-10} , and $8.093 \times 10^{-10} \text{ m}^2/\text{s}$. The D_{AVG} values for carrot slices clearly increase as the microwave power is increased. When samples were dried at a higher microwave strength, the behavior of water molecules increased, resulting in higher moisture diffusivities. The moisture diffusivity values obtained in this study are common for food products, ranging from 10^{-11} to $10^{-9} \text{ m}^2/\text{s}$ for food materials (Madamba et al., 1996). The values of the D_{AVG} are consistent with the reported values of 2.434 to 14.199×10^{-10} for microwave drying black pepper at the microwave power range of 180 to 540 W (Amarasinghe et al., 2018), 2.16 to 7.89×10^{-10} for microwave drying celery leaves in the microwave power range of 180 to 900 W (Demirhan and Özbek, 2011), and 6.210 to 55.290×10^{-10} for the microwave vacuum drying of carrot slices at microwave power range of 100 to 600 W (Sutar and Prasad, 2007). Moreover, Table 12 exhibits an average D_{AVG} at different phases of the MFD process. The D_{AVG} in the sublimation and desorption phases also increased from 2.255×10^{-10} to $3.580 \times 10^{-10} \text{ m}^2/\text{s}$ and 8.760×10^{-10} to $10.377 \times 10^{-10} \text{ m}^2/\text{s}$, as the microwave power increased. The D_{AVG} in the sublimation phase was lower than the D_{AVG} in the desorption phase. This was because the ice structure limits the vapor to diffuse from inside out to the

environment in the sublimation phase. After the ice was removed entirely, in the desorption phase, the dry layer's pore structure was created and remained open after the ice in the carrot slices sublimed. Thus, the vapor inside the material can flow towards the surface of the materials in the desorption phase faster than in the sublimation phase, causing a higher D_{AVG} in the desorption phase.

Table 12 The average moisture diffusivity for different microwave power levels.

Microwave power (W)	Average of moisture diffusivity ($D_{AVG} \times 10^{-10} \text{ m}^2/\text{s}$)		
	Overall	Sublimation phase	Desorption phase
100	6.406	2.255	8.760
200	7.404	3.158	9.792
300	8.093	3.580	10.377

4.4.2 Strategic development of dynamic microwave logic control (DMLC)

Since the microwave absorption ability of the carrot slices in each phase of MFD was different, it was necessary to regulate the microwave power to correspond to some critical parameters, such as, moisture content, drying rate, and material temperature. Thus, the DMLC was strategically developed to increase the efficiency of the MFD process based on the moisture content and temperature profiles from Figure 40 and the k values in Table 10. The DMLC shown in Figure 42 was divided into three processes as follows:

Process I - Sublimation: During the first hour of the MFD process (Figure 40), the drying curve of MC 100W was similar to MC 300W. Thus, the microwave power of 100 W was selected at the beginning of the sublimation phase to reduce the energy consumption because the microwave absorption in the carrot was limited by the non-rotating ice molecules. As the drying process carried on until the moisture content dropped below $84 \pm 1\%$, the profile of MC 100W became different from that of MC 300W. Therefore, the microwave power of 300 W was selected to increase the drying rate because it was able to

maximize the k values to $780.9 \times 10^{-6} \text{ min}^{-1}$ (Table 10), it was selected for the next part of the sublimation phase to increase the drying rate. This setting was continued until the moisture content was reduced below the transition phase of $21 \pm 1\%$ moisture content, indicating the onset of the desorption phase in Process II. In Process I, the real-time moisture content of the carrot slices was used as feedback to the CLC system for process regulation.

Process II - Desorption: The microwave power was regulated at 200 W to reduce energy consumption and to avoid product shrinkage. Since the k values (Table 10) during the desorption phase at microwave powers 300 W and 200 W were not significantly different ($p > 0.05$), both levels of the microwave power did not affect the drying time. As in Process I, the temperature of the carrot slices was likewise used as feedback for the CLC system in the Process II.

Process III - Final desorption: As the MFD process continued to the final desorption phase, the carrot temperature reached 40°C . At this stage, the carrot temperature was held at $40 \pm 1^\circ\text{C}$ to maintain the color and quality of the carrot slices (Gamboa-Santos et al., 2013). The MFD process was terminated when the moisture content of the carrot dropped to $6 \pm 1\%$. In Process III, both the temperature and the real-time moisture content of the carrot slices were used as feedback for the CLC system to control the final state temperature and detect the final moisture content of carrot slices.

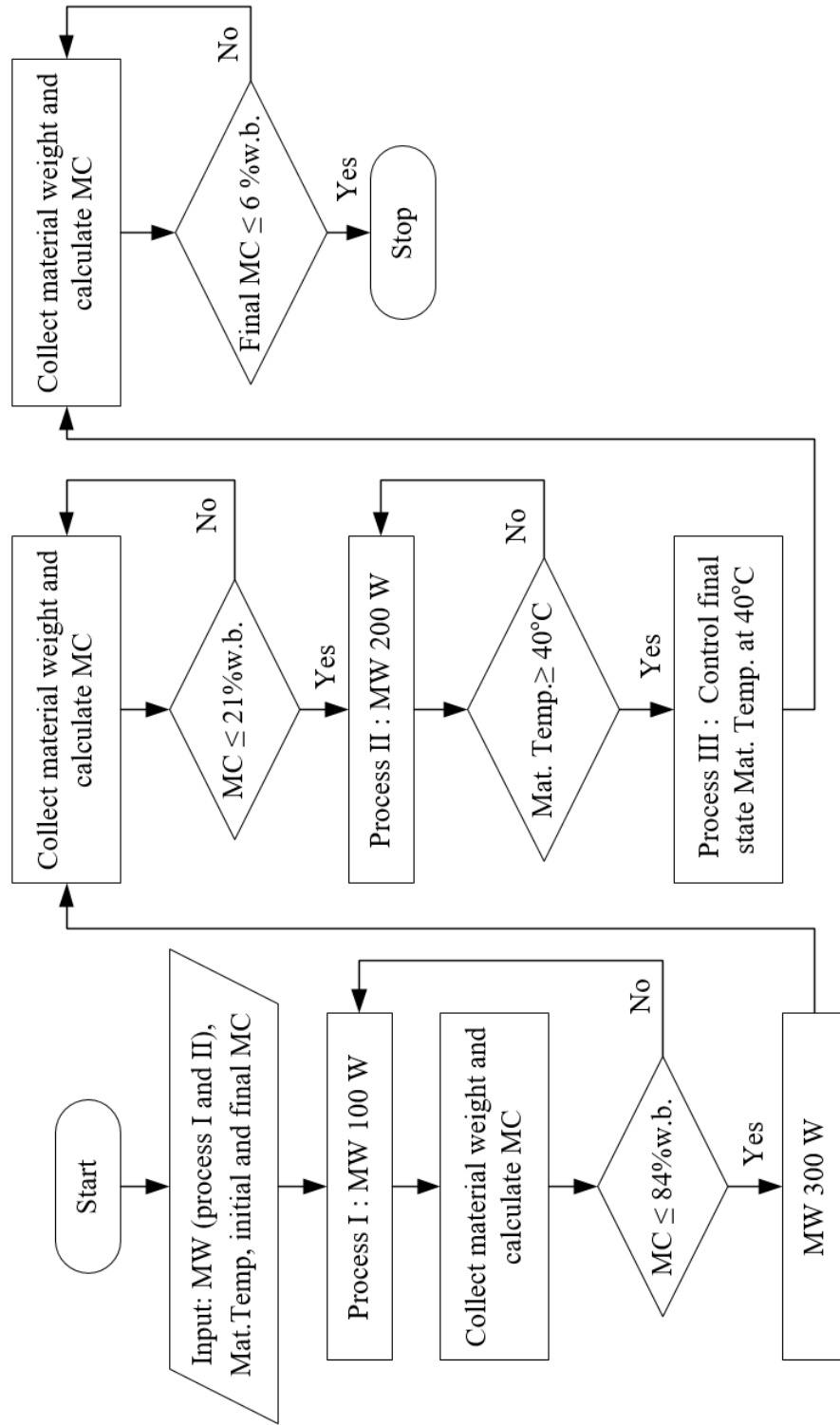


Figure 42 Flow process diagram of dynamic microwave logic control for microwave freeze drying of carrot slices.

After the development of the DMLC, according to Figure 42, the DMLC was program into the central processing unit (Figure 26), and the software for the CLC system was developed to display the MFD drying status, input the initial values, and config the process control strategy (Figure 32 and 33). This software helps the operation of the CLC system was more flexible and convenient. During the MFD-DMLC process, the MFD with an embedded DMLC and the CLC system software was found to work correctly during the MFD process of carrot slices. The CLC system can detect the material temperature and material weight accurately. It can calculate the moisture content in real-time, and the process regulation works smoothly with no logical error control during the drying process. After applied the CLC system with an embedded DMLC to the MFD process, the results show that the drying characteristic of the MFD-DMLC was similar to that of the general MFD in Figures 40 and 43 but slightly different in magnitude. During the MFD-DMLC process, the moisture content decreased exhibiting a Sigmoidal-shaped trend (Jiang et al., 2011; Li et al., 2019; Wang et al., 2012). The phase transition of the moisture content ($21\pm 1\%$) and the temperature profile of the MFD-DMLC were similar to those of other MFDs. In the sublimation phase, the increasing material temperature of MFD-DMLC is not significantly different from the general MFD with all drying conditions. The MFD-DMLC reached the phase transition point at the same drying time as MFD-300W (nearly 4th hours of drying time). In the desorption phase, even the drying characteristic of the MFD-DMLC is similar to the MFD-300W; however, it took a bit longer drying time. The drying time of the MFD-DMLC (6.2 ± 0.1 hours) was similar to the MFD-300W (6.0 ± 0.1 hours), which was shorter than the FD (16.5 ± 0.1 hours) by about 60%. The MFD-DMLC produced a similar product quality as that of FD.

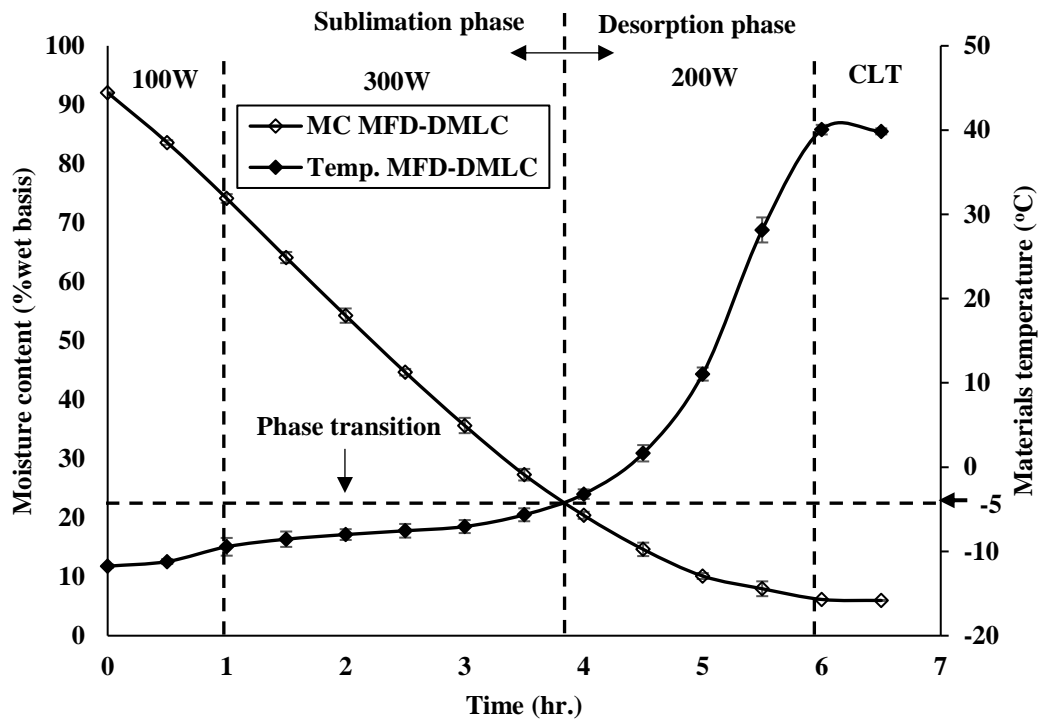


Figure 43 Temperature and moisture content profiles of carrot slices during the MFD-DMLC.

Figure 44 shows the drying rate as a function of the moisture content of carrot dried with MFD-DMLC and MFD under three different levels of microwave power. It was found that higher microwave power yielded a higher drying rate than lower microwave power. The higher drying rates were due to the higher microwave power that was also in good agreement with the higher moisture diffusion. As the moisture content inside the carrot slices was heated up by the microwave energy, the vapor inside the solid matrix of the carrot slices generated the vapor pressure. This created the pressure gradient between the internal vapor pressure and vacuum pressure at the carrot surface's surroundings. This pressure gradient was responsible for moisture transportation (Datta and Anantheswaran, 2001). The increasing of the microwave power leads to an increase in the vapor pressure inside the carrot slices, which helps the vapor inside the material flow towards the surface of the carrot slices more quickly, causing the increase in the moisture diffusivity with increasing the

microwave power. Thus, the drying rate and the moisture diffusivity increased with increasing the microwave power.

Moreover, in Figure 44, It was possible that most of the MFD processes took place in the falling rate period and constant rate periods, similar to the findings by Azimi-Nejadian and Hoseini (2019), Esehaghbeygi et al. (2014), and Varith et al. (2007). During the initial stage, the drying rate of the MFD-DMLC was similar to the others. The carrot slices absorbed a small amount of microwave energy due to the fixed water molecules in the ice which prevented ion or dipole rotation and led to low dielectric permittivity in the ice. Once the drying process continued until the moisture content dropped below $84\pm 1\%$, the level of the microwave power was changed by the controller to 300 W to increase the drying rate. The drying rate of the MFD-DMLC increased significantly and differed with the MFD-100W and MFD-200W. Without any moisture in the product, this exhibited a reduction in the concentration of the microwave power and drying rate (Soysal et al., 2009). When the moisture content dropped below $21\pm 1\%$ (Phase transition point), the DMLC was changed to Process II. In this process, the controller changed the microwave power to 200 W to reduce the energy consumption and avoid any over-burning damage to the product. At this stage, the drying rate of the MFD-DMLC was not significantly different with those of MFD-200W and MFD-300W. Process II was continued until the carrot slices temperature reached the desired final state temperature at 40°C . Then, the DMLC changed to Process III and the closed-loop temperature control (CLT) was activated to control the final state temperature of the carrot slices at 40°C . The drying rate of the MFD-DMLC at the final stage was not significantly different with the other MFD due to the control of the heat generated by the CLT (Sujinda et al., 2020). The trend of the MFD-DMLC drying rate agreed with the drying rate constant (k) in each phase of the MFD process (Table 13).

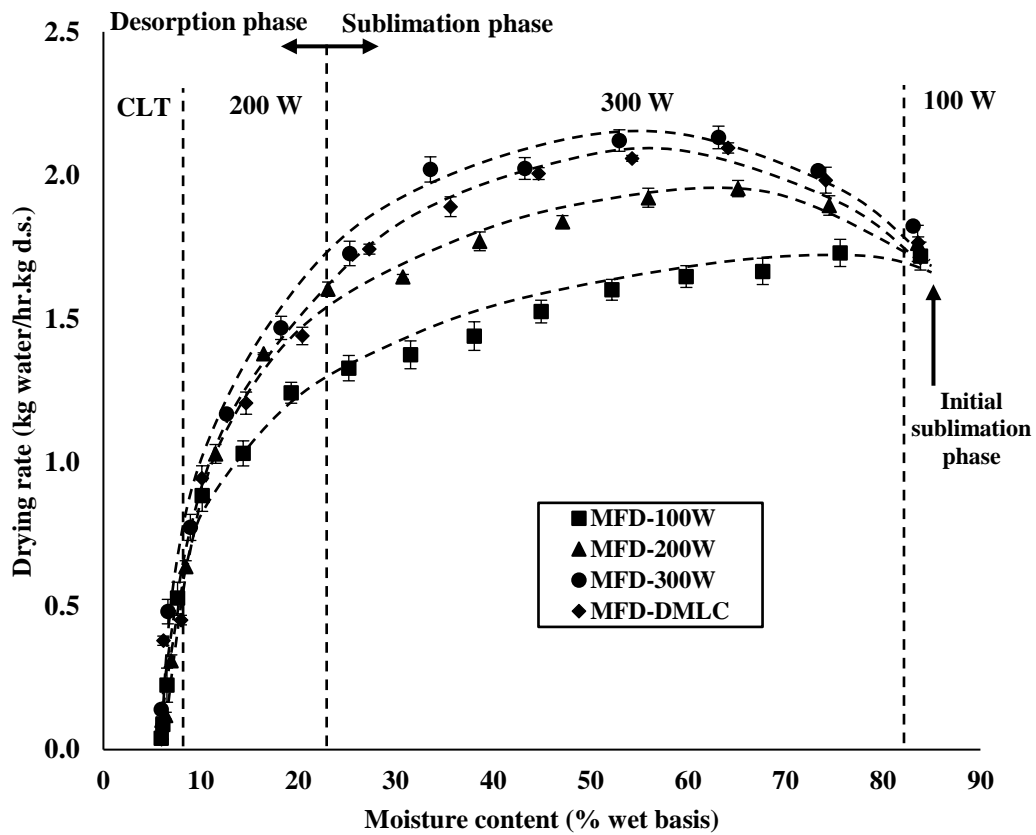


Figure 44 Drying rate profiles of carrot slices during the MFD process.

Table 13 The average moisture diffusivity and drying rate constant of MFD-DMLC.

Drying Phase	D_{AVG} ($\times 10^{-10} \text{ m}^2/\text{s}$)	k ($\times 10^{-6} \text{ min}^{-1}$)	a	b ($\times 10^{-4}$)	n	$RMSE$	r^2
Overall	7.734	433.0 ± 17.5	0.9847	0	1.483	0.010	0.999
Sublimation	3.545	775.1 ± 20.0	1.0246	1.6992	1.393	0.014	0.998
Desorption	9.852	157.7 ± 5.8	1.3955	1.1937	1.720	0.002	0.997

Table 13 shows that the k values of MFD-DMLC were similar to the MFD-300W (Table 10), which is the highest value of all drying conditions while providing the better product quality. This indicates that using microwave power 100 W in the beginning and microwave power 200 W in Process II for reduced energy consumption was not affected the drying rate of the MFD process and the product quality. In

addition, Table 13, shows the D_{AVG} of the MFD-DMLC. The overall D_{AVG} of the MFD-DMLC was slightly lower than the D_{AVG} of the MFD-300W, but the D_{AVG} of the MFD-DMLC in the sublimation phase was not significantly different from that of the MFD-300W. With the MFD-DMLC, the D_{AVG} in the sublimation phase was lower than that of the desorption phase. The trend of the D_{AVG} during the MFD-DMLC process agreed well with the D_{AVG} from the regular MFD process as presented previously in Table 13.

4.4.3 Product quality and energy consumption

The quality of the carrot slices processed by the FD, MFD, and MFD-DMLC in terms of the textures, colors, rehydration ratio, and shrinkage are presented in Table 14. The overall product quality of MFD with fixed microwave power at 300 W was significantly different ($p < 0.05$) from those of other MFD drying conditions. The effect of MFD-300W on the carrot's charring was not noticeable, but the samples appeared to have some burned spots on the surface. The dried carrot slices were observed to retain their initial shapes with minor shrinkage in the drying methods since the removal of moisture content from the dried carrot slices occurred under low vacuum pressure, low temperature, and low microwave power. These observations are in good agreement with the findings in other studies (Duan et al., 2010b; Wang et al., 2010b; Zhang et al., 2012). However, the shrinkage of the carrot subjected to MFD-300W was 37.8%, resulting in the highest shrinkage among the MFD and FD treatments. The effects of the microwave power levels of the MFD process compared with FD can be physically observed, as shown in Figure 45. The high levels of microwave power provided the highest drying rate in the desorption phase. It led to an increase in the internal vapor pressure and the collapse of the cell-matrix of the carrot's opened pores. It is critical to note that the moisture content inside the carrot slices gets heated up by microwave energy and starts changing to the vapor inside the solid matrix of the carrot slices, which generates significant pressure. This raises the vapor pressure within the pores, causing them to expand due to the pressure. The high microwave strength, which increased the rate of moisture removal from the carrot slice, increased the vapor pressure within the pores structure and increased the pressure for opening the pores, causing the matrix in the carrot slices

to collapse. The collapse of the pore structure leads to reducing the number of the pore, causing the shrinkage of the carrot slice. This can observe physically with Figure 45c. The shape and the color of the product are significantly different from those of other drying methods, consistent with the statistical analysis results in Table 14. This phenomenon was confirmed by the rehydration ratio, as well as the crispness and hardness of the carrot subjected to MFD-300W, which had significant differences compared with those of carrot subjected to MFD-100W, MFD-200W, MFD-DMLC, and FD processes. The collapse of the pore structure in MFD-300W led to the reduction in the number of pores able to rehydrate it. At the same time, the texture of the carrot slices was case-hardened. Moreover, a significant decrease in the L^* and an increase in a^* and b^* values indicated that the carrot slices subjected to MFD-300W were darker in color than others. Thus, the MFD-300W exhibited negative effects on the overall quality of the carrot slices compared with other treatments.

Table 14 The quality of carrot slices under different MFD and FD drying conditions.

Product quality	Drying conditions				
	FD	MFD-100W	MFD-200W	MFD-300W	MFD-DMLC
L^*	64.69 ±1.50 ^a	62.76 ±1.50 ^a	61.99 ±4.37 ^a	54.35 ±4.53 ^b	62.35 ±0.82 ^a
a^*	25.16 ±3.06 ^a	26.43 ±2.63 ^a	26.25 ±0.93 ^a	33.07 ±3.31 ^b	26.78 ±1.33 ^a
b^*	29.79 ±1.46 ^a	29.79 ±1.46 ^a	31.41 ±6.06 ^a	35.95 ±2.32 ^b	31.71 ±1.85 ^a
Crispness	15.5 ±0.54 ^a	14.33 ±1.36 ^{ab}	13.83 ±0.98 ^b	10.67 ±1.63 ^c	14.00 ±0.89 ^b
Hardness (N)	7.55 ±1.96 ^a	7.35 ±1.96 ^a	7.74 ±1.96 ^{ab}	8.63 ±1.08 ^b	7.65 ±1.47 ^a
Rehydration ratio	5.66 ±0.31 ^a	5.48 ±0.49 ^{ab}	5.31 ±0.23 ^{ab}	4.97 ±0.35 ^b	5.36 ±0.11 ^{ab}
%Shrinkage	25.1 ±0.6 ^a	25.6 ±1.7 ^{ab}	27.8 ±1.1 ^b	37.8 ±0.9 ^c	27.0 ±1.9 ^{ab}

Note: Values followed by the same superscript letters within the same row are not significantly different ($p \geq 0.05$).

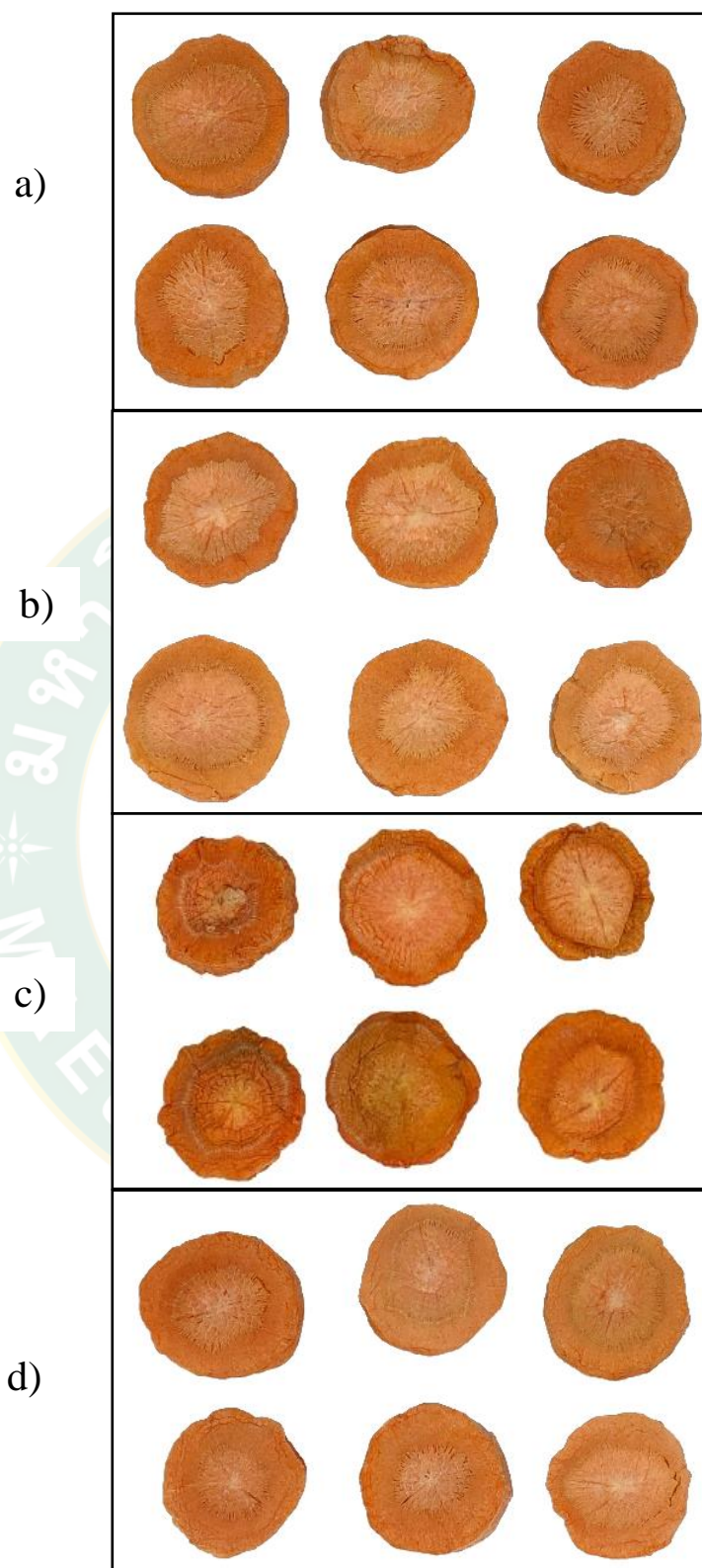


Figure 45 Carrot slices dried a various microwave power levels compared with FD:

(a) MFD 100W; (b) MFD 200W; (c) MFD 300W; (d) FD

The ultimate goal of the MFD-DMLC was to maintain the quality of the product and to optimize the energy consumption (EC). The efficiency in terms of the EC and SMER was evaluated (Table 15). The EC of all drying conditions was estimated using the actual kWh reading from the optical power meter and converting it to MJ. Table 15 showed the highest and lowest ECs needed to minimize the moisture content of carrot slices from $92\pm 0.5\%$ (wet basis) to a final $6\pm 0.1\%$ (wet basis) at FD (70.9 MJ) and MFD-300W (39.0 MJ). The microwave power and drying time were found to be the most significant factors affecting EC. The SMER is a parameter that is used to define the drying process efficiency. It is measured by multiplying the mass of water evaporated or extracted from the product (kg) by the appropriate input energy (kWh). The SMER is a term used to describe the drying efficiency of a material. Equation 53 can be used to calculate the SMER for all drying conditions. The higher value of SMER indicate the more efficient drying process with lower energy consumption (Stawreberg and Nilsson, 2010). The calculated average SMER of the FD, MFD-100W, MFD-200W, MFD-300W, and MFD-DMLC were 4.4×10^{-3} , 6.8×10^{-3} , 7.3×10^{-3} , 7.9×10^{-3} , and 7.9×10^{-3} $\text{kg}_{\text{moisture}}/\text{kWh}$, respectively. Although it was clear that the MFD-300W could achieve the lowest EC and the highest SMER, it yielded the downside of low product quality (Table 14). On the other hand, the EC and SMER of the MFD-DMLC were not significantly different ($P \geq 0.05$) from that of the MFD-300W, but the MFD-DMLC provided superior product quality equivalent to that of the FD treatment (Table 14). Table 15 indicates that MFDs provided better energy efficiency than that of the FD. With the MFD-DMLC, the carrot was dried with EC of 39.5 MJ which was about 44.2% lower than energy used in the FD (70.9 MJ). The SMER and total drying time (TDT) of the MFD-DMLC was higher by 44.3% and lower by 62.4% than those of the FD process. The better SMER means better energy usage while the lower TDT means shorter drying time. Both parameters together with product quality are good indicators supporting the better process efficiency of the MFD than that of the FD. Also, it can also be concluded that the MFD-DMLC successfully enhance the efficiency of the MFD processes in this work.

Table 15 Energy consumption, specific moisture extraction rate, and total drying time of FD and MFD processes.

Drying condition	EC (MJ)	SMER $\times 10^{-3}$ (kg _{moisture} /kWh)	Δ SMER (%)	TDT (hr)	Δ TDT (%)
FD	70.9 \pm 0.2 ^a	4.4 \pm 0.1 ^a	-	16.5 \pm 0.1 ^a	-
MFD-100W	45.7 \pm 0.4 ^b	6.8 \pm 0.1 ^b	+35.3	8.1 \pm 0.2 ^b	-50.9
MFD-200W	42.7 \pm 0.4 ^c	7.3 \pm 0.1 ^c	+39.7	7.2 \pm 0.2 ^c	-56.4
MFD-300W	39.0 \pm 0.1 ^d	7.9 \pm 0.1 ^d	+44.3	6.0 \pm 0.1 ^d	-63.6
MFD-DLMC	39.5 \pm 0.2 ^d	7.9 \pm 0.1 ^d	+44.3	6.2 \pm 0.1 ^d	-62.4

Note: 1. Values followed by the same superscript letters within the same row are not significantly different from each other ($p \geq 0.05$).

2. EC = Energy Consumption; SMER = Specific Moisture Extraction Rate; TDT = Total Drying Time.

3. Δ = % Difference, calculated using the FD as reference.

4.5 Discussion

This research consisted of three parts: the uncertainty of measurement and moisture calculation, a variation of temperature during the MFD process, and the development of a CLC system for MFD. In the first part of this research, the uncertainty of temperature measurement, weight measurement, and moisture calculation was evaluated following the GUM after designing the hardware for the control system to verify the accuracy of the measurement system and the moisture content calculation. The results show that the uncertainty of temperature measurement is $\pm 1.5^\circ\text{C}$ or 3.9% from a full-scale range of 30 – 50 $^\circ\text{C}$, the uncertainty of weight measurement is ± 0.347 grams or 0.8% from a full-scale range of 0 – 150 g, and the uncertainty of real-time moisture content calculation is $\pm 1\%$ (wet basis). As the results, the measurement systems were acceptable for use in the CLC system with no affected in terms of process control and product quality which confirm by the same later results in repetition of each treatment in this research.

In the second part of this research, the temperature variations during MFD of carrot slices and how CLT improved such variations were investigated. The carrot slices were dried to a final moisture content of 6% (wet basis) with a terminal temperature of 40°C using 100 W microwave power under 100 Pa vacuum pressure. The results showed that the MFD process consisted of two phases, viz. sublimation and desorption drying. In the sublimation drying phase, ice, due to its low dielectric permittivity, absorbed little microwave energy. This caused a slow rising in the temperature of carrot slices at the early stage of drying. After the moisture decreased below 22% (wet basis), the sample temperature sharply increased until it reached the final state temperature of the samples, indicating the onset of the desorption drying phase. In this phase, the sample temperature rose faster than that in the sublimation phase. Without CLT, the temperature of carrot slices varied by 30°C in the desorption drying phase of MFD, which leads to low product quality. However, after applying CLT to the MFD process, the variation in temperature of the carrot slices was reduced to 12°C, equivalent to a temperature control improvement of 60% during the desorption drying phase, and it provided a good product quality similar to FD. This improvement can be a part of DMLC development by integrating with the CLC to control the carrot slices temperature in the final stage of the MFD process. This can help to maintain the better final product quality. Thus, the CLT was applied to the MFD process for developing CLC in the final part of this research.

In the final part, The CLC was developed to improve the MFD process. The development process consisted of two sections: the MFD experiment to develop the DMLC and the implementation of the CLC with the DMLC on the MFD process. In the first section, the MFD process was examined to obtain the drying strategy on the carrot slices using microwave power of 100 W, 200 W, and 300 W with a temperature profile of the sample from -15°C to 40°C, the final moisture content of 6% (wet basis), and the final state of materials temperature was controlled at 40°C by the CLT. The results show that the drying curves of all drying conditions were not different in the first hour of the drying time. However, after that, the higher microwave power can reduce the moisture content of the carrot slices faster than the lower microwave power. The microwave power of 300 W took the shortest

drying time. In addition, the drying rate (k values) of microwave power 300 W was maximum in the sublimation phase compared to the other drying conditions. In the desorption phase, the k values were lower than those of the sublimation phase at the same power. However, the k values between the microwave power of 200 W and 300 W were not significantly different ($p \geq 0.05$) in this phase. Even though the microwave power 300 W took the shortest drying time and the highest drying rate, but its quality was low. In contrast, the microwave power 100 W can obtain the product quality similar to FD but take longer drying time and higher energy consumption than microwave power 300 W. As a result, the MFD process should be optimized by designing the process control strategy to improve the MFD process. It was designed by selecting the microwave power 300 W and 200 W to apply in the development of the DMLC for the MFD of the carrot slices to increase the drying rate in the sublimation phase and minimize the energy consumption in the desorption phase.

In the second section of the final part of this research, the DMLC was strategically developed and integrated into the CLC system. The results showed that in the MFD process, the DMLC was developed based on a drying-phase configuration and dynamic control between the microwave power and real-time moisture content sensing to provide feedback to the CLC system. The DMLC consisted of three processes. Process I, the microwave power 100 W, was applied in the first hour to reduce the energy consumption due to the drying curve of MFD-100W was similar to MFD-300W until the moisture content dropped below 84% (wet basis) then the microwave power was changed to 300 W. The microwave power 300 W can increase the drying rate in this stage because the drying rate was maximum at this condition. As the drying process carried on until the moisture content dropped below the transition phase of the moisture content of 22% (wet basis), which indicates that the desorption phase began, then the DMLC was changed to Process II. In this stage, the real-time moisture content of the carrot was used as feedback for the CLC system, and the microwave power was regulated at 200 W to reduce energy consumption because the drying rate of MFD-200W and MFD-300W were not significantly different ($p \geq 0.05$) and did not affect the drying time. As the MFD process continued to the

final desorption phase, the carrot temperature reached 40°C, and then the DMLC was changed to Process III. In this stage, the temperature of the carrot slices was used as feedback for the CLC system. The CLT, which improved from the first part of this research, was applied to control the carrot slices at 40°C ($\pm 1^\circ\text{C}$) as the final stage to maintain the color and quality of the carrot slices. After applying the DMLC into the CLC system to maintain the quality of the product and to optimize the energy consumption (EC) for the MFD of carrot slices, the result shows that the MFD with an embedded DMLC (MFD-DMLC) was found to work properly during the MFD process of the carrot slices. The EC and SMER of the MFD-DMLC were not significantly different ($P \geq 0.05$) from that of the MFD-300W, but the MFD-DMLC provided superior product quality equivalent to that of the FD treatment. The SMER and total drying time (TDT) of the MFD-DMLC were higher by 44.3% and lower by 62.4% than those of the FD process. A better SMER means better energy usage, while a lower TDT means shorter drying time. Both parameters together with product quality are good indicators supporting the better process efficiency of the MFD than that of the FD. Thus, it can also be concluded that the MFD-DMLC successfully enhances the efficiency of the MFD processes in this research.

4.6 Novelty of this research

The novelty of this research is the use of drying parameters, such as drying rate constant (k) and moisture diffusion (D), as a theoretical basis to develop the drying strategy by integrating with the closed-loop control theory to design the MFD-dynamic microwave logic control. From this research, we can identify the phase-transition moisture content of the MFD process and monitor the drying rate and moisture diffusivity in the sublimation phase and desorption phase. Moreover, we can control the MFD process in real-time using the real-time moisture content and temperature as a feedback control to automatically control the process to enhance the efficiency of the MFD while obtaining the best product quality. This is a new technique in the microwave drying research field. All of the findings have not been reported elsewhere but rather important to understand the in-depth MFD drying characteristics.

CHAPTER 5

CONCLUSIONS

5.1 Conclusions

Our findings indicate that MFD with CLT positively reduces the variation in temperature of carrot slices during the desorption drying phase by 60% compared to MFD without CLT. The drying time and energy consumption of the MFD with CLT are also reduced by 35-40%, while product quality similar to the FD process is obtained. The improvement of CLT involving a more accurate temperature feedback control and obtained a smoother temperature control in the desorption drying phase. After applying DMLC into the CLC system, which developed based on a drying-phase configuration and dynamic control between the microwave power and real-time moisture content and applying the CLT to control the final stage temperature. The CLC system can work properly with the MFD of carrot slices under the uncertainty of temperature measurement of 3.9%, weight measurement of 0.8%, and moisture content calculation of 1%. The moisture content and temperature of carrot slices were shown to be important factors influencing the drying characteristics. The carrot's moisture content played a role in the absorption of the microwave energy during the MFD process; therefore, it was used as feedback for the CLC. The temperature played an important role in maintaining the final product quality; hence, it was used as another form of feedback for the CLC in the final stage of the MFD process. Integrating both factors into the DMLC, the MFD process could be controlled appropriately and was able to shorten the drying time by 62.4% and 23.4% compared to the FD and MFD with no DMLC, respectively. The MFD-DMLC provided the final product with a quality equivalent to that of the FD process but achieved 44.3% better SMER. The CLC-MFD was successfully developed, and the objective of this research was achieved. The findings from this research suggested that the DMLC based on the moisture content and temperature of the samples could be combined with the MFD process to enhance its efficiency of the general

MFD and FD process while maintaining the superior quality to the FD product which achieved the goals of this research.

5.2 Recommendations

While in this research, the PLC system was successfully developed for improving the MFD process, little is known on theoretical studies, modeling, and simulation for MFD processes. Such research is needed for the optimization of complex drying technologies. The typical simulation models, which have been validated through experiments, should be able to predict the impact of important parameters on drying time and energy efficiency, as well as assist in improving operational output for various combination drying processes. Furthermore, the laboratory-scale MFD was applied that was designed based on a domestic microwave oven with a 2.4 GHz microwave generator and a microwave power range of 0 – 900W as the main microwave energy sources in this study. This makes scaling up lab-scale findings to industrial-scale implementations, which could have a different design. As a result, future research should concentrate on larger MFD systems or pilot-scale systems that can model continuous processes using industrial-scale MFD equipment. An analysis of continuous and automatic control is very important for the further potential for industrial applications in the MFD process.

REFERENCES

- Abbasi, S. & Azari, S. 2009. Novel microwave–freeze drying of onion slices. **International Journal of Food Science & Technology**, 44(5), 974-979.
- Adams, D. J. 1981. Theory of the dielectric constant of ice. **Nature**, 293(5832), 447-449.
- Akoy, E. O. M. 2014. Experimental characterization and modeling of thin-layer drying of mango slices. **international food research journal**, 21(1), 1911-1917.
- Akpinar, E. K. 2006a. Determination of suitable thin layer drying curve model for some vegetables and fruits. **Journal of Food Engineering**, 73(1), 75-84.
- Akpinar, E. K. 2006b. Mathematical modelling of thin layer drying process under open sun of some aromatic plants. **Journal of Food Engineering**, 77(4), 864-870.
- Akpinar, E. K., Bicer, Y. & Cetinkaya, F. 2006. Modelling of thin layer drying of parsley leaves in a convective dryer and under open sun. **Journal of Food Engineering**, 75(3), 308-315.
- Amarasinghe, B. M. W. P. K., Aberathna, A. J. M. L. M. & Aberathna, K. K. P. P. 2018. Kinetics and mathematical modeling of microwave drying of sri lankan black pepper (*Piper Nigrum*). **International Journal of Environmental & Agriculture Research**, 4(2), 6-13.
- Ambros, S., Mayer, R., Schumann, B. & Kulozik, U. 2018. Microwave-freeze drying of lactic acid bacteria: Influence of process parameters on drying behavior and viability. **Innovative Food Science & Emerging Technologies**, 48(1), 90-98.
- Ambros, S., Oezcelik, M., Dachmann, E. & Kulozik, U. 2017. Microwave freeze drying of fruit foams for the production of healthy snacks. **Nutrition and Food Engineering**, 4(4), 1135-1135.
- Amiri Chayjan, R., Dibagar, N. & Alaei, B. 2017. Drying characteristics of zucchini slices under periodic infrared-microwave vacuum conditions. **Heat and Mass Transfer**, 53(12), 3473-3485.
- Amiri Chayjan, R., Kaveh, M. & Khayati, S. 2015. Modeling drying characteristics of hawthorn fruit under microwave-convective conditions. **Journal of Food**

Processing and Preservation, 39(3), 239-253.

Azimi-Nejadian, H. & Hoseini, S. S. 2019. Study the effect of microwave power and slices thickness on drying characteristics of potato. **Heat and Mass Transfer**, 55(10), 2921-2930.

Berk, Z. 2018. **Food Process Engineering and Technology**. 3rd ed. London: Academic Press.

Brooker, D. B., Bakker-Arkema, F. W. & Hall, C. W. 1992. **Drying and Storage of Grains and Oilseeds**. New York: Van Nostrand Reinhold.

Bruce, D. M. 1985. Exposed-layer barley drying: Three models fitted to new data up to 150°C. **Journal of Agricultural Engineering Research**, 32(4), 337-348.

Cao, X., Zhang, M., Mujumdar, A. S., Zhong, Q. & Wang, Z. 2018a. Effect of microwave freeze-drying on quality and energy supply in drying of barley grass. **Journal of the Science of Food and Agriculture**, 98(4), 1599-1605.

Cao, X., Zhang, M., Mujumdar, A. S., Zhong, Q. & Wang, Z. 2018b. Effects of ultrasonic pretreatments on quality, energy consumption and sterilization of barley grass in freeze drying. **Ultrasonics Sonochemistry**, 40(1), 333-340.

Carrin, M. & Crapiste, G. (2008). Convective drying of foods. In **Advances in Food Dehydration** (pp. 123-152). Boca Raton: CRC Press.

Ceballos, A. M., Giraldo, G. I. & Orrego, C. E. 2012. Effect of freezing rate on quality parameters of freeze dried soursop fruit pulp. **Journal of Food Engineering**, 111(2), 360-365.

Chua, K. J., Chou, S. K., Ho, J. C. & Hawlader, M. N. A. 2002. Heat pump drying: Recent developments and future trends. **Drying Technology**, 20(8), 1579-1610.

Crank, J. 1975. **The Mathematics of Diffusion**. 2nd ed. London: Oxford University Press.

Cui, Z.-W., Li, C.-Y., Song, C.-F. & Song, Y. 2008. Combined microwave-vacuum and freeze drying of carrot and apple chips. **Drying Technology**, 26(12), 1517-1523.

Datta, A. K. & Anantheswaran, R. C. (2001). Fundamentals of Heat and Moisture Transport for Microwaveable Food Product and Process Development. In **Handbook of Microwave Technology for Food Applications** (A. K. and Anantheswaran ed., pp. 115–166). New York: Marcel Dekker.

- Demirhan, E. & Özbek, B. 2011. Thin-layer drying characteristic and modeling of celery leaves undergoing microwave treatment. **Chemical Engineering Communications**, 198(7), 957-975.
- Doymaz, I. 2005. Drying behaviour of green beans. **Journal of Food Engineering**, 69(1), 161-165.
- Doymaz, İ. 2004. Convective air drying characteristics of thin layer carrots. **Journal of Food Engineering**, 61(3), 359-364.
- Doymaz, İ. 2007. The kinetics of forced convective air-drying of pumpkin slices. **Journal of Food Engineering**, 79(1), 243-248.
- Doymaz, İ. & İsmail, O. 2011. Drying characteristics of sweet cherry. **Food and Bioproducts Processing**, 89(1), 31-38.
- Drof, R. C. & Bishop, R. H. 2017. **Modern Control System**. 13th ed. Boston: Pearson.
- Duan, X., Liu, W. C., Ren, G. Y., Liu, L. L. & Liu, Y. H. 2016. Browning behavior of button mushrooms during microwave freeze-drying. **Drying Technology**, 34(11), 1373-1379.
- Duan, X., Ren, G. Y. & Zhu, W. X. 2012. Microwave freeze drying of apple slices based on the dielectric properties. **Drying Technology**, 30(5), 535-541.
- Duan, X., Zhang, M., Li, X. & Mujumdar, A. S. 2008a. Microwave freeze drying of sea cucumber coated with nanoscale silver. **Drying Technology**, 26(4), 413-419.
- Duan, X., Zhang, M., Li, X. & Mujumdar, A. S. 2008b. Ultrasonically enhanced osmotic pretreatment of sea cucumber prior to microwave freeze-drying. **Drying Technology**, 26(4), 420-426.
- Duan, X., Zhang, M. & Mujumdar, A. S. 2007a. Studies on the microwave freeze-drying technique and sterilization characteristics of cabbage. **Drying Technology**, 25(10), 1725-1731.
- Duan, X., Zhang, M. & Mujumdar, A. S. 2007b. Study on a combination drying technique of sea cucumber. **Drying Technology**, 25(12), 2011-2019.
- Duan, X., Zhang, M., Mujumdar, A. S. & Wang, R. 2010a. Trends in microwave-assisted freeze drying of foods. **Drying Technology**, 28(4), 444-453.
- Duan, X., Zhang, M., Mujumdar, A. S. & Wang, S. 2010b. Microwave freeze-drying of sea cucumber (*Stichopus japonicus*). **Journal of Food Engineering**, 96(4), 491-

497.

- Erbay, Z. & Icier, F. 2010. A review of thin layer drying of foods: theory, modeling, and experimental results. **Critical Reviews in Food Science and Nutrition**, 50(5), 441-464.
- Feng, H. & Tang, J. 1998. Microwave finish drying of diced apples in a spouted bed. **Journal of Food Science**, 63(4), 679-683.
- Feng, H., Tang, J., Cavalieri, R. P. & Plumb, O. A. 2001. Heat and mass transport in microwave drying of porous materials in a spouted bed. **AIChE Journal**, 47(7), 1499-1512.
- Franks, F. & Auffret, T. 2008. **Freeze-drying of Pharmaceuticals and Biopharmaceuticals: Principles and Practice**. Cambridge: RSC Publishing.
- Fryer, P. J. & Robbins, P. T. 2005. Heat transfer in food processing: ensuring product quality and safety. **Applied Thermal Engineering**, 25(16), 2499-2510.
- Gallawa, J. C. 2000. **The Complete Microwave Oven Service Handbook**. New Jersey, United States: Prentice Hall.
- Gamboa-Santos, J., Soria, A. C., Fornari, T., Villamiel, M. & Montilla, A. 2013. Optimisation of convective drying of carrots using selected processing and quality indicators. **International Journal of Food Science & Technology**, 48(10), 1998-2006.
- Ghazanfari, A., Emami, S., Tabil, L. G. & Panigrahi, S. 2006. Thin-layer drying of flax fiber: II. Modeling drying process using semi-theoretical and empirical models. **Drying Technology**, 24(12), 1637-1642.
- Giri, S. K. & Prasad, S. 2007. Drying kinetics and rehydration characteristics of microwave-vacuum and convective hot-air dried mushrooms. **Journal of Food Engineering**, 78(2), 512-521.
- Guiné, R., Pinho, S. & Barroca, M. 2011. Study of the convective drying of pumpkin (*Cucurbita maxima*). **Food and Bioproducts processing**, 89(4), 422-428.
- Hammack, B., Ryan, P. E. & Ziech, N. 2012. **Eight Amazing Engineering Stories**. Lexington: Articulate Noise Books.
- Haseley, P. & Oetjen, G. W. 2018. **Freeze-Drying**. 3rd ed. Weinheim: Wiley-VCH.
- Hasted, J. B. (1972). Liquid Water: Dielectric Properties. In F. Franks (Ed.), **The Physics**

- and Physical Chemistry of Water** (pp. 255-309). Boston: Springer New York.
- Henderson, S. M. 1974. Progress in developing the thin layer drying equation. **Transactions of the ASAE**, 17(6), 1167-1168.
- Hii, C. L. & Ogugo, J. F. 2014. Effect of pre-treatment on the drying kinetics and product quality of star fruit slices. **Journal of Engineering Science and Technology**, 9(1), 123-135.
- Huang, L.-l., Zhang, M., Mujumdar, A. S., Sun, D.-f., Tan, G.-w. & Tang, S. 2009. Studies on decreasing energy consumption for a freeze drying process of apple slices. **Drying Technology**, 27(9), 938-946.
- ISO, E. 2008. **Guide to the Expression of Uncertainty in Measurement**. Geneva: International Organization for Standardization.
- Janjai, S., Lamlert, N., Mahayothee, B., Bala, B. K., Precoppe, M. & Muller, J. 2011. Thin layer drying of peeled longan (*Dimocarpus longan* Lour.). **Food Science and Technology Research**, 17(4), 279-288.
- Jazini, M. H. & Hatamipour, M. S. 2010. A new physical pretreatment of plum for drying. **Food and Bioproducts Processing**, 88(2), 133-137.
- Jia, Y., Khalifa, I., Hu, L., Zhu, W., Li, J., Li, K. & Li, C. 2019. Influence of three different drying techniques on persimmon chips' characteristics: A comparison study among hot-air, combined hot-air-microwave, and vacuum-freeze drying techniques. **Food and Bioproducts Processing**, 118(1), 67-76.
- Jiang, H., Zhang, M., Liu, Y., Mujumdar, A. S. & Liu, H. 2013. The energy consumption and color analysis of freeze/microwave freeze banana chips. **Food and Bioproducts Processing**, 91(4), 464-472.
- Jiang, H., Zhang, M. & Mujumdar, A. S. 2010. Microwave freeze-drying characteristics of banana crisps. **Drying Technology**, 28(12), 1377-1384.
- Jiang, H., Zhang, M., Mujumdar, A. S. & Lim, R.-X. 2011. Comparison of the effect of microwave freeze drying and microwave vacuum drying upon the process and quality characteristics of potato/banana re-structured chips. **International Journal of Food Science & Technology**, 46(3), 570-576.
- Jiang, H., Zhang, M., Mujumdar, A. S. & Lim, R.-X. 2014. Comparison of drying characteristic and uniformity of banana cubes dried by pulse-spouted

- microwave vacuum drying, freeze drying and microwave freeze drying. **Journal of the Science of Food and Agriculture**, 94(9), 1827-1834.
- Kaatze, U. 1997. The dielectric properties of water in its different states of interaction. **Journal of Solution Chemistry**, 26(11), 1049-1112.
- Kadam, D. M., Goyal, R. K. & Gupta, M. K. 2011. Mathematical modeling of convective thin layer drying of basil leaves. **Journal of Medicinal Plants Research**, 5(19), 4721-4730.
- Kaur, K. & Singh, A. K. 2014. Drying kinetics and quality characteristics of beetroot slices under hot air followed by microwave finish drying. **African Journal of Agricultural Research**, 9(1), 1036-1044.
- Kumar, N., Sarkar, B. C. & Sharma, H. K. 2012. Mathematical modelling of thin layer hot air drying of carrot pomace. **Journal of food science and technology**, 49(1), 33-41.
- Li, L., Zhang, M. & Wang, W. 2019. A novel low-frequency microwave assisted pulse-spouted bed freeze-drying of Chinese yam. **Food and Bioproducts Processing**, 118(1), 217-226.
- Liu, W. C., Duan, X., Ren, G. Y., Liu, L. L. & Liu, Y. H. 2017. Optimization of microwave freeze-drying strategy of mushrooms (*Agaricus bisporus*) based on porosity change behavior. **Drying Technology**, 35(11), 1327-1336.
- Lombraña, J. I., Zuazo, I. & Ikara, J. 2001. Moisture diffusivity behavior during freeze drying under microwave heating power application **Drying Technology**, 19(8), 1613-1627.
- Lopez-Quiroga, E., Antelo, L. T. & Alonso, A. A. 2012. Time-scale modeling and optimal control of freeze drying. **Journal of Food Engineering**, 111(4), 655-666.
- Love, W. (1995). Chapter 2 - Magnetrons. In T. Koryu Ishii (Ed.), **Handbook of Microwave Technology** (pp. 33-55). San Diego: Academic Press.
- Madamba, P. S., Driscoll, R. H. & Buckle, K. A. 1996. The thin-layer drying characteristics of garlic slices. **Journal of Food Engineering**, 29(1), 75-97.
- Maskan, M. 2000. Microwave/air and microwave finish drying of banana. **Journal of food engineering**, 44(2), 71-78.
- Mayr, O. & Bryant, L. 1971. The origins of feedback control. **IEEE Transactions on**

- Systems, Man, and Cybernetics**, SMC-1(4), 407-407.
- McMinn, W. A. M., McLoughlin, C. M. & Magee, T. R. A. 2005. Thin-layer modeling of microwave, microwave-convective, and microwave-vacuum drying of pharmaceutical powders. **Drying Technology**, 23(3), 513-532.
- Meda, L. & Ratti, C. 2005. Rehydration of freeze-dried strawberries at varying temperatures. **Journal of Food Process Engineering**, 28(3), 233-246.
- Mellor, J. D. 1978. **Fundamentals of Freeze-drying**. London: Academic Press.
- Midilli, A., Kucuk, H. & Yapar, Z. 2002. A new model for single-layer drying. **Drying Technology**, 20(7), 1503-1513.
- Mishra, A., Vats, T. & Clark, H. J. 2015. **Microwave-Assisted Polymerization**. Cambridge: Royal Society of Chemistry.
- Mudgett, R. E. (1985). Dielectric properties of foods. In R. V. Decareau (Ed.), **Microwaves in the Food Processing Industry** (pp. 15-37). Toronto: Academic Press Inc.
- Murthy, T. & Manohar, B. 2012. Microwave drying of mango ginger (*Curcuma amada* Roxb): prediction of drying kinetics by mathematical modelling and artificial neural network. **International Journal of Food Science & Technology**, 47(6), 1229-1236.
- Nail, S. L., Jiang, S., Chongprasert, S. & Knopp, S. A. (2002). Fundamentals of Freeze-Drying. In **Development and Manufacture of Protein Pharmaceuticals** (pp. 281-360). Boston: Springer US.
- Narjes, M., Zahra, E.-D., Seyed Hassan, H. & Gholam Reza, A. 2018. Modeling thin layer drying kinetics, moisture diffusivity and activation energy of hazelnuts during microwave-convective drying. **International Journal of Food Engineering**, 14(2), 20170100.
- Nguyen, M.-H. & Price, W. E. 2007. Air-drying of banana: Influence of experimental parameters, slab thickness, banana maturity and harvesting season. **Journal of Food Engineering**, 79(1), 200-207.
- Nijhuis, H. H., Topping, H. M., Muresan, S., Yuksel, D., Leguijt, C. & Kloek, W. 1998. Approaches to improving the quality of dried fruit and vegetables. **Trends in Food Science & Technology**, 9(1), 13-20.

- Okos, M. R., Narishman, G., Singh, R. K. & Weitnauer, A. C. (1992). Food dehydration. In **Handbook of Food Engineering** (pp. 437-562). New York: Marcel Dekker.
- Omolola, A. O., Jideani, A. I. & Kapila, P. F. 2014. Modeling microwave drying kinetics and moisture diffusivity of Mabonde banana variety. **International Journal of Agricultural and Biological Engineering**, 7(1), 107-113.
- Orsat, V., Raghavan, G. S. V. & Krishnaswamy, K. (2017). Microwave technology for food processing: An overview of current and future applications. In M. Regier, K. Knoerzer & H. Schubert (Eds.), **The Microwave Processing of Foods** (2nd ed., pp. 100-116). Cambridge: Woodhead Publishing.
- Ozcelik, M., Ambros, S., Heigl, A., Dachmann, E. & Kulozik, U. 2019. Impact of hydrocolloid addition and microwave processing condition on drying behavior of foamed raspberry puree. **Journal of Food Engineering**, 240(1), 83-91.
- Özdemir, M. & Onur Devres, Y. 1999. The thin layer drying characteristics of hazelnuts during roasting. **Journal of Food Engineering**, 42(4), 225-233.
- Ozkan, I. A., Akbudak, B. & Akbudak, N. 2007. Microwave drying characteristics of spinach. **Journal of Food Engineering**, 78(2), 577-583.
- Panchariya, P. C., Popovic, D. & Sharma, A. L. 2002. Thin-layer modelling of black tea drying process. **Journal of Food Engineering**, 52(4), 349-357.
- Pardeshi, I. L., Arora, S. & Borker, P. A. 2009. Thin-layer drying of green peas and selection of a suitable thin-layer drying model. **Drying Technology**, 27(2), 288-295.
- Prasertsan, S. & Saen-saby, P. 1998. Heat pump drying of agricultural materials. **Drying Technology**, 16(1-2), 235-250.
- Raikham, C., Prachayawarakorn, S., Nathakaranakule, A. & Soponronnarit, S. 2013. Optimum conditions of fluidized bed puffing for producing crispy banana. **Drying Technology**, 31(6), 726-739.
- Ratti, C. 2001. Hot air and freeze-drying of high-value foods: a review. **Journal of Food Engineering**, 49(4), 311-319.
- Rayaguru, K. & Routray, W. 2012. Mathematical modeling of thin layer drying kinetics of stone apple slices. **international food research journal**, 19(1), 1503-1510.
- Regier, M., Knoerzer, K. & Schubert, H. 2016. **The Microwave Processing of Foods**.

Cambridge: Woodhead publishing.

- Ren, G. Y., Zeng, F. L., Duan, X., Liu, L. L., Duan, B., Wang, M. M., Liu, Y. H. & Zhu, W. X. 2015. The effect of glass transition temperature on the procedure of microwave freeze-drying of mushrooms (*Agaricus bisporus*). **Drying Technology**, 33(2), 169-175.
- Requena-Perez, M. E., Pedreno-Molina, J. L., Monzo-Cabrera, J. & Diaz-Morcillo, A. 2005. Multimode cavity efficiency optimization by optimum load location-experimental approach. **IEEE Transactions on Microwave Theory and Techniques**, 53(6), 2114-2120.
- Sacilik, K., Keskin, R. & Elicin, A. K. 2006. Mathematical modelling of solar tunnel drying of thin layer organic tomato. **Journal of Food Engineering**, 73(3), 231-238.
- Saxena, J. & Dash, K. 2015. Drying kinetics and moisture diffusivity study of ripe Jackfruit. **international food research journal**, 22(1), 414-420.
- Scaman, C. H. & Durance, T. D. (2005). Combined Microwave Vacuum-drying. In D.-W. Sun (Ed.), **Emerging Technologies for Food Processing** (pp. 507-533). London: Academic Press.
- Sharma, G. P. & Prasad, S. 2001. Drying of garlic (*Allium sativum*) cloves by microwave-hot air combination. **Journal of Food Engineering**, 50(2), 99-105.
- Sharma, G. P. & Prasad, S. 2004. Effective moisture diffusivity of garlic cloves undergoing microwave-convective drying. **Journal of Food Engineering**, 65(4), 609-617.
- Simal, S., Femenia, A., Garau, M. C. & Rosselló, C. 2005. Use of exponential, Page's and diffusional models to simulate the drying kinetics of kiwi fruit. **Journal of Food Engineering**, 66(3), 323-328.
- Sochanski, J. S., Goyette, J., Bose, T. K., Akyel, C. & Bosisio, R. 1990. Freeze dehydration of foamed milk by microwaves. **Drying Technology**, 8(5), 1017-1037.
- Song, C., Wu, T., Li, Z., Li, J. & Chen, H. 2018. Analysis of the heat transfer characteristics of blackberries during microwave vacuum heating. **Journal of Food Engineering**, 223(1), 70-78.

- Soysal, Y. 2004. Microwave drying characteristics of parsley. **Biosystems Engineering**, 89(2), 167-173.
- Soysal, Y., Ayhan, Z., Eştürk, O. & Arıkan, M. F. 2009. Intermittent microwave–convective drying of red pepper: Drying kinetics, physical (colour and texture) and sensory quality. **Biosystems Engineering**, 103(4), 455-463.
- Srinivasa, P. C., Ramesh, M. N., Kumar, K. R. & Tharanathan, R. N. 2004. Properties of chitosan films prepared under different drying conditions. **Journal of Food Engineering**, 63(1), 79-85.
- Stawreberg, L. & Nilsson, L. 2010. Modelling of specific moisture extraction rate and leakage ratio in a condensing tumble dryer. **Applied Thermal Engineering**, 30(14), 2173-2179.
- Süfer, Ö., Sezer, S. & Demir, H. 2017. Thin layer mathematical modeling of convective, vacuum and microwave drying of intact and brined onion slices. **Journal of Food Processing and Preservation**, 41(6), 13239.
- Sujinda, N., Varith, J., Jaturonglumert, S. & Shamsudin, R. 2020. Closed-loop temperature control during microwave freeze-drying of carrot slices. **Maejo International Journal Science and Technology**, 14(1), 81-92.
- Sumnu, G. & Sahin, S. (2005). Recent Developments in Microwave Heating. In D.-W. Sun (Ed.), **Emerging Technologies for Food Processing** (pp. 419-444). London: Academic Press.
- Sutar, P. P. & Prasad, S. 2007. Modeling microwave vacuum drying kinetics and moisture diffusivity of carrot slices. **Drying Technology**, 25(10), 1695-1702.
- Tanaka, M. & Sato, M. 2007. Microwave heating of water, ice, and saline solution: Molecular dynamics study. **The Journal of Chemical Physics**, 126(3), 034509.
- Torki-Harchegani, M., Ghanbarian, D., Ghasemi Pirbalouti, A. & Sadeghi, M. 2016. Dehydration behaviour, mathematical modelling, energy efficiency and essential oil yield of peppermint leaves undergoing microwave and hot air treatments. **Renewable and Sustainable Energy Reviews**, 58(1), 407-418.
- Torringa, E., Esveld, E., Scheewe, I., van den Berg, R. & Bartels, P. 2001. Osmotic dehydration as a pre-treatment before combined microwave-hot-air drying of mushrooms. **Journal of Food Engineering**, 49(2), 185-191.

- Varith, J., Dijkanarukkul, P., Achariyaviriya, A. & Achariyaviriya, S. 2007. Combined microwave-hot air drying of peeled longan. **Journal of Food Engineering**, 81(2), 459-468.
- Wang, J. & Sheng, K. 2006. Far-infrared and microwave drying of peach. **LWT - Food Science and Technology**, 39(3), 247-255.
- Wang, J. & Xi, Y. S. 2005. Drying characteristics and drying quality of carrot using a two-stage microwave process. **Journal of Food Engineering**, 68(4), 505-511.
- Wang, R., Zhang, M. & Mujumdar, A. S. 2010a. Effect of food ingredient on microwave freeze drying of instant vegetable soup. **LWT - Food Science and Technology**, 43(7), 1144-1150.
- Wang, R., Zhang, M. & Mujumdar, A. S. 2010b. Effects of vacuum and microwave freeze drying on microstructure and quality of potato slices. **Journal of Food Engineering**, 101(2), 131-139.
- Wang, R., Zhang, M., Mujumdar, A. S. & Sun, J.-C. 2009. Microwave freeze-drying characteristics and sensory quality of instant vegetable soup. **Drying Technology**, 27(9), 962-968.
- Wang, Z., Sun, J., Chen, F., Liao, X. & Hu, X. 2007a. Mathematical modelling on thin layer microwave drying of apple pomace with and without hot air pre-drying. **Journal of Food Engineering**, 80(2), 536-544.
- Wang, Z., Sun, J., Liao, X., Chen, F., Zhao, G., Wu, J. & Hu, X. 2007b. Mathematical modeling on hot air drying of thin layer apple pomace. **Food Research International**, 40(1), 39 - 46.
- Wu, H., Tao, Z., Chen, G., Deng, H., Xu, G. & Ding, S. 2004. Conjugate heat and mass transfer process within porous media with dielectric cores in microwave freeze drying. **Chemical Engineering Science**, 59(14), 2921-2928.
- Wu, X.-f., Zhang, M., Ye, Y. & Yu, D. 2020. Influence of ultrasonic pretreatments on drying kinetics and quality attributes of sweet potato slices in infrared freeze drying (IRFD). **LWT**, 109801.
- Yaldýz, O. & Ertekýn, C. 2001. Thin layer solar drying of some vegetables. **Drying Technology**, 19(3-4), 583-597.
- Younis, M., Abdelkarim, D. & Zein El-Abdein, A. 2018. Kinetics and mathematical

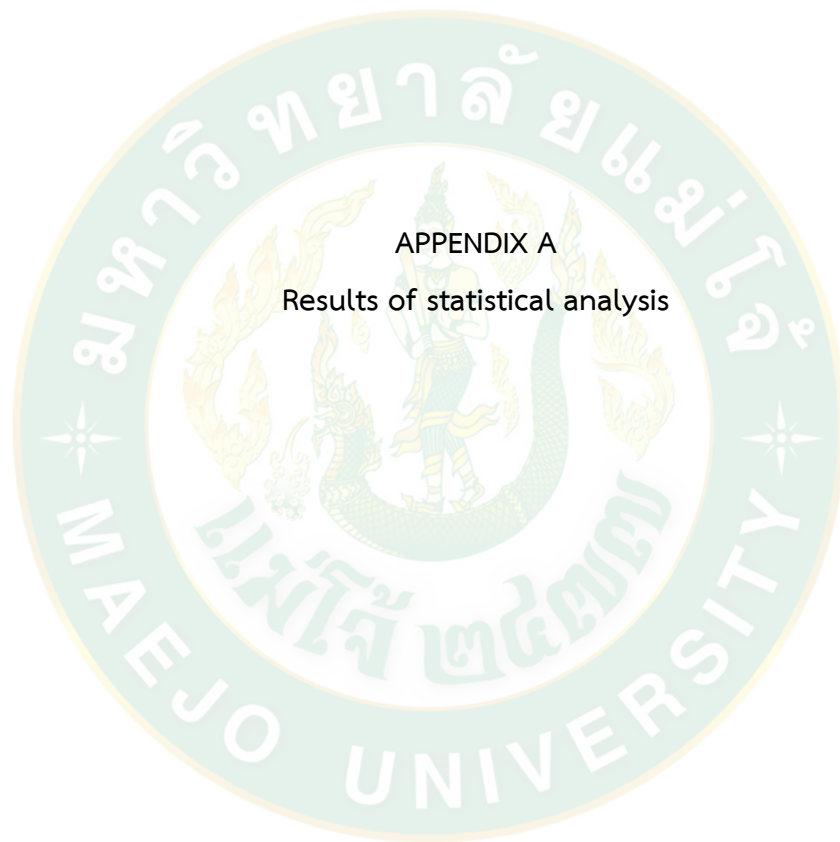
modeling of infrared thin-layer drying of garlic slices. **Saudi Journal of Biological Sciences**, 25(2), 332-338.

Zhang, Q., Zhang, G., Mu, G. & Liu, Y. 2012. Freeze and microwave vacuum combination drying technique for sea cucumber. **International Journal of Agricultural and Biological Engineering**, 5(3), 83-89.





APPENDIX



APPENDIX A

Results of statistical analysis

Table A1 Duncan table for the color (L^*) of carrot slices affected by the FD, MFD with CLT, and MFD without CLT.

		L^*		
	Drying methods	N	Subset for alpha = 0.05	
			1	2
Duncan ^a	MFD non CLT	9	45.7600	
	MFD with CLT	9		61.7912
	FD	9		64.6900
	Sig.		1.000	.062

Means for groups in homogeneous subsets are displayed.

a. Uses Harmonic Mean Sample Size = 9.000.

Table A2 Duncan table for the color (a^*) of carrot slices affected by the FD, MFD with CLT, and MFD without CLT.

		a^*		
	Drying methods	N	Subset for alpha = 0.05	
			1	2
Duncan ^a	MFD with CLT	9	25.1589	
	FD	9	26.8422	
	MFD non CLT	9		31.4567
	Sig.		.112	1.000

Means for groups in homogeneous subsets are displayed.

a. Uses Harmonic Mean Sample Size = 9.000.

Table A3 Duncan table for the color (b*) of carrot slices affected by the FD, MFD with CLT, and MFD without CLT.

		b*		
	Drying methods	N	Subset for alpha = 0.05	
			1	2
Duncan ^a	FD	9	29.7889	
	MFD with CLT	9	32.9500	32.9500
	MFD non CLT	9		38.1156
	Sig.		1.000	.112

Means for groups in homogeneous subsets are displayed.

a. Uses Harmonic Mean Sample Size = 9.000.

Table A4 Duncan table for the crispness of carrot slices affected by the FD, MFD with CLT, and MFD without CLT.

		Crispness		
	Drying methods	N	Subset for alpha = 0.05	
			1	2
Duncan ^a	MFD non CLT	27	11.2163	
	MFD with CLT	27		14.8863
	FD	27		15.4383
	Sig.		.262	.140

Means for groups in homogeneous subsets are displayed.

a. Uses Harmonic Mean Sample Size = 27.000.

Table A5 Duncan table for the hardness of carrot slices affected by the FD, MFD with CLT, and MFD without CLT.

Hardness				
	Drying methods	N	Subset for alpha = 0.05	
			1	2
Duncan ^a	FD	27	7.6887	
	MFD with CLT	27	7.7544	7.7544
	MFD non CLT	27		8.2545
	Sig.		.260	.532

Means for groups in homogeneous subsets are displayed.

a. Uses Harmonic Mean Sample Size = 27.000.

Table A6 Duncan table for the rehydration ratio of carrot slices affected by the FD, MFD with CLT, and MFD without CLT.

Rehydration				
	Drying methods	N	Subset for alpha = 0.05	
			1	
Duncan ^a	MFD with CLT	9	5.3871	
	MFD non CLT	9	5.4628	
	FD	9	5.6578	
	Sig.		.577	

Means for groups in homogeneous subsets are displayed.

a. Uses Harmonic Mean Sample Size = 9.000.

Table A7 Duncan table for the energy consumption of the FD, MFD with CLT, and MFD without CLT.

EC				
	Drying methods	N	Subset for alpha = 0.05	
			1	2
Duncan ^a	MFD with CLT	3	45.8469	70.9805
	MFD non CLT	3	46.4017	
	FD	3		
	Sig.		1.000	.134

Means for groups in homogeneous subsets are displayed.

a. Uses Harmonic Mean Sample Size = 3.000.

Table A8 Duncan table for the color (L*) of carrot slices affected by the different drying conditions.

L*				
	Drying methods	N	Subset for alpha = 0.05	
			1	2
Duncan ^a	MFD-300W	9	54.3467	61.9878
	MFD-200W	9		
	MFD-DMLC	9		
	MFD-100W	9		
	FD	9		
	Sig.		1.000	.062

Means for groups in homogeneous subsets are displayed.

a. Uses Harmonic Mean Sample Size = 9.000.

Table A9 Duncan table for the color (a*) of carrot slices affected by the different drying conditions.

		a*		
	Drying methods	N	Subset for alpha = 0.05	
			1	2
Duncan ^a	FD	9	25.1589	
	MFD-200W	9	26.2544	
	MFD-100W	9	26.4267	
	MFD-DMLC	9	26.7756	
	MFD-300W	9		33.0667
	Sig.		.187	1.000

Means for groups in homogeneous subsets are displayed.

a. Uses Harmonic Mean Sample Size = 9.000.

Table A10 Duncan table for the color (b*) of carrot slices affected by the different drying conditions.

		b*		
	Drying methods	N	Subset for alpha = 0.05	
			1	2
Duncan ^a	MFD-100W	9	29.7889	
	FD	9	29.7889	
	MFD-200W	9	31.4056	
	MFD-DMLC	9	31.7078	
	MFD-300W	9		35.9544
	Sig.		.494	1.000

Means for groups in homogeneous subsets are displayed.

a. Uses Harmonic Mean Sample Size = 9.000.

Table A11 Duncan table for the crispness of carrot slices affected by the different drying conditions.

Crispness					
	Drying methods	N	Subset for alpha = 0.05		
			1	2	3
Duncan ^a	MFD-300W	27	10.6742		
	MFD-200W	27		13.8310	
	MFD-DMLC	27		14.0015	
	MFD-100W	27		14.3317	14.3317
	FD	27			15.4837
	Sig.			1.000	.211

Means for groups in homogeneous subsets are displayed.

a. Uses Harmonic Mean Sample Size = 27.000.

Table A12 Duncan table for the hardness of carrot slices affected by the different drying conditions.

Hardness				
	Drying methods	N	Subset for alpha = 0.05	
			1	2
Duncan ^a	MFD-100W	27	7.3537	
	FD	27	7.5512	
	MFD-DMLC	27	7.6503	
	MFD-200W	27	7.7422	7.7422
	MFD-300W	27		8.6334
	Sig.			.532

Means for groups in homogeneous subsets are displayed.

a. Uses Harmonic Mean Sample Size = 27.000.

Table A13 Duncan table for the rehydration ratio of carrot slices affected by the different drying conditions.

Rehydration				
	Drying methods	N	Subset for alpha = 0.05	
			1	2
Duncan ^a	MFD-300W	9	4.9667	
	MFD-200W	9	5.3133	5.3133
	MFD-DMLC	9	5.3600	5.3600
	MFD-100W	9	5.4833	5.4833
	FD	9		5.6667
	Sig.			.099

Means for groups in homogeneous subsets are displayed.

a. Uses Harmonic Mean Sample Size = 9.000.

Table A14 Duncan table for the shrinkage of carrot slices affected by the different drying conditions.

Shrinkage					
	Drying methods	N	Subset for alpha = 0.05		
			1	2	3
Duncan ^a	FD	9	25.0895		
	MFD-100W	9	25.5864	25.5864	
	MFD-DMLC	9	26.9845	26.9845	
	MFD-200W	9		27.7951	
	MFD-300W	9			37.8647
	Sig.			.095	.336

Means for groups in homogeneous subsets are displayed.

a. Uses Harmonic Mean Sample Size = 9.000.

Table A15 Duncan table for the energy consumption (EC) of the different drying conditions.

EC						
	Drying methods	N	Subset for alpha = 0.05			
			1	2	3	4
Duncan ^a	MFD-300W	3	39.0127			
	MFD-DMLC	3	39.5346			
	MFD-200W	3		42.7437		
	MFD-100W	3			45.7504	
	FD	3				70.9805
	Sig.			.347	1.000	1.000

Means for groups in homogeneous subsets are displayed.

a. Uses Harmonic Mean Sample Size = 3.000.

Table A16 Duncan table for the SMER of the different drying conditions.

SMER						
	Drying methods	N	Subset for alpha = 0.05			
			1	2	3	4
Duncan ^a	FD	9	4.4133			
	MFD-100W	9		6.8400		
	MFD-200W	9			7.2833	
	MFD-DMLC	9				7.9133
	MFD-300W	9				7.9343
	Sig.			1.000	1.000	1.000

Means for groups in homogeneous subsets are displayed.

a. Uses Harmonic Mean Sample Size = 9.000.

Table A17 Duncan table for the SMER of the different drying conditions.

SMER						
	Drying methods	N	Subset for alpha = 0.05			
			1	2	3	4
Duncan ^a	FD	9	4.4133			
	MFD-100W	9		6.8400		
	MFD-200W	9			7.2833	
	MFD-DMLC	9				7.9133
	MFD-300W	9				7.9343
	Sig.			1.000	1.000	1.000

Means for groups in homogeneous subsets are displayed.

a. Uses Harmonic Mean Sample Size = 9.000.

Table A18 Duncan table for the total drying time (TDT) of the different drying conditions.

TDT						
	Drying methods	N	Subset for alpha = 0.05			
			1	2	3	4
Duncan ^a	FD	3	16.5315			
	MFD-100W	3		8.1020		
	MFD-200W	3			7.2133	
	MFD-DMLC	3				6.1567
	MFD-300W	3				6.0448
	Sig.			1.000	1.000	1.000

Means for groups in homogeneous subsets are displayed.

a. Uses Harmonic Mean Sample Size = 3.000.

Table A19 Duncan table for the overall drying rate constant (k values) of the different microwave power.

k					
	MW power	N	Subset for alpha = 0.05		
			1	2	3
Duncan ^a	100 W	3	286.0466		
	200 W	3		344.2871	
	300 W	3			410.0012
	Sig.		1.000	1.000	1.000

Means for groups in homogeneous subsets are displayed.

a. Uses Harmonic Mean Sample Size = 3.000.

Table A20 Duncan table for the drying rate constant (k values) of the sublimation phase of the different microwave power.

k					
	MW power	N	Subset for alpha = 0.05		
			1	2	3
Duncan ^a	100 W	3	530.5720		
	200 W	3		628.6825	
	300 W	3			780.8804
	Sig.		1.000	1.000	1.000

Means for groups in homogeneous subsets are displayed.

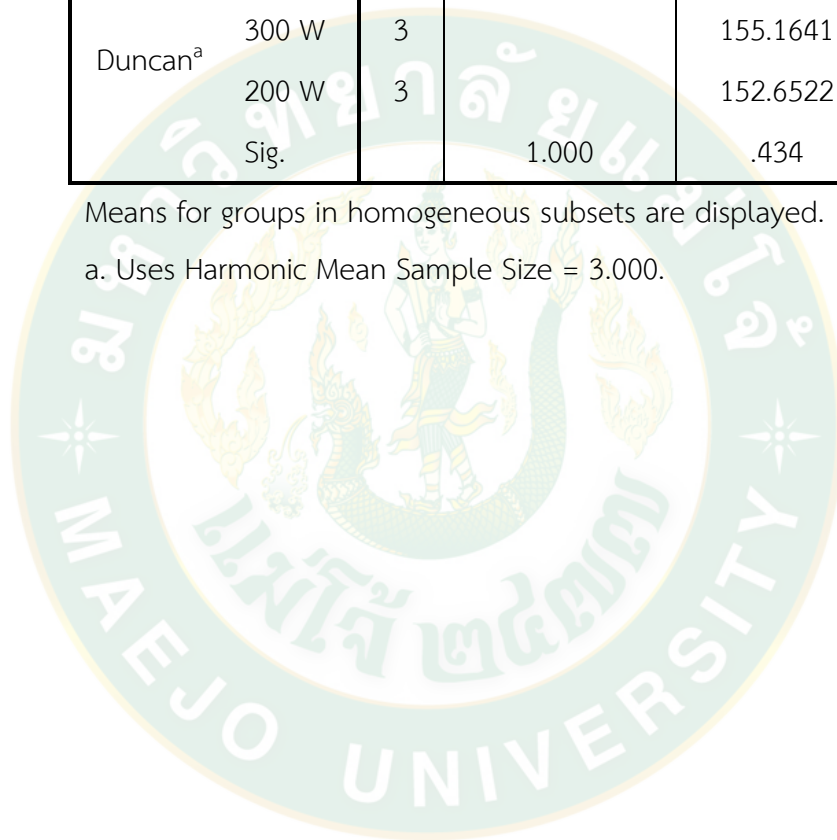
a. Uses Harmonic Mean Sample Size = 3.000.

Table A21 Duncan table for the drying rate constant (k values) of the desorption phase of the different microwave power.

		k		
	MW power	N	Subset for alpha = 0.05	
			1	2
Duncan ^a	100 W	3	136.5420	
	300 W	3		155.1641
	200 W	3		152.6522
	Sig.		1.000	.434

Means for groups in homogeneous subsets are displayed.

a. Uses Harmonic Mean Sample Size = 3.000.





APPENDIX B
Research Publication

*Full Paper***Closed-loop temperature control during microwave freeze-drying of carrot slices****Narathip Sujinda^{1, 2}, Jaturapatr Varith^{1, *}, Somkiat Jaturonglumlert¹ and Rosnah Shamsudin²**¹ Graduate Program of Food Engineering, Faculty of Engineering and Agro-industry, Maejo University, Chiang Mai 50290, Thailand² Department of Process and Food Engineering, Faculty of Engineering, Universiti Putra Malaysia, Selangor 43400, Malaysia* Corresponding author, e-mail: varithj@maejo.mju.ac.th*Received: 11 November 2018 / Accepted: 16 March 2020 / Published: 23 March 2020*

Abstract: Temperature variations during microwave freeze-drying (MFD) of carrot slices and how closed-loop temperature control (CLT) improved such variations were investigated. The carrot slices were dried to a final moisture content of 6% with a terminal temperature of 40°C using 100-watt microwave power under 100-Pa vacuum pressure. The results showed that the MFD process consisted of two phases, viz. sublimation and desorption drying. In the sublimation drying phase, ice, due to its low dielectric permittivity, absorbed little microwave energy. This caused a slow rising of temperature of carrot slices at the early stage of drying. After the moisture decreased below 45%, the sample temperature increased sharply until it reached the temperature of the chamber, indicating the onset of desorption drying phase. In this phase, the sample temperature rose faster than that in the sublimation phase. Without CLT, the temperature of carrot slices varied by 25°C in the desorption drying phase of MFD. After applying CLT to the MFD process, the variation in temperature of the carrot slices was reduced to 11°C, equivalent to a temperature control improvement of 56%. The MFD with CLT system also significantly reduced the drying time and energy consumption by 35-40%.

Keywords: carrot slices, microwave freeze-drying, sublimation, desorption, closed-loop temperature control

Figure B1 Publication in Maejo International Journal of Science and Technology.



Development of a closed-loop control system for microwave freeze-drying of carrot slices using a dynamic microwave logic control

Narathip Sujinda^{a, b}, Jaturapatr Varith^{a, *}, Rosnah Shamsudin^b, Somkiat Jaturonglumert^a, Saranyapak Chamnan^a

^a Division of Food Engineering, Faculty of Engineering and Agro-Industry, Maejo University, Chiang Mai, Thailand

^b Department of Process and Food Engineering, Faculty of Engineering, Universiti Putra Malaysia, Malaysia

ARTICLE INFO

Keywords:

Microwave freeze-drying
Closed-loop control system
Dynamic microwave logic control
Drying characteristics
Carrot slices

ABSTRACT

This research aimed to develop a closed-loop control (CLC) system to improve the microwave freeze-drying (MFD) process and to examine the effects of a dynamic microwave logic control (DMLC) on the drying characteristics of MFD. The development process consisted of two parts: (1) the MFD experiment to develop the DMLC, and (2) the implementation of the CLC with the DMLC on the MFD process. In the first part, the MFD process was examined to obtain the strategy for drying the carrot slices using microwave powers of 100 W, 200 W, and 300 W, with a temperature profile of the sample from -15°C to 40°C , and the final moisture content of 6% (wet basis). In the second part, the DMLC was strategically developed and integrated into the CLC system. The results showed that in the MFD process, the DMLC was developed based on a drying-phase configuration and dynamic control between the microwave power and real-time moisture content sensing to provide feedback to the CLC system. After applying the DMLC into the CLC system, the efficiency of the MFD process was improved by up to 62.4% by shortening the drying time, as compared with the freeze-dry (FD) process. The MFD-DMLC also resulted in the quality of carrot equivalent to that of a traditional FD process. Since the DMLC exhibited great potential to improve the MFD process, it could be developed for future industrial use for a high-performance MFD process in terms of product quality and process efficiency.

1. Introduction

Carrot (*Daucus carota* L.) is considered a significant root vegetable owing to its medicinal properties beneficial to human health. Because of its susceptibility to spoilage, an applicable technique would be needed to preserve its nutritional value (Guo et al., 2020). Of the drying methods, freeze-drying (FD) has been suggested as a good option for storage of fruits and vegetables in food industries due to retention of organoleptic and nutritional qualities. Contrastingly, it is time- and energy-consuming and high in operational cost because of inadequate heat supply coming from the heated plate (Cao et al., 2018b; Wu et al., 2020). Hence, a process that reduces the drying period and energy usage while retaining the product's quality resolves this issue.

Microwave freeze-drying (MFD) is a drying method that applies microwave energy as a heating source to the FD process (Duan et al., 2010a). Thus, microwave energy offers a better option for reducing the drying period and energy usage (Cao et al., 2018a; Huang et al., 2009), while considerably increasing the drying rate (Ozcelik et al., 2019) due

to rapid heating in materials. Microwave energy generates heat inside the materials by two mechanisms: a dipole rotation and an ionic conduction. These mechanisms occur simultaneously as the ions are induced by electrical oscillation for alignment within the electromagnetic field. The electromagnetic energy in this process is converted to thermokinetic energy and is absorbed in all parts of the material (Song et al., 2018; Varith et al., 2007). For this reason, the MFD process can reduce the drying time by half (Duan et al., 2010b; Wang et al., 2010) and the energy consumption by up to 30%, while obtaining a product quality similar to that of FD (Jiang et al., 2013). Thus, MFD is an effective drying method that could address the weakness of traditional FD.

In the MFD process, complex parameters, such as, microwave power levels, moisture content, material temperature, and vacuum pressure are found to affect the drying rate, product quality and energy consumption. Although the higher microwave power reduces the drying time and increases the drying rate better than the lower microwave power, it typically results in poor product quality (Ambros et al., 2018; Duan et al., 2007; Wang et al., 2009). Additionally, the relationship

* Corresponding author.

E-mail address: varithj@mju.ac.th (J. Varith).

<https://doi.org/10.1016/j.jfoodeng.2021.110559>

Received 27 November 2020; Received in revised form 23 February 2021; Accepted 24 February 2021

0260-8774/© 2021

Figure B2 Publication in Journal of Food Engineering.

CURRICULUM VITAE

NAME Mr. Narathip Sujinda

DATE OF BIRTH 23 May 1986

EDUCATION 2015-Present : Dual Doctoral Degree Programme at Food Engineering Program, Faculty of Engineering and Agro-industry, Maejo University and Agricultural Process Engineering Program, Faculty of Engineering, Universiti Putra Malaysia.

2009-2011 : Master degree in Agricultural Process Engineering at Faculty of Engineering and Agro-industry, Maejo University.

2005-2008 : Bachelors degree in Food Engineering at Faculty of Engineering and Agro-industry, Maejo University

WORK EXPERIENCE 2014-Present : Managing Director at Quality Sense Engineering Co., Ltd., Chiangmai, Thailand

2014-2015 Plant supervisor and Engineer at Crispy Veg and Fruit Co. Ltd., Chiangmai, Thailand

2011-2014 : Head of Production and Engineer at Crispy Veg and Fruit Co. Ltd., Chiangmai, Thailand

2008-2013 : Managing Partner at Quality Sense Limited Partnership., Chiangmai, Thailand

